DYNAMIC ANALYSIS OF ASSEMBLED STRUCTURES WITH NONLINEARITY

A thesis submitted for the degree of
Doctor of Philosophy

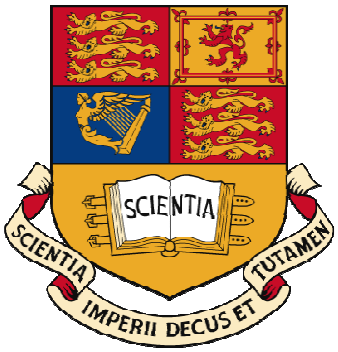

by

SEN HUANG
BEng, Nanyang Technological University, Singapore, 1999
MSc, National University of Singapore, Singapore, 2002

Department of Mechanical Engineering
Imperial College London
August, 2007

Dedicated to my beloved wife,
Seik-Yuun Emily Woon
for her love and patience

Abstract

Mathematical models are widely used in the field of structural dynamics. They are often found at the design stage of a mechanical product, when the effect of physical modifications on the total dynamic response of the structure needs to be understood before the real fabrication is carried out. In recent years they are also used in real-time machine diagnosis and prognosis applications, in which fast and precise decision-making requires highly accurate and efficient structural mathematical models. The problem we are facing now is: as the structure becomes more complicated, consisting more segments and joints, the accuracy and efficiency of the corresponding mathematical model deteriorates fast due to the difficulties in joint modelling and the nonlinearities existing in those joints. The purpose of this thesis is to develop and demonstrate a generalised approach for constructing a mathematical model that is capable of predicting accurately and efficiently dynamic responses of a complex structural assembly, in which nonlinearity at the joint must be counted.

This work takes a 'bottom-up' approach. It is reckoned that an accurate assembly model is only achievable and meaningful when all the constituent component models are constructed correctly. Hence, the first part of the thesis investigates linear structural component modelling methods and issues in mechanical joint modelling. The second part of the thesis looks into general nonlinear structural dynamic analysis. Both time-domain and frequency-domain methods are examined. In particular, the frequency-domain Harmonic Balance Method (HBM) is reviewed in detail and proven via simulations of a 1-DOF strongly nonlinear system that it can solve steady-state solutions accurately and much more efficiently than the more common time-domain methods. For a structural assembly model of moderate complexity and significant nonlinearity, HBM alone is not enough to provide efficient calculation due to the size of the problem. A new method, based on HBM and the concept of Frequency Response Function (FRF) coupling is explored. It takes advantage of the fact that nonlinearity is a localised property in most practical structural assembly. A test rig is designed and constructed to verify the above modelling approach. The rig consists of key flexible structural components that can be found in normal rotating machines. One of the bearing supports is specially-designed to exhibit adjustable nonlinear stiffness. Results from amplitude-controlled dynamic tests match the simulation very closely, which proves that the HBM together with the FRF coupling concept is a very promising approach to tackle problems of large scale structures with localised nonlinearity. The success is also attributed to the great attention to the component and joint models.

Acknowledgement

I feel privileged and indeed very proud to be one of the fifty or so PhD students that have ever studied under Prof. Ewins. Like all the previous ones, I am very grateful for his guidance and encouragement throughout this project. Apart from being inspired by his great enthusiasm and insight in the field of structural dynamics, I am very impressed by the way he manages his busy schedule, excelling in both research and important administrative duty for the college.

I am also very grateful to my co-supervisor Mr. Robb. He is always very approachable, despite his busy schedule being a College and Mechanical Department Tutor. His door is always open to me whenever I had problems, be it work-related or personal. I have learned much hands-on experience in testing and measurement from him. In this field, he is second to none.

My thanks also go to all the staffs in the section of Dynamics of Machines & Structures, especially to Dr. Petrov, a dedicated and outstanding researcher in the league of his own, whom I have bothered too many times for ideas as well as the use of the FORSE code. The helps from Margaret and Nina are also very much appreciated. In this pretty much male-dominated research group, they never failed to bring in a touch of tenderness.

I would like to say thanks to John and Paul (Sooty), two outstanding lab technicians, who have played significant roles in the completion of my project. Some of John's brilliant ideas have been shamelessly 'stolen' by me, which should be worth more than one line of recognition here. I also enjoyed many enlightening conversations with him, from engineering topics to life in general.

I feel fortunate to meet a group of intelligent people: my previous and current colleagues at Imperial College, with whom I had many interesting discussions on all sorts of topics. In the sequence of appearance, they are Enrique, Dario, Hugo, Matthew, Marija, Osamu, Gan, Wenjie, Chaoping, Giovanna, Christoph and Stefano.

During these five years, I had the opportunity to guide some final year students from Italy (Gigliola, Leonardo and Mauro) and Germany (Bernd and Christoph). It was not an easy task and it did frustrate me sometimes when I could not take things more lightly; nevertheless, it had been a great experience. Nothing is more joyful when I saw my name in their theses, when I heard they did great in final presentations, and when we have still been in contact until today.

Outside the college, I have met many great friends, who have made my life in London more enjoyable. It is difficult to list down all the names here. Just to name a few: Yuan Liang and Puay Sze, for the great friendship and many memorable dinner gatherings; Peifang, a lovely girl and an avid listener of my jokes; Ma Jian, Xinxin, Helen, Rui, Norman, Ting Kuei, Yu-Chuan, Iris and many likewise for the great times we have spent together.

The support of my family is where the ultimate comfort and happiness is from. A very big ‘thank you’ to my wife, Emily, whose love and patience has driven me forward at difficult times. Without her, I would not be able to imagine I can be where I am now. I am also indebted to my parents back in China. Even though for the first a few months they had difficulties to understand why I should spent another a few years in school; nevertheless they supported my decision ever since.

Last but not least, I shall thank the financial support of MagFly project, and all the people I met there, Dr. Becker, Dr. Bucher, Thomas, Norbert, Beat, Kai, Luc, etc. They have been very helpful to me throughout this period.

Table of Contents

List of Figures

Nomenclature

In the general context

m, c, k : SDOF mass, damping and stiffness, respectively

M, C, D, K : MDOF system matrices of mass, viscous damping, structural damping and stiffness, respectively

$u, \dot{u}, \ddot{u}$: displacement, velocity and acceleration at one DOF

$\mathbf{u}, \dot{\mathbf{u}}, \ddot{\mathbf{u}}$: displacement, velocity and acceleration of a MDOF system in vector form

$\mathbf{U}$: amplitude of the displacement vector

$\bar{\mathbf{U}}$: amplitude of the displacement vector in complex form

$\bar{\mathbf{U}}^n$: amplitude of the n^{th} harmonic component of the displacement vectors in complex form

$\mathbf{U}_S^n$: amplitude of the n^{th} sine harmonic term of the displacement

$\mathbf{U}_C^n$: amplitude of the n^{th} cosine harmonic term of the displacement

$f_i, f_{Ii}, f_{Di}, f_{Si}$: external excitation force, inertia force, damping force and elastic force respectively at i^{th} DOF

$\mathbf{f}, \mathbf{f}_I, \mathbf{f}_D, \mathbf{f}_S$: external excitation force, inertia force, damping force and elastic force respectively in a vector form for a MDOF system

$\bar{\mathbf{F}}$: external excitation force amplitude in complex form

g_k : nonlinear internal force at k^{th} DOF

p_{kj} : nonlinear internal reaction force between DOF k and DOF j

$\bar{P}_{kj}$: amplitude of g_{kj} in complex form

$\mathbf{g}$: nonlinear internal reaction force vector

$\mathbf{G}_S^n$: amplitude of the n^{th} sine harmonic term of the nonlinear interaction force vector

$\mathbf{G}_C^n$: amplitude of the n^{th} cosine harmonic term of the nonlinear interaction force vector

T: excitation period

ω : excitation frequency

ω_r : r^{th} natural frequency

$\mathbf{\Omega}$: eigenvalue matrix

$\boldsymbol{\psi}_r$: r^{th} eigenvector

$\boldsymbol{\psi}_X, \boldsymbol{\psi}_A$: eigenvectors derived from experimental and analytical models respectively

$\boldsymbol{\Psi}$: eigenvector matrix

$\mathbf{H}(\omega)$: Frequency Response Function matrix

$\mathbf{Z}(\omega)$: dynamic stiffness matrix

N: total number of harmonic terms included in the Fourier series expansion

v_{kj}: describing function that links DOF k and DOF j

$[\boldsymbol{\Delta}]$: generalised quasi-linear matrix comprising describing functions

${}_A[\ ], {}_B[\ ]$: corresponding matrices or vectors related to component A and B, respectively

$[\ ]_i, [\ ]_c$: corresponding matrices or vectors related to internal and connecting DOFs, respectively

$\{\ \}^n$: n^{th} harmonic component

$[\ ]_{\text{nln}}$: parameters related to nonlinear DOFs

$[\ ]_{\text{nln\_r}}$: parameters related to retained linear DOFs

$[\ ]_{\text{nln\_d}}$: parameters related to discarded linear DOFs

$\boldsymbol{R}_1, \boldsymbol{R}_2, \boldsymbol{R}_3, \boldsymbol{R}_4$: 4th order Runge-Kutta parameters

In the joint description

F: external force

N: normal clamping force at the frictional interface

μ: dynamic friction coefficient

k_1, k_2, k_3: first, second and third order stiffness factors

In the experiment

v: voltage input to the shaker's coil

$\bar{V}^n$: amplitude of the n^{th} harmonic component of the voltage in complex form

$\{\ \}^{(n)}$: number of iterations

Abbreviations

AMB:	Active Magnetic Bearing
CAD:	Computer Aided Design
CMS:	Component Mode Synthesis
CPU:	Central Processing Unit
DOF:	Degree of Freedom
FE:	Finite Element
FEM:	Finite Element Method
FFT:	Fast Fourier Transform
FRF:	Frequency Response Function
HBM:	Harmonic Balance Method
LDV:	Laser Doppler Vibrometer
MAC:	Modal Assurance Criteria
MDOF:	Multi-Degree of Freedom
NBS:	Nonlinear Bearing Support
NFD:	Natural Frequency Difference
SDOF:	Single Degree of Freedom

Chapter 1

Introduction

1.1 Introduction to the Problem

Structural models are used in the field of engineering to study and predict the behaviour of real structures. Our ancestors have already known how to use physical, scaled-down models to assure themselves of the structural soundness before they started to construct those magnificent buildings that still stand firmly today. 'Model' is a very general term. It is referred to as a physical or an abstract representation of another object that is difficult to be directly applied analysis on; as an alternative, a model which bears the resemblance to the object in one or a few aspects is created to undertake those analyses. In the field of engineering, we have long passed the time when physical models were the only choice to assess the behaviour of an object. Of course, physical models are still very useful tools in engineering for their directness and visual impact. In this thesis, the name 'model' refers to the abstract type, unless it is stated otherwise. The abstract model is normally presented in the form of a set of variables and a set of logical and quantitative relationships between those variables. It is usually written in mathematical forms, so it is also known as the mathematical model.

Mathematical models are widely used in structural dynamic modelling. They are often used at the design stage of a product, during which frequent modifications

take place to optimise its performance. For a long time, physical modifications on the products were the only choice, and these are made mainly based on experience, if not via a pure trial-and-error approach. Before the final product can be rolled out of the factory floor, many physical alternations to the product and qualification tests have to be done. From the economic point of view, cutting down the time and resources spent on hardware modifications and tests can largely improve the productivity, which is in fact the driving force behind the development of structural modelling techniques in the aerospace and automobile industries.

Structural models also find their potential usage in real-time applications. It is envisaged that in future, machines for example aero-engines, will have more mechatronic systems incorporated. They are implemented to improve monitoring, diagnosis, prognosis and correction capabilities to make machines more reliable and durable. The emphasis on the structural models in these applications is different from those used in the product design. The structural models used in real-time applications need to be, and should remain to be, able to represent the structure accurately throughout its life span. Real-time applications require model processing to be conducted extremely fast. Any response change observed from the measurement at the running condition might be an indication of malfunction. The cause is identified and located from the model processing, and the outcome is quickly used in decision making as what action to be taken. A few European Union funded projects have been carried out to push for more development in this field.

The demand for high-quality structural models and the accompanying processing techniques is growing fast. As a summary, the reasons for such a demand are: firstly, the product development cycle is getting shorter and shorter because of the growing competitiveness in industry, which leads to the need to cut down the time on testing and simulation. Secondly, as products get more complex and delicate, those physical tests, from which useful information is drawn, can be too expensive, so to use more of the analytical model is a cheaper alternative. Thirdly, the fast development in computing technology fuels the idea that experiments and tests might one day be totally replaced by analytical simulation as long as we keep on pushing the boundary and make full use of the computing

power we can get. Last but not least, analytical models are increasingly used in real-time and more critical applications, in which both accuracy and efficiency of the model need to be at the highest standard.

The demand is clearly there, so is the challenge: how to construct high-quality structural models that can be efficiently processed to deliver accurate predictions of the dynamic behaviour of complex systems? The following few sections will provide some background information and difficulties that need to be overcome.

1.1.1 Structural Models: Component versus Assembly

The difference between a component and an assembly is the complexity in their constitution. Components tend to have uniformly distributed material properties and simple geometries. An assembly is the combination of at least two component. The modelling and dynamic response prediction techniques for individual structural components have been well developed. Using Finite Element (FE) models and various model validation techniques, we can get very good component models that produce accurate predictions. However, when a similar procedure is extended to a structural assembly, the prediction quality deteriorates quickly, especially so when the number of components in the assembly increases.

There are two possibilities for such deterioration. Firstly, the component models are not accurate enough; certain properties that do not affect the component model hence have not been validated may affect the assembly model. Secondly, which is a more likely situation, the connection mechanism between components has not been represented sufficiently. It is not fair to claim that mechanical joints have all along been neglected in structural modelling. They have indeed been studied quite extensively. The majority of studies treat the joints as isolated entities. Very detailed joint models are constructed trying to explain complex phenomenon at the connecting interface. These models try to provide physical insight, but they are too large to be incorporated into the assembly model for efficient calculations. Those extensive studies indicate that most of the mechanical joints' behaviour is nonlinear, which complicates the whole situation further.

1.1.2 Structural Models: Linear versus Nonlinear

In structural dynamics, most of the models are developed and applied with the assumption of linearity. Strictly speaking this is not true for real practical structures. Lightly or severely, a system displays nonlinearity in one way or another. A proper linearisation process can solve most problems with satisfactory accuracy; however, when the extent of the nonlinearity exceeds the capacity of a linear description, nonlinear techniques must be used. The problem can be solved analytically, which means solving the non-linear differential equations that govern the phenomena to get a closed-form solution. It can also be solved approximately to yield a result that is much more accurate than the case of direct linearisation. The former approach is only applicable when there are few variables, or when the problem can be simplified to be describable with a few variables. The approximate approach is more efficient, because it can work on larger systems and make good use of computing power.

With the approximation approach, the system differential equations are discretised and then processed either in the time domain or the frequency domain. Time-domain methods are more demanding for computational power, but they can provide solutions for any types of response and tend to be more accurate. In contrast, frequency-domain methods can substantially cut down computational cost, but are limited for steady-state solutions only. However, they might serve our purpose just as well. In both product development and many real-time application cases, what matters most is the machine's performance at its normal working condition, i.e. often the steady-state condition. It is also desirable to predict the responses at overload or other extreme conditions, at which the machine still operates continuously. The prediction can be approached with both methods. There are a few frequency-domain based methods available in the literature, which have shown their efficiency with reasonable accuracy on small models, but the application on large models that represent more realistic structures is still not available.

Even though nonlinearity in a structure is an unavoidable fact of life, we should still be able to find ways to work around it. Linearisation is one approach. Another one, which needs yet more exploration, is to make full use of the fact that in most complex structural assemblies, there are only a few noticeably

nonlinear elements, or in other words, the nonlinearity is a localised property in many practical structural assemblies. Normal nonlinear methods treat the whole structure as nonlinear, even if there is only one nonlinear Degree-of-Freedom (DOF) out of thousands of linear ones. Hence, it is valuable to look into the development of better nonlinear dynamic analysis algorithms, which shall fully take the advantage of 'localised' nonlinearity, so as to make the calculation more efficient.

1.1.3 Concluding Remarks on the Problem

Based on the above background information, here is what this thesis wants to achieve:

"To develop and demonstrate a structural modelling strategy that can accurately predict the steady-state dynamic behaviour of a complex and realistic machinery structural assembly."

Realistic machines have the following complexities: flexible components, multiple connecting interfaces and local nonlinearities. All these need to be addressed in order to achieve the target.

1.2 Solution Strategy

A bottom-up process is adopted here as a general approach. It is analogous to a product assembly line: small parts are specified in great detail and made to agreed standards before being checked individually to make sure of the quality. These parts are then joined together to form small sub-assemblies. Each of these sub-assemblies is also checked to make sure that the joining mechanism functions properly. Those small sub-assemblies are in turn linked to each other until the final complex assembly is formed, which, because of the careful and stringent preparation at the fundamental unit level, is expected to be of good quality.

A structural assembly model is made of a collection of component models which are connected to each other via various joint mechanisms. Without accurate component models, it is not possible to have any meaningful prediction results from the final assembly model. So, the first step is to create component models with good accuracy. Finite Element Method (FEM) is most often used to

construct structural component models. Improved computing power means that great detail now can be included in the FE model. The FE model can only be considered accurate and useful after it is validated. Model validation is the process of demonstrating or attaining the condition that the coefficients in a model are sufficiently accurate to enable that model to provide an acceptably correct description of the subject structure's dynamic behaviour [1]. Model validation is achieved via model updating, which is the process of correcting the numerical values of individual parameters in the mathematical model using experimental data. This is a well studied subject, and this thesis will focus more on the application side of it.

The next step focuses on mechanical joint modelling, and how it is best represented in the assembly model. Mechanical joints come with many different forms of configuration and a detailed study of each can be a daunting task. It is also well known that some of the most common types of joint, for example friction joints, are notoriously complicated, and even the exact physics of them is yet to be understood fully. From the whole assembly point of view, a simplified representation is the only feasible way to incorporate joints into an assembly model. Simplification does not necessarily lead to erroneous prediction results; rather, the predicted results for the whole assembly may be of acceptable quality at certain specific operating conditions with limited range of frequency.

Many joint connections can be considered as linear at normal working conditions. Some researchers have shown that joints can actually be modelled in the same way as other structural components, in the form of spring-damper or spring-mass-damper matrices. Direct construction of such matrices for a real assembly can be tedious; it is, from the application point of view, much more convenient and possibly more accurate to model the joints using FEM. Of course, the properties of the joint elements must be validated, preferably against test data. It is a more tricky business when a linear description is not enough to describe the joint behaviour, e.g. the behaviour at more extreme working conditions. Formulae are available for most types of joints, but generalisation is difficult, and each case has to be treated individually. Measurements on the joint itself must be carried out to derive a specific nonlinear model for the joint.

The third step, with individual component and joint models ready, is to construct the assembly model. If the joint is considered to be linear and represented with a validated FE model, this task can be easily accomplished in any FE software package by simply joining all the individual models together. If the joint is nonlinear, the calculation will be more complicated and time-consuming. This project will focus on nonlinear analysis in the frequency domain, i.e. focusing on steady-state solutions. The Harmonic Balance Method has shown its potential in dealing with large nonlinear systems. It will be further developed, combining with the fact that nonlinearity is a localised property in most practical structures, to locate the steady-state solutions more efficiently.

The final step is to design a rig and conduct tests on it to validate the whole modelling process. Theories and methods can be useless if they can not be validated against tests, no matter how beautifully they are presented; hence the test rig design is considered as important as the theory development. Bearing in mind that the modelling strategy is meant for complex practical structures, the test rig must contain some key features: complex configuration, close to practical structures, prominent and measurable nonlinearity. In real machines, nonlinearity normally occurs at extreme operation or malfunction conditions. This is quite difficult to achieve safely in a laboratory environment, so a purpose built-in nonlinearity is required. As a result, a simplified aero engine model was developed, which consists of the key structural components of a real engine: casing, rotor, shaft and bearing supports. In addition, a significant nonlinearity is embedded in one of its bearing supports.

1.3 Summary of the Thesis

The thesis is arranged in the same way as how this complex problem is tackled. Figure 1 - 1 presents a flowchart showing the interrelations between different chapters. The arrows indicate how the information flows.

Chapter 1 presents the problem of structural dynamic modelling of complex structures with nonlinearity. Background information is introduced to show the importance of tackling such problems. The solution strategy is laid out as a guideline for the whole thesis work.

Chapter 2 talks about linear structural component and assembly modelling techniques. It is very important to get the component model right before we take on a more complex assembly model. Different types of model representations, model updating methods and structural coupling methods are reviewed.

Chapter 3 is dedicated to mechanical joints. As the integral parts of the structural assembly, mechanical joints are often not represented sufficiently, even though they are the prime sources of uncertainties. Different types of mechanical joints are reviewed, showing the richness of the nonlinear behaviour that very often we do not include in linear structural modelling.

Chapter 4 shows how steady-state solutions are achieved by both time-domain methods and frequency-domain methods for a nonlinear system. One nonlinear model is used for demonstration. The special nonlinearity resembles the stiffness pattern of a buckled beam. Frequency-domain methods, in particular the Harmonic Balance Method, are elaborated in detail. Multiple steady-state solutions at one frequency point are observed. The Harmonic Balance Method is verified by the time-domain simulation of the same system.

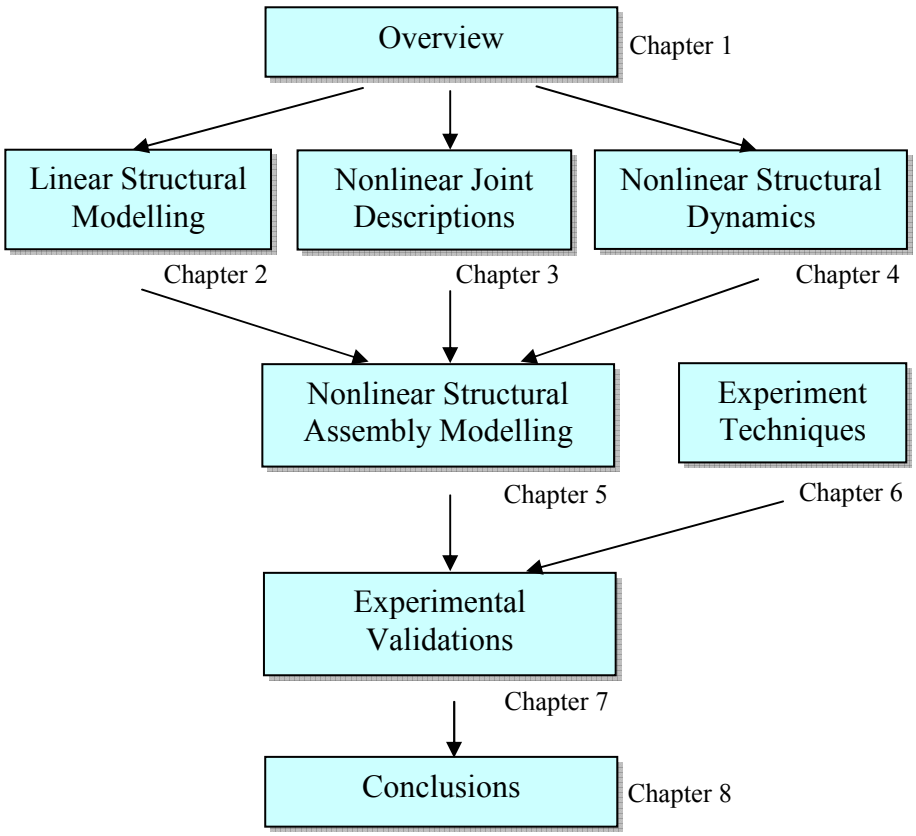

Figure 1 - 1 Organisation of the thesis

Chapter 5 takes in the knowledge from the previous three chapters, and introduces an efficient calculation algorithm that makes use of the Frequency Response Function (FRF) models of the linear components and the Harmonic Balance Method to predict the steady-state response of a complex structure with localised nonlinearity. The efficiency of such an algorithm is demonstrated by the comparison with a time-domain calculation carried out on the same assembly model.

Chapter 6 is devoted to experiment-related topics. Experiments serve two purposes here. Firstly, they are required to ensure the quality of component models and joint models, and this is done through the model validation process. Secondly, they are required to verify that the calculation algorithm introduced in Chapter 5 produces good prediction results. Different types of dynamic test and setup are discussed, emphasising two issues: good experimental practice and choosing the right setup according to the specific purpose. In order to dynamically measure the nonlinear effects accurately, a LabVIEW-based code has been developed to control force input to the structure and to calculate the required FRFs under specified input conditions.

Chapter 7 shows the construction of the test rig that is designed to demonstrate and evaluate the proper routines for achieving a good assembly model. Individual components are validated and linear joint parameters are identified. Both cases show the improvement in the prediction of the dynamic behaviour. Finally, a series of nonlinear dynamic tests are carried out on the whole test rig. A very close match between the prediction and experiment is reported.

Chapter 8 draws conclusions from the whole work and indicates the further development required.

Chapter 2

Linear Structural Modelling

2.1 Introduction

Most of the structural dynamic analyses are carried out with the assumption of linearity in structure's behaviour, even though nonlinearity is the underlying actuality. Such an assumption can be justified on the ground that it produces acceptably accurate solutions and at the same time simplifies the model processing. Creating good and reliable linear structural models is not a trivial task, and this chapter is dedicated to this task with a good look at what has been done in the past.

In this chapter, fundamental structural modelling techniques are discussed, trying to lay the foundation for the following more advanced analysis that relates to nonlinear structures. The concept of Finite Element Method (FEM), model validation and structural coupling are touched upon.

2.2 Linear Structural Component Modelling

Analytical modelling of a complex structure is a bottom-up process, in the same way as the counterpart physical model being constructed. Individual components are first specified with suitable representation and with enough accuracy. They are then linked to form the final assembly. It is important to make sure that the

analytical models at the component level are correct before trying to model the whole assembly.

In this section, different types of mathematical representation of a structural model are presented. Each type has its pros and cons and the choice is pretty much depended on the application.

2.2.1 Spatial Model

The first option of a structural model is derived from the structure's most tangible physical properties: its mass, elasticity and energy dissipation mechanisms. Although the resultant description of the model is somewhat abstract, in the form of matrices, it is closely linked to the geometric information of the structure. This is where the name Spatial Model originates. In the following a few paragraphs, we will show how the system matrices are derived, which, though very basic in concept, is the foundation of structural modelling.

The simplest Spatial Model consists of a single mass, spring and damper that form a so-called Single Degree of Freedom (SDOF) model. This model is usually inadequate in describing engineering structure with flexibilities. Both rigid body motion and deformation of the structure itself are important for a better understanding of the performance of the structure under dynamic loading. The deformation shape as well as its amplitude can only be described with more than one displacement coordinate, which is in the form of a set of discrete points along the structure. In principle, these points may be located anywhere, but in practice, they should be associated with specific features of the physical properties which may be significant and should be distributed accordingly so as to provide a good definition of the deflected shape [2]. This results in a Multi-Degree of Freedom (MDOF) model.

The MDOF structural model is derived from the equation of motion, which is formulated by expressing the equilibrium of the effective forces associated with each of its degree of freedom. In linear structural dynamics, four types of force are active at any DOF i: externally applied load f_i, inertial force f_{Ii}, damping force f_{Di} and elastic force f_{Si}. The dynamic equilibrium may be expressed as:

$$f_{Ii} + f_{Di} + f_{Si} = f_i(t) \tag{2.1}$$

When all the DOFs are counted at the same time, forces are represented in vector form for the MDOF system as:

$$\{\mathbf{f}_I\}+\{\mathbf{f}_D\}+\{\mathbf{f}_S\}=\{\mathbf{f}(t)\} \tag{2.2}$$

Each of the resistance forces is expressed most conveniently by means of an appropriate set of influence coefficients. As shown in equation (2.3), the elastic force at DOF i, f_{Si}, is a linear combination of the deformation at all the DOFs weighted by the corresponding coefficient k_{ij}, which is called stiffness influence coefficient.

$$\begin{Bmatrix} f_{S1} \\ f_{S2} \\ \vdots \\ f_{Si} \\ \vdots \\ f_{SN} \end{Bmatrix} = \begin{bmatrix} k_{11} & k_{12} & \cdots & k_{1i} & \cdots & k_{1N} \\ k_{21} & k_{22} & \cdots & k_{2i} & \cdots & k_{2N} \\ \vdots & \vdots & \ddots & \vdots & \ddots & \vdots \\ k_{i1} & k_{i2} & \cdots & k_{ii} & \cdots & k_{iN} \\ \vdots & \vdots & \ddots & \vdots & \ddots & \vdots \\ k_{N1} & k_{N2} & \cdots & k_{N1} & \cdots & k_{NN} \end{bmatrix} \begin{Bmatrix} u_1 \\ u_2 \\ \vdots \\ u_i \\ \vdots \\ u_N \end{Bmatrix} \tag{2.3}$$

More concisely, the above equation can be expressed in matrix form:

$$\{\mathbf{f}_S\}=[\mathbf{K}]\{\mathbf{u}\} \tag{2.4}$$

in which **[K]** is the $N\times N$ stiffness matrix, and $\{\mathbf{u}\}$ is the displacement vector representing the deformation shape of the structure.

Physically, the stiffness coefficients represent the forces developed in the structure when a unit displacement corresponding to one DOF is introduced and no other nodal displacements are permitted. The system stiffness matrix can be derived using this definition. However in practice the Finite Element (FE) concept, which will be discussed in more detail in a later section, provides the most convenient means for this task. In FEM, the structure is divided into a set of discrete elements, which are interconnected at nodal points. The stiffness coefficients of a typical element are calculated and the stiffness matrix of the whole system can be obtained by adding the element stiffness coefficients with consideration of the connectivity at those nodal points.

Damping is a trickier system property to model, because the physics of it is still not fully understood. Normally it is assumed that only viscous-type damping

exists in the concerned structure. In the same way as for the elastic forces, the damping force at a certain DOF is the linear combination of damping effects at all the DOFs, and this is expressed in equation (2.5).

$$\begin{Bmatrix} f_{D1} \\ f_{D2} \\ \vdots \\ f_{Di} \\ \vdots \\ f_{DN} \end{Bmatrix} = \begin{bmatrix} c_{11} & c_{12} & \cdots & c_{1i} & \cdots & c_{1N} \\ c_{21} & c_{22} & \cdots & c_{2i} & \cdots & c_{2N} \\ \vdots & \vdots & \ddots & \vdots & \ddots & \vdots \\ c_{i1} & c_{i2} & \cdots & c_{ii} & \cdots & c_{iN} \\ \vdots & \vdots & \ddots & \vdots & \ddots & \vdots \\ c_{N1} & c_{N2} & \cdots & c_{N1} & \cdots & c_{NN} \end{bmatrix} \begin{Bmatrix} \dot{u}_1 \\ \dot{u}_2 \\ \vdots \\ \dot{u}_i \\ \vdots \\ \dot{u}_N \end{Bmatrix} \tag{2.5}$$

In a more concise form:

$$\{\mathbf{f}_D\} = [\mathbf{C}]\{\dot{\mathbf{u}}\} \tag{2.6}$$

in which **[C]** is the $N \times N$ viscous damping matrix.

The mass matrix is defined in the similar way as shown in equation (2.7) and (2.8).

$$\begin{Bmatrix} f_{I1} \\ f_{I2} \\ \vdots \\ f_{Ii} \\ \vdots \\ f_{IN} \end{Bmatrix} = \begin{bmatrix} m_{11} & m_{12} & \cdots & m_{1i} & \cdots & m_{1N} \\ m_{21} & m_{22} & \cdots & m_{2i} & \cdots & m_{2N} \\ \vdots & \vdots & \ddots & \vdots & \ddots & \vdots \\ m_{i1} & m_{i2} & \cdots & m_{ii} & \cdots & m_{iN} \\ \vdots & \vdots & \ddots & \vdots & \ddots & \vdots \\ m_{N1} & m_{N2} & \cdots & m_{N1} & \cdots & m_{NN} \end{bmatrix} \begin{Bmatrix} \ddot{u}_1 \\ \ddot{u}_2 \\ \vdots \\ \ddot{u}_i \\ \vdots \\ \ddot{u}_N \end{Bmatrix} \tag{2.7}$$

$$\{\mathbf{f}_I\} = [\mathbf{M}]\{\ddot{\mathbf{u}}\} \tag{2.8}$$

All the off-diagonal items in the above mass matrix are zero if they are derived with the assumption that the element mass is concentrated at those nodal points and only translational degrees of freedom are used to describe the motion. The distribution of the element masses to those nodal points is determined by statics principles. The total mass concentrated at any node is the sum of the contribution from all the elements attached to the nodal point. The mass matrix created in this way is called Lumped Mass Matrix. The diagonal form of the mass matrix largely reduces the computation cost, as demonstrated in classical Modal Analysis [1]. For a refined and more realistic description of the mass distribution, the FE concept can also be applied to the derivation of the mass matrix, in the

same way as the stiffness matrix, in which appropriate shape functions are put into use.

Substituting equations (2.4), (2.6) and (2.8) into (2.2), we have the fundamental system equation that governs the dynamic behaviour of the modelled structure.

$$[\mathbf{M}]\{\ddot{\mathbf{u}}\}+[\mathbf{C}]\{\dot{\mathbf{u}}\}+[\mathbf{K}]\{\mathbf{u}\}=\{\mathbf{f}\} \tag{2.9}$$

Mathematically, equation (2.9) represents a coupled system of linear second order ordinary differential equations. The matrices **[M], [C]** and **[K]** represent the Spatial model of the structure.

2.2.2 Modal Model

Without any external excitation each structure's dynamic behaviour is unique and can be described by a set of natural frequencies and the corresponding vibration mode shapes. Both sets of values can be derived from the calculation of the steady-state solution of equation (2.9) when $\{\mathbf{f}\}=\{\mathbf{0}\}$. For demonstration purposes, the damping matrix $[\mathbf{C}]$ is set at $[\mathbf{0}]$.

It can be assumed that $\{\mathbf{u}\}=\{\mathbf{U}\}e^{i\omega t}$ when the structure is vibrating naturally, in which $\{\mathbf{U}\}$ is the $N\times 1$ vector of time-independent amplitudes of the response. Rearranging equation (2.9):

$$\left[\mathbf{K}-\omega^2\mathbf{M}\right]\{\mathbf{U}\}e^{i\omega t}=\mathbf{0} \tag{2.10}$$

The only non-trivial solutions are those which satisfy:

$$\det\left|\mathbf{K}-\omega^2\mathbf{M}\right|=0 \tag{2.11}$$

The solution of this equation is N values of ω^2, the undamped system's natural frequencies. Substituting each of the natural frequencies back into equation (2.10) yields a corresponding set of relative values of response amplitudes $\{\boldsymbol{\psi}_r\}$, the so-called mode shape corresponding to that natural frequency [1]. In mathematical expression, these two sets of values are represented in matrix form as:

$$\boldsymbol{\Omega} = \begin{bmatrix} \omega_1^2 & \cdots & 0 \\ \vdots & \ddots & \vdots \\ 0 & \cdots & \omega_N^2 \end{bmatrix} \qquad \boldsymbol{\Psi} = \begin{bmatrix} \{\boldsymbol{\psi}_1\} & \cdots & \{\boldsymbol{\psi}_r\} & \cdots & \{\boldsymbol{\psi}_N\} \end{bmatrix} \tag{2.12}$$

They are called eigenvalues and eigenvectors respectively, and form the Modal model of a structure.

2.2.3 Response Model

As the name itself indicates, this type of model describes how a structure responds under a given excitation. On the surface, the response depends not only on the structure's inherent properties but also on the amplitude of the imposed excitation. However, it is found that for linear structures specifically, the ratio between the response and excitation is unique to the structure under study. It can also be derived analytically from the system equation (2.9) by substituting $\{\mathbf{u}\} = \{\mathbf{U}\}e^{i\omega t}$ and $\{\mathbf{f}\} = \{\mathbf{F}\}e^{i\omega t}$ into it. Setting $[\mathbf{C}] = [\mathbf{0}]$ and rearranging the equation into:

$$\{\mathbf{U}\} = \left[\mathbf{K} - \omega^2\mathbf{M}\right]^{-1}\{\mathbf{F}\} = \left[\mathbf{H}(\omega)\right]\{\mathbf{F}\} \tag{2.13}$$

in which $\left[\mathbf{H}(\omega)\right]$ is the so-called Receptance matrix of the system with the size of $N \times N$ and is a representation of the Response model. Each entry of the Receptance matrix is defined as:

$$H_{jk}(\omega) = \left(\frac{U_j}{F_k}\right) \tag{2.14}$$

The response U_j is a displacement; it can also be in the form of velocity or acceleration. The ratio between the response and the external excitation is known as the Frequency Response Function (FRF). In this thesis, $\left[\mathbf{H}(\omega)\right]$ will be referred to as the FRF matrix.

2.2.4 Finite Element Method

The Finite Element Method (FEM) is a modelling and numerical analysis technique for obtaining approximate solutions to a wide variety of engineering problems. In the field of structural dynamics, it involves creating a mathematical

model of a material or design that is stressed and analysed to assess its dynamic properties. It is a well-developed method and is widely used in industry in the process of new product design, refinement of existing products, etc. FEM is being discussed here because it provides a vigorous mathematical foundation, as well as a physical interpretation of the application of the Spatial model. In addition, the dynamic analysis of complex structures nowadays relies on the FEM to generate the Spatial model for further processing.

The label *Finite Element Method* first appeared in a paper on plane elasticity problems by Clough [3] in 1960, but the ideas of finite element analysis date back much further into 1940s, and were developed independently across different scientific communities with different purposes and prospects. In the engineering community, this method was originated from physical intuition that a continuum structure could be analogised with a truss problem by dividing the structure into elements or structural sections interconnected at only a finite number of node points [4]. More developments followed, which concentrated on finding improved ways to discretise the structure to yield better results [5]. This method only took off seriously in the late 1950s when automatic digital computation emerged and opened the way to the numerical solution of complex problems, which had previously been hindered by the amount of numerical calculations involved. Engineers began to recognise the efficacy of the Finite Element Method, and it has been receiving widespread acceptance ever since. This was further fuelled by the advancement in Personal Computer and the introduction of many commercial software packages that are developed based on the concept of FEM, notably a few big names: ABAQUS®, MSC/NASTRAN® and ANSYS®, which is used in the modelling work in this thesis.

Regardless of which software package being used, the solution of a continuum problem by the Finite Element Method always follows an orderly step-by-step process as described in [5]:

1. *Discretise the continuum*
2. *Select interpolation equation*
3. *Define element properties*
4. *Assemble element properties to obtain the system equations*

5. *Impose the boundary conditions*
6. *Solve the system equations*
7. *Make additional computation if required*

The modern FEM software packages make Finite Element Analysis a relatively easy task compared with twenty years ago; however, by no means does this imply that the requirement for the user to understand FEM is of any less importance. Computer Aided Design (CAD) is now integrated in the FEM software package, which allows the analysis of structures with complex geometries. The discretisation is accomplished by defining a mesh density or mesh size along a line, surface or solid, and the software will automatically fill the continuum with elements. The user is responsible for choosing the most suitable element type, which governs the interpolation equations to be applied by the software, as well as the final system assembly equation that represents the structural model. Material properties, boundary and loading conditions, numerical algorithms and results presentation format need to be defined before engaging the software into computation.

FEM is today still the dominant method for obtaining approximate solutions of many engineering problems, and its development is still a hot topic in both research and industry fields. Efforts made in improving iterative solvers and error indicators, implementing special-purpose elements and applying meshless formations can be found in many commercial software packages [5].

2.2.5 Remarks on Different Types of Linear Structural Models

Spatial, Modal and Response models of the same structural component are interrelated. It is possible to progress from the Spatial model through to a Response model with the application of FEM and solving the constitutional equations either in the frequency domain or in the time domain. It is also possible to carry out an analysis in the reverse direction – to derive Modal and Spatial models from the Response properties, which are normally obtained from vibration tests. The interdependence of these three representations of a structural component forms the linkage between test and simulation.

The Modal model is the most concise one among the three in terms of the amount of information it carries. It contains only the key information of a

structure's dynamic properties as far as the steady-state solution is concerned. Because of this, Modal properties are most often used to compare the likeness of the analytical model and experimental model of the same structure. This topic will be further explored in the next section.

2.3 Model Validation

The purpose of creating analytical models is economically driven. It is meant to reduce the design cycle time, and cut down the capital spending on fabrication and testing of prototypes. However, if the analytical model has not been validated, there will be no assurance to confirm that it can reliably represent the real structure and be used in further design stages. From the structural dynamics point of view, the validated analytical model should be able to predict the dynamic behaviour of the structure at the experiment condition. It should also be able to predict, with certain accuracy, the dynamic properties of the structure in situations different to those in which the experiment was undertaken [6]. To achieve this, the first step is to make a direct and objective comparison of specific dynamic properties, measured versus predicted. This is followed by making adjustments or modifications to one set of results, normally the predicted one, to bring them closer to each other. When this is achieved, the analytical model can be said to have been validated an is fit to be used for further analysis [7].

Up to this point, we can define model validation as a process of determining and attaining the 'correct' parameters of an analytical model so that it can provide an acceptably correct description of the real structure's dynamic behaviour. It is a process that should be performed at every stage of the modelling of a complex structure. It should start from the component level, and this is the reason for it being discussed here.

2.3.1 Model Correlation

The simulation results from the analytical model need to be compared with experimental data of the same structure to assess its suitability for further process. The discrepancies between these two sets of data may be quantified and used as a reference to modify the analytical model. The whole business about

assessing the likeness between the analytical and experimental models of the same structure is referred to as model correlation.

As far as the dynamic properties are concerned, natural frequencies, mode shapes and response properties are used for comparison.

2.3.1.1 Comparison of natural frequencies

The most obvious comparison to make is the measured versus the predicted natural frequencies. It is not a process as straightforward as it seems, because in many cases it is not correct to compare directly the modes that are identified in experiment and prediction in the same sequential order. The reasons are: firstly, there are modes that are only registered in either experiment or prediction; secondly, there are modes which have very close natural frequencies though they have totally different vibration patterns. Therefore, it is essential to identify associated mode pairs before comparing the corresponding natural frequencies. The association between experimental and predicted modes is based on the degree of similarity of the vibration patterns of the compared mode pairs.

The result of the comparison is represented in the form of Natural Frequency Difference (NFD), which is normally taken percentage-wise and used as a reference for model updating.

2.3.1.2 Comparison of mode shapes

It is stated in the previous section that comparing the natural frequencies alone is not enough, unless of course the structure is very simple and all the modes are well separated. Otherwise we need to perform a comparison of the mode shapes that are derived from experiment and prediction. Mode shapes describe the relative position of selected points on a structure for a given vibration mode. Each vibration mode has its unique mode shape, and if the structure is linear the mass normalised mode shapes are supposed to be orthogonal to each other. This leads to the concept of Modal Assurance Criterion (MAC), which quantifies the likeness of a pair of mode shapes. It is defined as:

$$\mathrm{MAC}(A,X)=\frac{\left|\sum_{j=1}^{n}\{\psi_X\}_j\{\psi_A\}_j^*\right|^2}{\left(\sum_{j=1}^{n}\{\psi_A\}_j\{\psi_A\}_j^*\right)\bullet\left(\sum_{j=1}^{n}\{\psi_X\}_j\{\psi_X\}_j^*\right)} \tag{2.15}$$

in which $\{\psi_X\}$ and $\{\psi_A\}$ are the mode shapes derived from the experiment and analytical models, respectively. The same equation can be expressed more concisely in the vector operation form:

$$\mathrm{MAC}(A,X)=\frac{\left|[\psi_X]^T[\psi_A]\right|^2}{\left([\psi_A]^T[\psi_A]\right)\bullet\left([\psi_X]^T[\psi_X]\right)} \tag{2.16}$$

It is found that in general a value of MAC in excess of 0.9 should be attained for well-correlated modes while a value of less than 0.1 indicates uncorrelated modes.

2.3.1.3 Comparison of responses

Ideally, comparing the time histories of the response makes the most sense, because the raw data from an experiment is presented in time domain, and fundamentally the analytical model is meant to predict the response at any point of time under any sort of excitation. However, it is actually a very difficult task to accomplish, mainly because calculation in time domain is very time consuming, even for a moderate size structural model.

The Frequency Response Function (FRF), normally the amplitude of it at every frequency point, is another form of response data that can be used for comparison. Calculation of FRFs is not a problem for analytical models of a linear structure, because the symmetric property of the system matrices heavily cuts down the calculation time. On the experimental side, time-domain data can be converted into the frequency domain and form the corresponding FRFs, but depending on the types of experiment conducted, FRFs may not be of perfect quality over the entire frequency range. For example, in the popular impact test, signal-to-noise ratios tend to be poor, and this will affect more on the FRFs at non-resonant frequencies. FRF comparisons in those regions showing big difference will not necessarily be an indication of a poor match between

analytical and experiment models. Signal-to-noise ratios can be improved if other types of experiment are carried out, e.g. sine sweep test etc. Another difficulty in FRF comparison is that FRFs are very sensitive to geometric information, more specifically, to the exact location of excitation and response. It is found that two FRFs relating to two response points that are very close to each other on the same structure can be very different [7].

In nonlinear structural modelling, FRFs can be the only feasible choice for comparison to assess the dynamic properties. As we shall see in future chapters that even for a weak nonlinearity, the FRFs are distorted considerably, while in the time domain, the distortion may be hard to notice or in any way deemed to be meaningful.

2.3.2 Model Updating

After the model correlation, if the discrepancies are small and within the error margin due to the limitations in the construction of analytical model and experiments conducted on the physical structure, the analytical model can be passed as suitable for further processing, e.g. joining to other analytical models to form an assembly. Otherwise, some adjustment has to be made in order to bring the analytical model closer to the experimental one. This process is called model updating. This subject has become a very extensive one, with already one textbook [8] and several hundred papers devoted to its details [9]. Some of the concepts and methods have been well developed and applied successfully in many cases. This section is more meant to show the importance of model updating, and how it is employed in the process of achieving good assembly model in the end.

Broadly speaking, there are two types of model updating methods. The first one is called the Direct Matrix Method, in which the individual elements of the system matrices **M**, **C** and **K** are adjusted directly according to the comparison between the test data and analytical model prediction. This type of method has the advantage of being computationally straightforward and can be very efficient in matching closely the dynamic properties. However, physical interpretations can hardly be drawn from the direct matrices adjustment. The other type of method, generally called Indirect Method, is where the physical properties of the

model are adjusted instead. The physical properties can be material-related, e.g. density and Young's modulus, or geometry-related. Change of these properties will indirectly change the system matrices, so is the prediction result. This type of method gives more physical sense to the analytical models that need to be updated.

Throughout these years there are many algorithms proposed to implement the concept of model updating. Very detailed surveys can be found in the following references [6, 10, 11]. One of the most popular methods is summarised here, which is also applied in this thesis for updating component models.

2.3.2.1 Inverse eigensensitivity method

This method is one type of the Indirect Method approach. Its calculation is based on the initial dynamic properties of the model and the first order sensitivity function of those properties. The fully-fledged mathematical derivation is very lengthy. A simplified version, which is sufficient for updating simple component models, is presented here.

This method attempts to minimise the discrepancy between corresponding pairs of natural frequencies, also known as eigenvalues, from the experiment and analytical model prediction. The following penalty function is normally used, assuming only one parameter p is updated:

$$J(p) = \sum_{i=1}^{m} \left(\left(\omega_A\right)_i - \left(\omega_X\right)_i \right)^2 \tag{2.17}$$

where $\left(\omega_A\right)_i$ and $\left(\omega_X\right)_i$ are the i^{th} corresponding analytical and experimental eigenvalues, while $J(p)$ is a function of updating parameter p. Using Taylor series to expand the above equation and truncate those items of second order and above, we will have:

$$J(p) \cong \sum_{i=1}^{m} \left(\left(\omega_A\right)_i \Big|_{p=p_0} + \frac{\partial \left(\omega_A\right)_i}{\partial p} \delta p - \left(\omega_X\right)_i \right)^2 \tag{2.18}$$

where, p_0 is the initial value of the updating parameter, and δp is the increment of the updating parameter, which will be decided during the updating process. A

minimum value of J can be achieved if we partial-differentiate the above equation with respect to δp and set the new equation equal to 0:

$$\frac{\partial J}{\partial(\delta p)} \cong \sum_{i=1}^{m} 2\times\left((\omega_A)_i \Big|_{p=p_0} + \frac{\partial(\omega_A)_i}{\partial p}\delta p - (\omega_X)_i \right)\frac{\partial(\omega_A)_i}{\partial p} = 0 \qquad (2.19)$$

Further simplifying the above equation, we will have:

$$\frac{\partial(\omega_A)_i}{\partial p}\delta p = (\omega_X)_i - (\omega_A)_i \qquad (2.20)$$

Considering all the mode pairs we can write the above equation in matrix form:

$$[\mathbf{S}_\omega]\{\delta\mathbf{p}\} = \{\mathbf{R}_\omega\} \qquad (2.21)$$

In which $[\mathbf{S}_\omega]$ is called the sensitivity matrix of the eigenvalues with respect to the updating parameter. $\{\mathbf{R}_\omega\} = \{\mathbf{\Omega}_X\} - \{\mathbf{\Omega}_A\}$ is the residual vector between the experiment eigenvalues and the predicted ones. To derive the unknown $\{\delta\mathbf{p}\}$, the sensitivity matrix needs to be inverted. This is where the name for this kind of methods is derived. Eigenvalues are usually non-linear functions with respect to almost all kinds of updating parameter [6]; hence equation (2.21) can only be solved iteratively.

2.3.3 Remarks on Model Validation

Model validation is an extensive topic and still in the course of development. This section presents the philosophical background of this topic and is meant to raise the awareness that model validation is an essential part of structural dynamic modelling, even though it may seem tedious and in certain cases rather additional to an already adequate model. As the Finite Element Method, computing power and operator's modelling skills get improved continuously, we can now sometimes make an analytical model that matches the experiment close enough to achieve the required accuracy in prediction without any adjustment, but at what kind of confidence level can we safely take in an analytical model without any experimental validation? There have not been any rules that can reliably answer this question. Model validation is still the safest and yet necessary step in every stage of structural dynamic modelling.

Model validation must start at the component level. The argument is always the same: without accurate component models, we will not feel confident in the final assembly model. A case study of component model validation will be shown in Chapter Seven, in which a cylindrical casing model has been improved by applying Inverse Eigensesitivity method upon the experimental result.

Last but not least, a meaningful and successful model validation relies on good experiment practice. This topic will be touched upon in Chapter Six.

2.4 Linear Structural Coupling Techniques

After the component models have been properly validated, the next step is to join them together to form an assembly, and this falls into another large topic in structural dynamics: structural coupling. It is also sometimes known as substructure analysis. This branch of structural dynamic analysis originated during the time when computing power was still limited and the demand for modelling of more complex structure was growing. It was known that for an N degree-of-freedom system, the CPU effort for an eigensolution is approximately proportional to N^3. Therefore if the system is subdivided into two equal subsystems the solution time may be expected to be reduced by a factor of 4 [12]. Therefore, lots of effort was devoted to developing new techniques to take advantage of such properties to improve the computation efficiency.

Besides time saving, there are other advantages that attributes to the fast development in this field. Firstly, the problem of modelling a complex structure can be greatly simplified by dividing the structure into substructures where each substructure can be better represented by a smaller, more accurate and refined mathematical model [13]. Secondly, with proper coupling techniques, it is possible to couple models from different sources, for example to couple an analytical model with experiment model. In today's product development field, complex machines are finely dissected into small segments and each are studied in detail. Modifications tend to be at the very local level. With suitable coupling techniques, the integration between different parts can be operated more smoothly and economically.

Structural coupling is also closely linked to model reduction, a topic in structural dynamics that concentrates on reducing the complexity of the problem definition

while preserving the essential dynamic behaviour. It may be seen as part of the structural coupling process, because in some of the coupling techniques, the size of the substructure is first reduced before they are joined to form the final assembly. How to reduce the size, how to keep the fidelity etc. are the questions to answer in the area of model reduction.

2.4.1 Spatial Coupling

This method is mainly used in theoretical analysis, in which physical spatially-distributed properties of the components are required as the inputs. FE software packages are best for this task. A simple demonstration of this method is shown in the following, as we are trying to get the system matrix of an assembled structure with components A and B. The corresponding mass and stiffness matrices are of the order N_A and N_B respectively, and each is partitioned according to the selected interior and connection DOFs, which are described with the subscription *i* and *c* respectively. The equilibrium equation for component A and B, with damping matrices omitted for clarity, are expressed as:

$$\begin{bmatrix} {}_A\mathbf{M}_{ii} & {}_A\mathbf{M}_{ic} \\ {}_A\mathbf{M}_{ci} & {}_A\mathbf{M}_{cc} \end{bmatrix} \begin{Bmatrix} {}_A\ddot{\mathbf{u}}_i \\ {}_A\ddot{\mathbf{u}}_c \end{Bmatrix} + \begin{bmatrix} {}_A\mathbf{K}_{ii} & {}_A\mathbf{K}_{ic} \\ {}_A\mathbf{K}_{ci} & {}_A\mathbf{K}_{cc} \end{bmatrix} \begin{Bmatrix} {}_A\mathbf{u}_i \\ {}_A\mathbf{u}_c \end{Bmatrix} = \begin{Bmatrix} {}_A\mathbf{0}_i \\ {}_A\mathbf{f}_c \end{Bmatrix} \tag{2.22}$$

$$\begin{bmatrix} {}_B\mathbf{M}_{ii} & {}_B\mathbf{M}_{ic} \\ {}_B\mathbf{M}_{ci} & {}_B\mathbf{M}_{cc} \end{bmatrix} \begin{Bmatrix} {}_B\ddot{\mathbf{u}}_i \\ {}_B\ddot{\mathbf{u}}_c \end{Bmatrix} + \begin{bmatrix} {}_B\mathbf{K}_{ii} & {}_B\mathbf{K}_{ic} \\ {}_B\mathbf{K}_{ci} & {}_B\mathbf{K}_{cc} \end{bmatrix} \begin{Bmatrix} {}_B\mathbf{u}_i \\ {}_B\mathbf{u}_c \end{Bmatrix} = \begin{Bmatrix} {}_B\mathbf{0}_i \\ {}_B\mathbf{f}_c \end{Bmatrix} \tag{2.23}$$

The compatibility and equilibrium equations at the interface of A and B are :

$$\{ {}_A\mathbf{f}_c \} = -\{ {}_B\mathbf{f}_c \} = \{\mathbf{f}_c\} \quad \text{and} \quad \{ {}_A\mathbf{u}_c \} - \{ {}_B\mathbf{u}_c \} = \{\mathbf{0}\} \tag{2.24}$$

The overall system equation can then be derived directly with the total number of DOF being $N_C = N_A + N_B - n_c$, where n_c is the connecting DOFs.

$$\left[{}_C\mathbf{M} \right] = \begin{bmatrix} {}_A\mathbf{M}_{ii} & {}_A\mathbf{M}_{ic} & \mathbf{0} \\ {}_A\mathbf{M}_{ci} & {}_A\mathbf{M}_{cc} + {}_B\mathbf{M}_{cc} & {}_B\mathbf{M}_{ci} \\ \mathbf{0} & {}_B\mathbf{M}_{ic} & {}_B\mathbf{M}_{ii} \end{bmatrix} \tag{2.25}$$

$$\left[{}_C\mathbf{K} \right] = \begin{bmatrix} {}_A\mathbf{K}_{ii} & {}_A\mathbf{K}_{ic} & \mathbf{0} \\ {}_A\mathbf{K}_{ci} & {}_A\mathbf{K}_{cc} + {}_B\mathbf{K}_{cc} & {}_B\mathbf{K}_{ci} \\ \mathbf{0} & {}_B\mathbf{K}_{ic} & {}_B\mathbf{K}_{ii} \end{bmatrix} \tag{2.26}$$

2.4.2 FRF Coupling

There are different formulations for the FRF Coupling method. The basic one makes use of the component models derived directly from FRF data.

$$\left[{}_A\mathbf{H}(\omega)\right]=\begin{bmatrix} {}_A\mathbf{H}_{ii} & {}_A\mathbf{H}_{ic} \\ {}_A\mathbf{H}_{ci} & {}_A\mathbf{H}_{cc} \end{bmatrix} \tag{2.27}$$

$$\left[{}_B\mathbf{H}(\omega)\right]=\begin{bmatrix} {}_B\mathbf{H}_{ii} & {}_B\mathbf{H}_{ic} \\ {}_B\mathbf{H}_{ci} & {}_B\mathbf{H}_{cc} \end{bmatrix} \tag{2.28}$$

With the application of the same boundary conditions as in equation (2.24), the whole system FRF matrix is represented as:

$$\begin{aligned}\left[{}_C\mathbf{H}(\omega)\right]&=\left[\left[{}_A\mathbf{H}(\omega)\right]^{-1}\oplus\left[{}_B\mathbf{H}(\omega)\right]^{-1}\right]^{-1}\\ &=\begin{bmatrix} {}_A\mathbf{Z}_{ii} & {}_A\mathbf{Z}_{ic} & \mathbf{0} \\ {}_A\mathbf{Z}_{ci} & {}_A\mathbf{Z}_{cc}+{}_B\mathbf{Z}_{cc} & {}_B\mathbf{Z}_{ci} \\ \mathbf{0} & {}_B\mathbf{Z}_{ic} & {}_B\mathbf{Z}_{ii} \end{bmatrix}^{-1}\end{aligned} \tag{2.29}$$

in which $\left[\mathbf{Z}(\omega)\right]=\left[\mathbf{H}(\omega)\right]^{-1}$.

The main advantage of FRF Coupling method is that it can use the component Response models derived from experiments directly. Within the frequency range of interest, the input and output relations are truly represented by the FRF matrices. However, as shown in equation (2.29), three matrix inverses are required before the derivation of the system FRF matrix, which, on one hand, requires excessive computation time, and on the other hand, matrices are easily ill-conditioned at the region of natural frequencies, which results in errors after inversion. This problem is more serious for lightly-damped structures. An alternative FRF Coupling method introduced by Jetmundsen et. al. [14] reduces the number of matrix inversions at each frequency point from three to one. In addition, the size of the matrices to be inversed is restricted to the connecting DOFs. The resultant system FRF matrix is expressed as the following:

$$\left[{}_C\mathbf{H}(\omega)\right]=\begin{bmatrix} {}_A\mathbf{H}_{ii} & {}_A\mathbf{H}_{ic} & \mathbf{0} \\ {}_A\mathbf{H}_{ci} & {}_A\mathbf{H}_{cc} & \mathbf{0} \\ \mathbf{0} & \mathbf{0} & {}_B\mathbf{H}_{ii} \end{bmatrix}-\begin{bmatrix} {}_A\mathbf{H}_{ic} \\ {}_A\mathbf{H}_{cc} \\ -{}_B\mathbf{H}_{ic} \end{bmatrix}\left[{}_A\mathbf{H}_{cc}+{}_B\mathbf{H}_{cc}\right]^{-1}\begin{bmatrix} {}_A\mathbf{H}_{ci} \\ {}_A\mathbf{H}_{cc} \\ -{}_B\mathbf{H}_{ci} \end{bmatrix}^{T} \tag{2.30}$$

2.4.3 Modal Coupling

Modal coupling methods are also called Component Mode Synthesis (CMS). The first CMS method was proposed by Hurty [15]. Depending on the boundary conditions applied to the substructure interfaces, the CMS methods can be classified into four groups: fixed interface methods; free interface methods; hybrid interface methods and loaded interface methods. Reviews of these methods can be found in [16] and [17]. The formulation of fixed interface method is summarised here. The dynamic equation at the component level is:

$$\begin{bmatrix} \mathbf{M}_{ii} & \mathbf{M}_{ic} \\ \mathbf{M}_{ci} & \mathbf{M}_{cc} \end{bmatrix} \begin{Bmatrix} \ddot{\mathbf{u}}_i \\ \ddot{\mathbf{u}}_c \end{Bmatrix} + \begin{bmatrix} \mathbf{K}_{ii} & \mathbf{K}_{ic} \\ \mathbf{K}_{ci} & \mathbf{K}_{cc} \end{bmatrix} \begin{Bmatrix} \mathbf{u}_i \\ \mathbf{u}_c \end{Bmatrix} = \begin{Bmatrix} \mathbf{f}_i \\ \mathbf{f}_c \end{Bmatrix} \tag{2.31}$$

It is assumed that the connecting interface is fixed and there is no force applied to all the internal DOFs, i.e. $\{\mathbf{u}_c\} = \{\mathbf{0}\}$ and $\{\mathbf{f}_i\} = \{\mathbf{0}\}$. The corresponding equation of motion becomes:

$$[\mathbf{M}_{ii}]\{\ddot{\mathbf{u}}_i\} + [\mathbf{K}_{ii}]\{\mathbf{u}_i\} = \{\mathbf{0}\} \tag{2.32}$$

This can be solved to deduce eigenvalues $[\mathbf{\Omega}_i]$ and eigenvectors $[\mathbf{\Psi}_i]$ of this fixed interface structure. The internal DOFs can be represented by the linear combination of the known fixed interface modes as:

$$\{\mathbf{u}_i\} = [\mathbf{\Psi}_i]\{\mathbf{p}_i\} \tag{2.33}$$

The displacement of internal DOFs also has the contribution from the connection DOFs, boundary modes or restrained modes as they are normally called. In this case, the relationship is described by Guyan reduction [18]. Hence, a transformation matrix can now be constructed, which is commonly known as Craig-Bampton method:

$$\begin{Bmatrix} \mathbf{u}_i \\ \mathbf{u}_c \end{Bmatrix} = \begin{bmatrix} \mathbf{\Psi}_i & \mathbf{\Psi}^*_{ic} \\ \mathbf{0} & \mathbf{I} \end{bmatrix} \begin{Bmatrix} \mathbf{p}_i \\ \mathbf{u}_c \end{Bmatrix} = [\mathbf{T}] \begin{Bmatrix} \mathbf{p}_i \\ \mathbf{u}_c \end{Bmatrix} \tag{2.34}$$

where $\left[\mathbf{\Psi}^*_{ic}\right]$ is the Guyan transformation matrix and it is defined as:

$$\left[\mathbf{\Psi}^*_{ic}\right] = -[\mathbf{K}_{ii}]^{-1}[\mathbf{K}_{ic}] \tag{2.35}$$

It is common, especially for experimentally derived models where there are only *k* number of modes available, that the above equation still can be used to count for all the physical DOFs:

$$\begin{Bmatrix} \mathbf{u}_i \\ \mathbf{u}_c \end{Bmatrix} = \begin{bmatrix} \boldsymbol{\Psi}_{ik} & \boldsymbol{\Psi}^*_{ic} \\ \mathbf{0} & \mathbf{I} \end{bmatrix} \begin{Bmatrix} \mathbf{p}_{ik} \\ \mathbf{u}_c \end{Bmatrix} = \begin{bmatrix} \mathbf{T}_k \end{bmatrix} \begin{Bmatrix} \mathbf{p}_{ik} \\ \mathbf{u}_c \end{Bmatrix} \tag{2.36}$$

Substitute equation (2.36) into (2.31) and pre-multiply $\begin{bmatrix} \mathbf{T}_k \end{bmatrix}^{-1}$, with some tedious but straightforward mathematical transformation, we can finally get the combined system equation as the following:

$$\begin{bmatrix} {}_A\mathbf{I}_{kk} & \mathbf{0} & {}_A\mathbf{M}_{kc} \\ \mathbf{0} & {}_B\mathbf{I}_{kk} & {}_B\mathbf{M}_{kc} \\ {}_A\mathbf{M}_{ck} & {}_B\mathbf{M}_{ck} & {}_A\mathbf{M}_{cc} + {}_B\mathbf{M}_{cc} \end{bmatrix} \begin{Bmatrix} {}_A\ddot{\mathbf{p}}_{ik} \\ {}_B\ddot{\mathbf{p}}_{ik} \\ \ddot{\mathbf{u}}_c \end{Bmatrix} + \begin{bmatrix} {}_A\boldsymbol{\Omega}_{ik} & \mathbf{0} & \mathbf{0} \\ \mathbf{0} & {}_B\boldsymbol{\Omega}_{ik} & \mathbf{0} \\ \mathbf{0} & \mathbf{0} & {}_A\mathbf{K}_{cc} + {}_B\mathbf{K}_{cc} \end{bmatrix} \begin{Bmatrix} {}_A\mathbf{p}_{ik} \\ {}_B\mathbf{p}_{ik} \\ \mathbf{u}_c \end{Bmatrix} = \begin{Bmatrix} \mathbf{0} \\ \mathbf{0} \\ \mathbf{0} \end{Bmatrix} \tag{2.37}$$

The above method can further be improved by including other types of modes, e.g. attachment modes, rigid body modes [19] and improved boundary modes [20] etc. to improve the accuracy.

2.4.4 Practical Consideration in Applications

The two prime considerations that drive the development of structural coupling techniques are computational efficiency and prediction accuracy. It is always a trade-off situation between these two objectives. In order to increase computational speed, the complexity of the problem must be reduced, which means some 'non-important' information, for example some DOFs and/or vibration data at high frequencies which are not relevant, must be sacrificed in order to reduce the amount of information that needs to be processed. The consequence is a reduced quality of the prediction results: less information and less accuracy. As far as the outcome is concerned, if there is enough computational power, full size modelling is always preferred.

The abovementioned structural coupling techniques do not necessarily require the component size to be reduced before they are joined. It is acceptable to keep the component model intact and to use the same interface constraints and equations for the coupling. This, however, still will not guarantee a good quality assembly model, because a key part is not represented sufficiently here: the joint.

It has generally been considered as rigid in those formulations. There are attempts being made to consider joints as elastic media [21], and in fact it is treated in the same way as the other structural components, being modelled as an individual entity.

The Finite Element Method is by far the most common way to construct an analytical structural model, so it is natural to use it to construct the joint model also. Actually in a rather isolated way FEM has already been used in studying the behaviour of various types of joints: bolted, welded, bonded etc. [22, 23], though all the studies concentrated on their static behaviour only. A joint is quite a complicated mechanism as will be shown in the next chapter. Thousands of DOFs may be need to model a single joint in order to acquire its nonlinear micro and macro stick-slip behaviour, for example. It is of course too much of a burden to try to incorporate this kind of massive joint model into the assembly model in studying the dynamic behaviour.

If, however, the joint can be assumed to be linear, it can be modelled as a simple layer of finite elements between the connected components. The element material properties can be adjusted to reflect the joint's correct flexibility and this can be achieved by carrying out a model updating exercise on the joint FE model only. In Chapter Seven, a linear structural coupling example is presented with experimental validation. The bolted joints are represented by a layer of FE elements. Their properties are updated via experiment.

The FE joint model is limited to linear case if the eigensolution or steady-state response is of the interest, because any nonlinearity in the FE definition has to be discarded in order to take the advantage of symmetric property in the system matrices when calculating the eigensolutions. If the nonlinearity cannot be neglected, some special algorithms must be used to derive the steady state solution in order to avoid the time-consuming time-domain calculation.

2.5 Concluding Remarks

This chapter is effectively an overview of a field that has already been well developed. It might seem to be basic, but it is crucial to get the fundamentals right before we embark on more complicated problems. The linear assumption is still largely used and actually it is acceptable in most applications. Methods and

techniques to perfect linear component models are crucial in achieving good final assembly model. Mechanical joints, even though their behaviour is better described as nonlinear, can often still be considered as linear at normal operation conditions, and linear coupling methods can be used efficiently to produce acceptable results.

Even though the theories have been well laid out, the actual application can be tricky and depends a lot on the thorough understanding of the subject.

Chapter 3

Nonlinear Joint Modelling

3.1 Introduction

The modern mechanical system design theory [24] states that an assembly represents an idea or concept greater than the sum of the individual parts. This indicates the direction for modern machinery development: innovative combinations of ever more number of specialised individual parts. To achieve so, various types of connection mechanisms are needed to properly link the individual parts into a functional assembly. From the structural modelling point of view, these jointed connections can be in different physical forms so long as the kinetic and kinematic constrains are considered properly, which is of course the difficult part of joint modelling.

Joints are normally treated separately from the remaining structural components. One of the reasons is that it is impossible to have a generalised joint model. This is in contrast to the structural components that can all be modelled by defining the mass, stiffness and damping matrices from the design data with FEM, or frequency response data from experiment. This has been well developed, and can be applied to all kinds of components, regardless of size and geometric complexity. In order to be incorporated into a whole assembly mathematical model, the joints need to be described with the same type of kinetic constraints

as those in the FE description of the structural component models. The physics of such constraints is rather different, and in some cases it is difficult to come up with a mathematical description without significant simplification. One typical example is a friction joint, the model of which is still more or less derived approximately from the experiment.

Joints are major sources of nonlinearity in an assembly. This is also part of the reason why joints should be treated separately from other components. The natural way of tackling this problem is to work from linear to non-linear in joint description. If linear joint models and normal structural coupling techniques can solve the problem within the required accuracy, there is no need to go for nonlinear methods. It is, however, necessary to deploy nonlinear models and calculation methods when the experimental results show discrepancies with simulations which can not be improved by merely enhancing the linear models and methods.

The concept of nonlinearity will be explored in detail in the next chapter. Briefly speaking, the fundamental difference between a linear system and a nonlinear one is that the latter's behaviour is not simply the sum of its parts or their multiples, as it is in a linear system. In mathematical terms, the rules of superposition and proportionality are true to linear systems but not to nonlinear ones. This difference is at the root of all the difficulties involved in nonlinear problems.

In the realm of nonlinear joint modelling, two issues are of particular concern. Firstly, extra care should be taken when a joint must be considered to be nonlinear. This is, of course, not to undermine the importance of linear joint modelling. The fact is that nonlinear models need more parameters to describe the behaviour sufficiently. In a linear system, less joint parameters are required and they can be easily adjusted based on the discrepancies between the experiment and simulation data. The same is difficult to do in a nonlinear system because of the large number of unknown parameters. Secondly, a nonlinear joint model must be presented in a form that is ready to be integrated with the remaining structural component models. This normally means a simplification of the joint model, even though in order to capture all the nonlinear phenomenon,

more parameters and conditions should be included in the description. To summarise, nonlinear joint models should be representative and concise.

There are two ways to obtain a nonlinear joint model. One is from the study of the fundamental physics of the joint, and the other is from expriment. The latter is known in the engineering world as 'parameter identification', which focuses on the reconstruction of the unknown governing equations of the joint. Both approaches have been carried out rather independently by physicists and engineers. It is nowadays believed that hybrid techniques that utilise both analytical and experimental data produce more reliable and accurate joint models [13].

This chapter focuses on a few representative nonlinear joint models which are commonly encountered in mechanical engineering, ranging from friction-induced nonlinearity to geometric nonlinearity. The main purpose is to raise awareness of the importance of joint modelling, and the complicated nature of it. Before embarking on the various detailed models, a list of different joint types is presented.

3.1.1 Joint Types

According to Maloney et al. [25], from the joint's effect on structural response point of view, joints can be broadly categorized into non-separable and separable joints. The former tends to be stronger, stiffer, more consistent and more predictable. Examples include welded joints [26, 27] and soldered joints [28]. This type of joint is mostly modelled with Finite Elements, and the concerns in research are more on their long-term reliability than on simulation of normal working conditions. Separable joints are often more difficult to predict and sensitive to many parameters that cannot readily be specified or controlled. There is a long list of separable joints that are presented in different physical forms: bolted joints, rivets, pin joints, thread connections, expansion joints, etc. [29-31].

The difficulties in modelling these separable joints are mainly caused by the existence of friction between the two joining parts. Friction provides resistance force against the relative movement and in fact this is how the joints bind the whole assembly together. Friction phenomena have been studied for centuries,

and the primary cause is yet to be fully understood by physicists. Mechanical engineers are keen on developing representative models from experiments, which should be accurate enough to represent the joint in its specific operating conditions. The friction joints will be discussed in detail in the following section.

It is also common to define some secondary components of an assembly, like angles, plates, gussets, gaskets and bearings as joints. They can indeed be modelled together with the other components, but depending on the computation capacity available and accuracy requirement for the whole assembly, these secondary components can be represented by joint models. A ball bearing in rotating machinery, for instance, connecting the rotor and stator, can be modelled as an individual structural component, containing details of sub-assemblies like balls, inner race, outer race etc. However, it can also be modelled as a simple mass-spring model connecting the rotor and stator, provided this simplification does not deteriorate the simulation quality.

3.2 Nonlinear Joint Models

3.2.1 Friction Models

Friction provides resistance to relative motion between two contacting bodies. This phenomenon is easy to perceive but difficult to model, and it is indeed not yet completely understood of its fundamental causes even today. Many types of joint can be stripped down to frictional elements. Some notable examples are bolted joints, fasteners, friction dampers and bearings etc. Friction has been studied extensively in classical mechanics, and at various times, numerous friction models, both phenomenological and empirical, have been proposed to provide predictive capabilities. One of the aims is to simplify the description of friction, with as few parameters as possible, in order to incorporate it easily with the rest of the structure in modelling the whole system; while at the same time the friction model itself is sufficient to replicate what is observed from experiment, even if it may lack physical insight in some cases.

In this section, the fundamentals about friction are first reviewed, which are followed by a few representative friction models most often seen in literature. Some of the main literature reviews on this subject can be referred to papers [32-34].

3.2.1.1 Friction Phenomenon

Experience with friction is as old as human history, but it was not until the Renaissance period when Leonardo Da Vinci first conducted controlled experiment to observe and quantify friction, that the phenomenon started attracting attentions of generations of scientists and engineers till today. In his famous static friction experiment with a block on horizontal and inclined planes, Da Vinci concluded that the force needed to start one object sliding over another is proportional to the force that presses the two objects together, but independent of the area of contact. This was later found out to be a not-so-accurate description, because the friction force does depend on the area of contact from the microscopic point of view. Nevertheless this is the first time the friction phenomenon was characterised.

From a structural dynamics point of view, we are more interested in the effect of friction on the whole assembly dynamic behaviour and therefore, the observable friction phenomenon, or macroscopic friction, are of concern and need to be quantified. From Da Vinci, macroscopic friction laws have since been enriched by Amontons, Euler, Coulomb and in more recent times notably by Bowden and Tabor [35]. Some of the typical frictional phenomena are summarised below:

- **Static friction and break-away force.** Static friction is the friction when sticking. The friction force opposes the direction of motion when the sliding velocity is zero, and it is equal to the externally applied tangential force until a maximum is reached. The break-away force is the tangential force required to initiate relative motion of two contacting bodies. It was found that the break-away force depends not only on the relative displacement between two contact surfaces, but also on the increment rate of the external force.
- **Coulomb friction.** For most engineering materials, the friction force between the two sliding surfaces is constant as long as relative motion continues. The force level only depends on the materials of the two bodies and the pressing force. This phenomenon was first documented by Amontons (1699) and Coulomb (1785).
- **Viscous friction.** This is the friction phenomenon observed when lubricant is used between two contacting surfaces. It was conclude by Reynolds (1866)

that the friction force caused by the viscosity of lubricants is proportional to the relative velocity of the two sliding surfaces.

- **Micro-slip and Macro-slip.** When two surfaces in contact slide against each other, localised deformation and slippage occurs before observable slide takes place. The stage when there is no relative motion between the two contacting surfaces is called micro-slip, and is widely observed in friction damping problems. Once the external force parallel to the interface surface exceeds the breakaway force level, relative motion will occur. This is called macro-slip. In some engineering applications, e.g. loose bolt joints under cyclic excitation, micro-slip and macro-slip happen repeatedly. This is known as stick-slip cycle. It is a major nonlinear source in assembly structures with bolted joints.

3.2.1.2 Friction Mechanisms

We are more interested here in the manifestation of friction, and a mathematical representation of it; nevertheless, it is also interesting and useful to know the underlying physical properties. As we know friction is the tangential reaction force between two surfaces in contact. Physically, these reaction forces are the result of many different mechanisms which depend on contact geometry and topology, properties of the bulk and surface materials of the bodies, displacement and relative velocity of the bodies and the presence of lubrication [36]. Some of the mechanisms are [36, 37]:

- In dry sliding contacts between flat surfaces, the elastic and plastic deformation of microscopic asperities in contact causes the resistance force, i.e. the friction force. It is accepted as a general rule that for each asperity contact, the tangential deformation is elastic until the applied shear pressure exceeds the shear strength of the surface material, when it becomes plastic. The break-away of the asperities finally leads to slip when the externally applied tangential force is large enough.
- In dry rolling contact, the frictional force is the result of a non-symmetric pressure distribution in the contact, and this uneven distribution is caused by elastic hysteresis in either of the contact bodies.

- When lubricants are added to the contact, the friction force is affected by the viscous property of the lubricant, the relative velocity of contacting surfaces, pressure and thickness of lubricant film, etc. Depending on the different combinations of the above physical properties, different mechanisms dominate in the inception of friction force. For example, at high velocity and low pressure, the friction is determined by the shear force built up in the fluid layer due to the hydrodynamic effects.
- Contamination also needs to be considered sometimes. The presence of small particles between the contact surfaces give rise to additional forces that strongly depend on the size and material properties of the contaminations.

There are many more different mechanisms, in addition to the above, cause friction. To construct a general friction model from physical principles is simply not possible [36]. Approximate models exist for certain configurations. These models were constructed based on the observations of friction phenomena.

3.2.1.3 Some Representative Friction Models

Though surface mechanics is useful knowledge, in the context of structural mechanics, however, such a detailed knowledge of surface mechanics is not always necessary. All we are looking for are the equivalent spring and damping forces displayed by a friction joint. Some of the mostly referred models in the literature are presented below.

Coulomb Friction Model

This is by far the most common model used to describe dry contact friction. It is widely used because of its simplicity and good approximation from the macroscopic point of view. The mathematical expression between the friction force f and relative velocity v can be written as:

$$f = \begin{cases} \mu N & v > 0 \\ F & v = 0 \\ -\mu N & v < 0 \end{cases} \tag{3.1}$$

in which:

F is the external force;

μ is the dynamic friction coefficient;

N is the normal clamping force;

Graphically, it is represented in Figure 3 - 1.

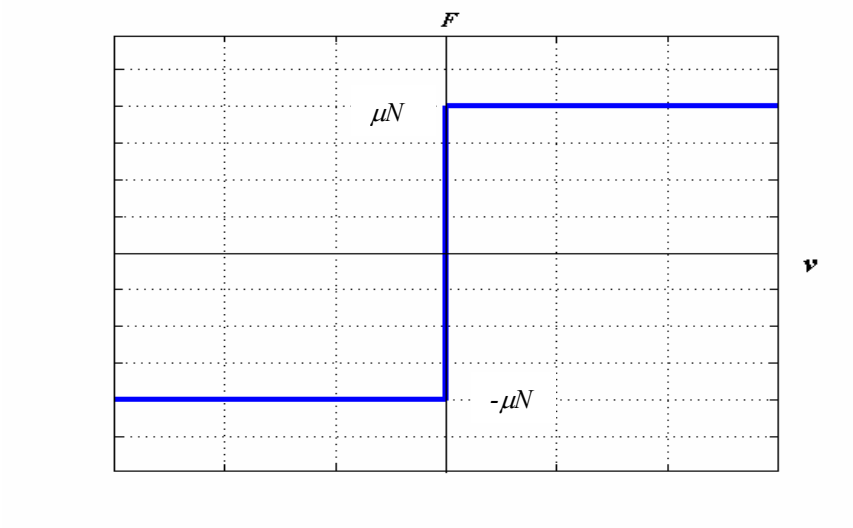

Figure 3 - 1 The Coulomb friction model

The above classical friction models can not capture the behaviour when there is relative velocity between the contacting surfaces. What is more, it neglects the small displacements that occur at the contacting interface during stiction. Therefore, as far as structural dynamics is concerned, a friction model involving dynamics is necessary for accurate description of the friction phenomena [38]. The following few models take care of the dynamic properties of the frictional joints.

1-D Jenkins Model

It is found from experiment that when the friction joint is under dynamic excitation, the joint response is similar to the elasto-plastic response of metals [34]. One of the simplest models to describe such a material property is the Jenkins spring slider element, which has also been successfully implemented in friction joint modelling.

Each Jenkins model consists of a spring and a Coulomb slider element, which has two possible arrangements, in series or in parallel as shown in Figure 3 - 2(a) and (b), respectively. In the case of Figure 3 - 2(a), the Coulomb element is connected in series with the spring element. Under a cyclic external excitation, the Coulomb element is firstly in its sticking state at the beginning of each cycle, which provides a resistive force equal and opposite to the input force to the

element, while the spring element provides the displacement representing micro-slip. When the friction capacity of the Coulomb element is passed, the sliding state starts. Once in the sliding state the Coulomb element provides constant resistance of magnitude equal to the coefficient of friction multiplied by the normal force. The typical force-displacement representation of this type of Jenkins model is shown in Figure 3 - 3. In the case of parallel connection of Coulomb element and spring element, as shown in Figure 3 - 2(b), the corresponding characteristic curve is shown in Figure 3 - 4.

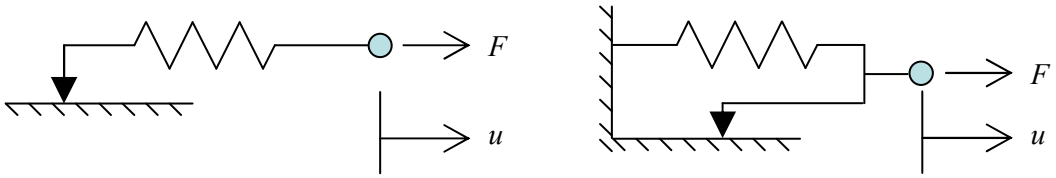

(a) In series **(b) In parallel**

Figure 3 - 2 Symbolic representation of Jenkins model

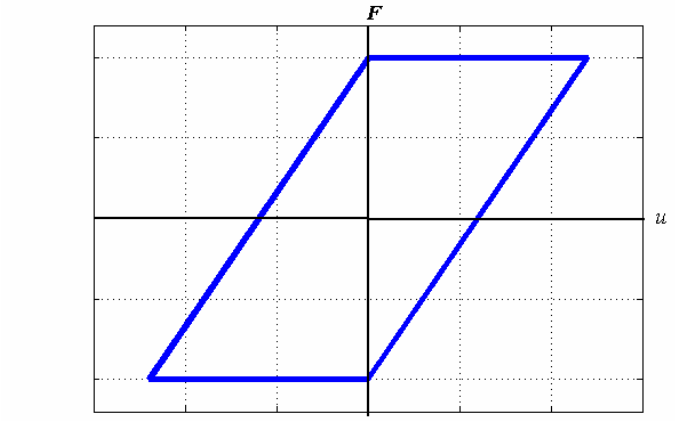

Figure 3 - 3 Characteristic curve of a Jenkins model with elements in series

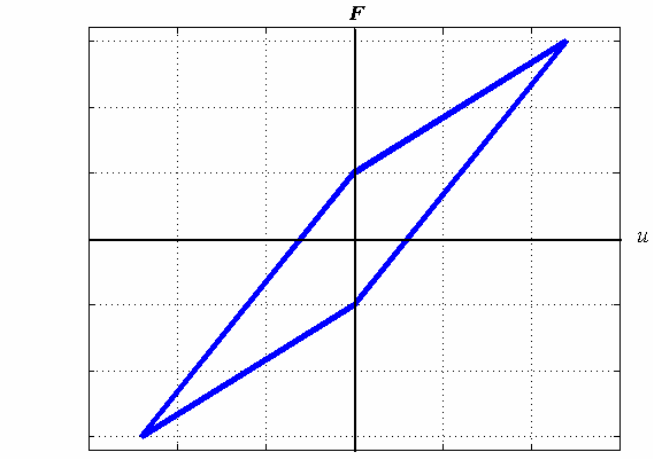

Figure 3 - 4 Characteristic curve of a Jenkins model with elements in parallel

The characteristic curve form a hysteresis loop which exhibits the energy dissipation property of a friction joint, a phenomenon observed from experiment and practical applications [39]. However, when only one Jenkins element is used to model the joint, the friction model displays bi-linear properties, indicating abrupt transition from stick to slip, which is not exactly the same as what is observed in reality, in which the transition is smooth. One way to solve this problem is to model the friction joint using a collection of Jenkins models. One of the most prominent developments along this line is Iwan's model [40, 41]. Iwan's model consists of several Jenkins elements connected in parallel. Each Jenkins element has the same stiffness, k, while the breaking away force of each Coulomb element is different, the arrangement of which is governed by a certain probabilistic distribution function $\rho(f)$, depending on the specific case under study. By carefully choosing k and $\rho(f)$, the resultant Iwan's model can match an actual measurement very well.

Valanis Model

This model was first proposed by Gaul and Lenz [42], who likened the force-displacement characteristics of a dynamically excited lap-joint to Valanis model of plasticity. The Valanis model in materials engineering shows the energy dissipation during the loading-unloading cycle, and the isotropic hardening effect, which is manifested as the proportionality between the increment in stress and the increment of strain after certain critical load point is passed. This is comparable to the transition between micro-slip and macro-slip observed in frictional joints. The governing equation is expressed in first order differential equation:

$$\dot{F} = \frac{E_0 \dot{u}\left[1+\operatorname{sgn}(\dot{u})\frac{\lambda}{E_0}(E_t u - F)\right]}{1+\kappa \operatorname{sgn}(\dot{u})\frac{\lambda}{E_0}(E_t u - F)} \tag{3.2}$$

The stiffness modulus of the stick condition is denoted by E_0 while the tangent modulus E_t describes the slope of slip motion. The parameter κ controls the influence of micro-slip. A re-plot from Gaul's paper [42] is show in Figure 3 - 5.

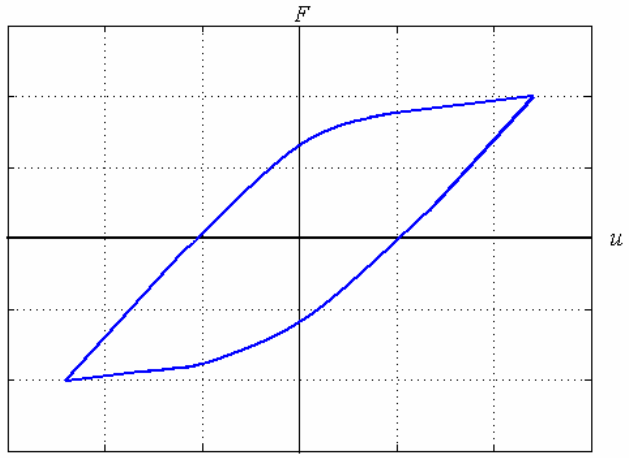

Figure 3 - 5 Characteristic curve of a typical Valanis model

The advantage of such a model is that the parameters needed to define the joint are far fewer than Iwan's model, and once all of them are derived from joint identification, the model can be readily integrated with FE models of the main bodies. However, the Vanalis model offers little physical interpretation of the friction phenomenon.

The LuGre Friction Model

This is a model with more physical insight. It was first proposed by Canudas De Wit et al. [38] to include the friction phenomenon in a control system. It is reckoned that the two contacting surfaces are very irregular at the microscopic level and the actual contacts are at a number of asperities, which are in the form of elastic bristles. As the external force increases, the elastic bristles deflect, and have similar effect as deformed springs. A schematic representation of such an interpretation is shown in Figure 3 - 6. For simplicity, the bristles on the low part are shown as rigid.

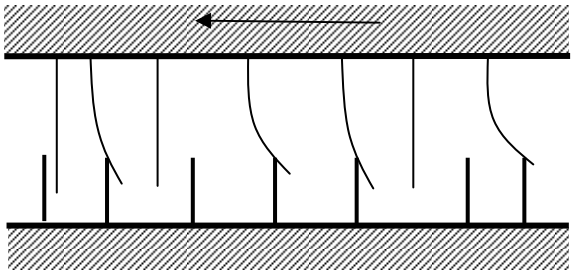

Figure 3 - 6 LuGre model - friction interface represented as bristle contacts

Once the deflection limits are reached, the bristles will restore to their normal unstressed state immediately, which is manifested as slip. Due to the highly

irregular distribution of the bristles, it is more economical to describe their behaviour in an average sense. The resultant governing equation is:

$$F(\dot{u}) = F_C \operatorname{sgn}(\dot{u}) + (F_S - F_C) e^{-\left(\dot{u}/v_s\right)^2} \operatorname{sgn}(\dot{u}) + \sigma \dot{u} \tag{3.3}$$

In which, F_C and F_S are the Coulomb friction level and Stiction force, respectively; v_s is the Stribeck velocity[1] and σ counts for the viscous effect.

3.2.1.4 Concluding Remarks on Friction Joint Models

This is not a complete review of friction joint models; rather, it is meant to show that friction is a very complicated physical issue, and that there is no single representative and conclusive enough model available. The choice of the best model to be used in any given case depends on many factors like operating conditions, accuracy requirement, calculation algorithm restrictions etc.

The Finite Element Method can be used to model linear joints. This method is straightforward and indeed preferred because the model is ready to be integrated with the remaining of the finite element structural component models. It is possible to extend this method into the nonlinear realm by meshing the joint regions finely enough to capture any relevant micromechanics. However, it proves to be impractical for large-scale structural systems because of the prohibitively small time steps required in calculation [39].

3.2.2 Geometric Nonlinear Models

This type of nonlinearity arises from the joints' geometric configurations. In some cases, joints are not much different from other structural components, other than the fact that the joints are located at critical areas, at which good flexibility and strength are needed. While still within the material elastic zone, the deformation of the joint material is so large that the assumption of linear stress-strain relationship is not valid any more. Geometric discontinuity is another source of nonlinearity. The load path across the joint is not smooth because of gap or material discontinuity. These two are discussed below.

[1] The friction phenomenon that arises from the use of fluid lubrication and gives rise to decreasing friction with increasing velocity at low velocity.

3.2.2.1 Cubic Stiffness

This is probably the most documented nonlinearity in structural dynamics. As the demand for faster, lighter and more efficient machine increases, some parts of such a structural assembly may undergo deformation so large that the relationship between force and displacement is no long a constant. It is possible that this type of nonlinearity is due to plastic deformation of the base material, but it is more common in practice that the base material is flexible and designed to work in its elastic region, and the only nonlinear source is the assumption of the infinite small deformation is no long valid in constructing the stress-strain relationship.

The stiffness nonlinearity can be analytically formulated and numerically simulated using FEM. The resultant equation to describe the relation between the force and the displacement can be written as:

$$F = k_1 u + k_3 u^3 \tag{3.4}$$

This characteristic is known as the cubic stiffening effect, and is best demonstrated with Figure 3 - 7. As the load F is increased steadily, the deflection increment gets less and less. If we take equivalent stiffness at every point along the curve, it is easy to see that the equivalent stiffness gets larger as the deflection increases.

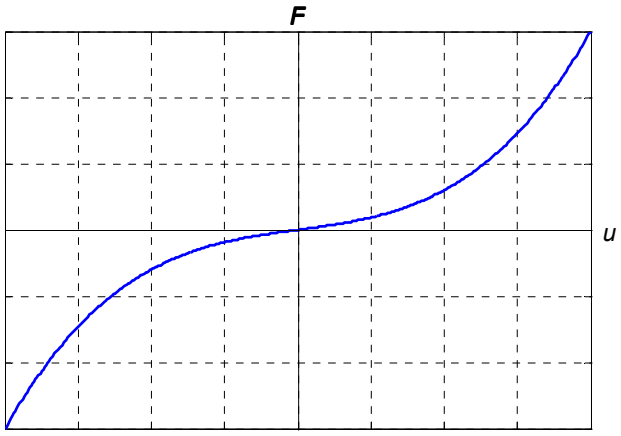

Figure 3 - 7 Characteristic plot of a typical cubic stiffness

3.2.2.2 Polynomial Stiffness

For a real structure experiencing large deflection, the stiffness function may include not only a cubic term but also higher-order terms in which the cubic term may dominate. There also exists in engineering application a cubic nonlinear stiffness with a negative first order term [43, 44], as $k_1 < 0$ in equation (3.4). Graphically the characteristic curve for this case is as shown in Figure 3 - 8:

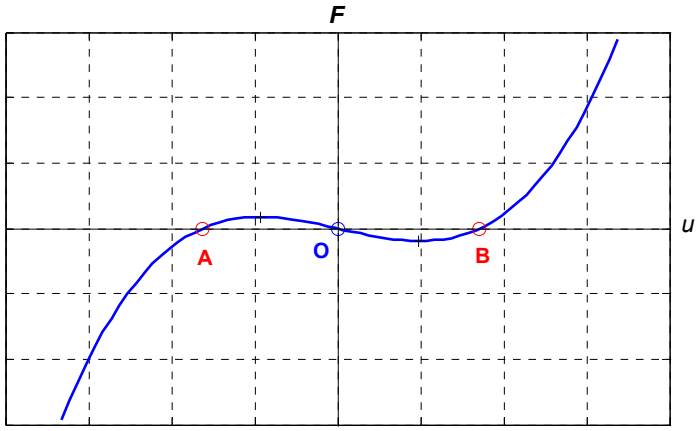

Figure 3 - 8 Characteristic curve of cubic stiffness with negative linear term

This is an interesting nonlinear case. Globally, it represents the case of stiffening spring. Locally, it has negative linear stiffness at its global centre O, and a weakening stiffness at its two static equilibrium points, A and B. The weakening effect can be visualised from the above plot. As the displacement leaves the equilibrium point and approaches the global centre, there is more and more deflection for a steadily increased load, until arriving at the point where the deflection is extreme for a very small increase in load. This local nonlinear stiffness can be fitted with a second order polynomial curve. In later chapters, it will be shown with an example that a slightly buckled beam possesses this type of nonlinearity.

3.2.2.3 Piecewise Linear Stiffness

This type of nonlinearity is caused by geometric discontinuity between two connecting components. It has a practical interest in many mechanical systems, such as the stiffness in the clutch of automobile power transmission system, backlash in the gear system, etc. A universal piecewise linear stiffness model is

shown in Figure 3 - 9(a) with different linear stiffness values at different displacement stages. There are two special cases worth mentioning here.

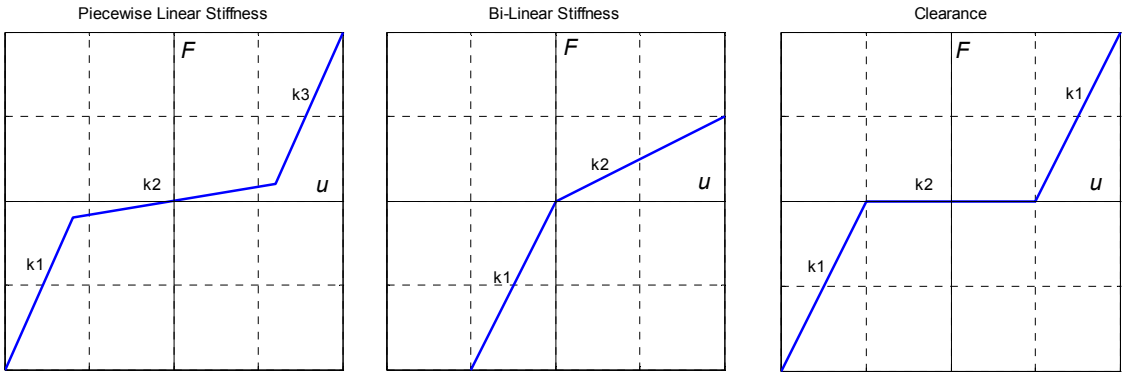

(a) **(b)** **(c)**

Figure 3 - 9 Piecewise linear stiffness models

Figure 3 - 9(b) shows a bi-linear stiffness case. One practical example is the bolted flange connection [45], in which the dominant stress-strain direction is along the bolt centre line. The stiffness k_1 in the compression regime is relatively higher because the compression load is shared by both the bolt stud and the flange; while the stiffness k_2 in the tension regime is smaller because the tensile load is only borne up by the bolt stud. Other bi-linear joint examples can be found in loosely joint structures [46].

Figure 3 - 9(c) shows a clearance type of nonlinearity. In some mechanical assemblies, a clearance is inevitable at the joint. Small suitable clearance is necessary to move a mechanism smoothly. In addition, through wear-and-tear, a small gap may be built up, e.g. the rattling problem in a gear system. Another example can be found in the application of Active Magnetic Bearing (AMB) systems in rotating machinery, in which an emergency 'catcher' bearing is used to support the rotor when the AMB is not functioning. It is a complicated problem involving impact mechanisms and rubbing etc., but it can be simplified and represented by a clearance type of joint as shown above. Here $k_2 = 0$ reflects the non-contact status.

3.3 Concluding Remarks

A few representative joint models have been presented in this chapter. The aim is to provide manageable joint models to the whole assembly model. It should be

noted that a joint is often extremely difficulty to model using a purely analytical approach. It always relies on experimental data to validate and correct the mathematical models. This is a research subject in its own right, known as joint identification. A large number of techniques have been proposed, notably collected in annual IMAC[1] and biennial ISMA[2] conferences.

[1] International Modal Analysis Conference
[2] International Conference on Noise & Vibration Engineering

Chapter 4

Dynamic Analysis of Nonlinear Structures

4.1 Introduction

Some forms of nonlinearity have been presented in the previous chapter when different structural joint models are described. From those various graphs that depict the relation between two parameters, e.g. displacement and restoring force, it is found that the relationship is not linearly proportional, as otherwise would be described by a straight line. This is the manifestation of nonlinearity that we most appreciate. The definition of nonlinearity can be expressed with a more stringent mathematical sense: the fundamental rule that judges whether a system is linear or nonlinear, is the conformance of the following two principles [47]:

• *The principle of superposition;*

• *The principle of proportionality.*

Violating either one means the existence of nonlinearity. This is because in a linear condition, the system is described by linear differential equations, which are the summation of dependent variables and their derivatives. Doubling the external excitation leads to doubling the responses, and the individual response

to each excitation components can simply be summed up to get the total response. In nonlinear situation, this is not true.

The existence of nonlinearity in a structure can be due to many different mechanisms, some of which have been covered in the previous chapter, but there is a long list to follow, and most of them are case-based. It is rather difficult to neatly categorise different types of nonlinearity based on its physical properties. It is, however, possible to classify the nonlinearity based on its extent: global nonlinearity and localised nonlinearity [13]. The former is found in problems related to nonlinear material properties; and the latter, which is to be focused on in this thesis, exists at the connection between two adjoining components, usually known as a joint. The large part of the remaining structure is effectively linear. This inspired the introduction of methods that take advantage of the localised properties of the nonlinearities to speed up the calculation for such type of structure on which nonlinearity only exists at a small number of DOFs. In this chapter we shall first examine a few methods that solve general nonlinear problems, which do not differentiate these two types of nonlinear problems in structural dynamics.

The principles of superposition and proportionality are the cornerstones of linear theory. Various analytical methods have been developed to make full use of these principles to simplify the process of solving problems of a linear system. The analytical solutions are described in algebraic form without the inclusion of numerical values for parameters. Once the solutions are obtained, any desired numerical values can be inserted and the entire possible range of solutions can be explored, which is certainly a time-saving practice, in addition to its exactness. Nonlinear structural dynamic problems are usually described by nonlinear differential equations, which can be notoriously difficult to solve in an analytical closed form. The existence and co-existence of many interesting nonlinear phenomena, e.g. bifurcation, sub-harmonic and super-harmonic motion, limited cycle and chaos, means that a direct analytical solution is indeed not possible. Therefore, indirect or approximation procedures must be applied.

There are two major branches in the modern developments of nonlinear analysis: the analytical methods of successive approximations and the topological methods of graphical integration [48]. The latter one originated from the

graphical representation of the solution of dynamic equilibrium equations in the phase plane. Phase planes are useful for visualising the behaviour of a physical system. Stability and unique vibration patterns can be assessed through the study of the integral curves in the phase planes. However, these methods are only applicable to lower order systems and are mostly used in the more mathematically inclined approaches. The concept of phase plane will be demonstrated in a later section. The main purpose of this thesis is to develop accurate and efficient structural modelling practices for large-scale structure assemblies; hence, only the first type of these methods is going to be investigated in more detail. Some of the important methods to find approximate analytical solutions are (i) the perturbation method, (ii) the iteration method, (iii) the averaging method, (iv) the harmonic balance method [48] and the step-by-step direct numerical integration of the differential equation in the time-domain method [13]. These can be grouped into two categories, time-domain methods and frequency-domain methods.

This thesis focuses on finding steady-state solutions of a nonlinear structure subjected to periodic excitation. It is understood from linear structural dynamic analysis that the dynamic properties of a linear system can be characterised by a set of frequency response functions, which relate the amplitude and phase of the response to harmonic excitation. This concept can be extended to nonlinear structural dynamic analysis to study how a nonlinear structure responds to harmonic excitation. It is noted that cyclic external excitation is very often experienced by engineering structures, e.g. vibration caused by unbalanced rotating machinery, so to analyse the steady-state solution of a structure subjected to periodic excitation has clear physical significance. In addition, from the model validation point of view, if the steady-state response calculation can be correlated with experiment, it will prove that the nonlinear structure is correctly modelled.

In the following sections, time-domain methods and frequency-domain methods are discussed. The focus is on the Runge-Kutta Method and Harmonic Balance Method respectively, which are used in the subsequent case study. This case study is an interesting one DOF nonlinear problem with a ‘strange’ nonlinear stiffness. A large collection of steady-state solutions have been found.

4.2 Time-Domain Analysis

'Time-domain' is a term used to describe the analysis of mathematical functions or physical signals, with respect to time. In this thesis, we refer this type of analysis as those numerical methods for solving ordinary differential equations with time as the independent variable. The signal or the state of a system is calculated step-by-step throughout the time history at discrete points.

In the case of using Spatial model to represent the structure, a set of differential equations are applied to describe the dynamic equilibrium at each DOF. For a linear system, the exact steady-state solution of this set of equations can be solved by an analytical method with respect to time. They can also be solved numerically to get approximate solutions at discrete time points. With carefully-selected time step size and a numerical calculation scheme, the result will be very close to the exact analytical solution. In linear case, numerical schemes are not preferred because it is far more expensive to run them.

For studying the dynamic response of a nonlinear structure, the analytical solution is extremely difficult to get. Time-domain numerical schemes are among the many procedures used to find the corresponding approximate solutions. They are renowned for being potentially accurate, even though a low computational efficiency is still unavoidable. In this thesis, we focus on examining efficient approximate methods to describe a nonlinear system under periodical external excitation. Time-domain calculation results will be used as the 'exact' solution, to be compared with those from other approximate methods.

4.2.1 Runge-Kutta Method

The fourth-order Runge-Kutta method is one of the standard algorithm to solve differential equations. No knowledge is required about the nonlinear system and it virtually always succeeds with reasonable accuracy [13]. This method is designed to imitate the Taylor series method without requiring analytic differentiation of the original differential equations [49]. The dynamic system can be described with the following second order differential equations:

$$[\mathbf{M}]\{\ddot{\mathbf{u}}\}+[\mathbf{C}]\{\dot{\mathbf{u}}\}+i[\mathbf{D}]\{\mathbf{u}\}+[\mathbf{K}]\{\mathbf{u}\}+\{\mathbf{g}\}=\{\mathbf{f}\} \tag{4.1}$$

in which, $\{\mathbf{g}\}$ is the nonlinear internal force vector. In order to accommodate the application of the numerical method, this second-order equation needs to be re-written into first order form:

$$\begin{aligned} &\{\dot{\mathbf{u}}\} = \{\mathbf{v}\} \\ &[\mathbf{M}]\{\dot{\mathbf{v}}\} + [\mathbf{C}]\{\mathbf{v}\} + i[\mathbf{D}]\{\mathbf{u}\} + [\mathbf{K}]\{\mathbf{u}\} + \{\mathbf{g}\} = \{\mathbf{f}\} \end{aligned} \tag{4.2}$$

The above equation can be arranged in a single matrix form as:

$$\begin{bmatrix} \mathbf{M} & \mathbf{0} \\ \mathbf{0} & \mathbf{I} \end{bmatrix} \begin{Bmatrix} \dot{\mathbf{v}} \\ \dot{\mathbf{u}} \end{Bmatrix} + \begin{bmatrix} \mathbf{C} & \mathbf{K}+i\mathbf{D} \\ \mathbf{I} & \mathbf{0} \end{bmatrix} \begin{Bmatrix} \mathbf{v} \\ \mathbf{u} \end{Bmatrix} = \begin{Bmatrix} \mathbf{f}-\mathbf{g} \\ \mathbf{0} \end{Bmatrix} \tag{4.3}$$

This is most commonly written in the state-space equation format as:

$$\{\dot{\mathbf{z}}\} = \{\mathbf{S}(t,\mathbf{z})\} \tag{4.4}$$

in which:

$$\{\mathbf{z}\} = \begin{Bmatrix} \mathbf{v} \\ \mathbf{u} \end{Bmatrix} = \begin{Bmatrix} \dot{\mathbf{u}} \\ \mathbf{u} \end{Bmatrix} \tag{4.5}$$

and

$$\{\mathbf{S}(t,\mathbf{z})\} = \begin{bmatrix} \mathbf{M} & \mathbf{0} \\ \mathbf{0} & \mathbf{I} \end{bmatrix}^{-1} \left(\begin{Bmatrix} \mathbf{f}-\mathbf{g} \\ \mathbf{0} \end{Bmatrix} - \begin{bmatrix} \mathbf{C} & \mathbf{K}+i\mathbf{D} \\ \mathbf{I} & \mathbf{0} \end{bmatrix} \begin{Bmatrix} \mathbf{v} \\ \mathbf{u} \end{Bmatrix} \right) \tag{4.6}$$

When the initial conditions $\{\mathbf{z}(t_0)\}$ is known, equation (4.4) is ready to be solved by the Runge-Kutta formulations:

$$\mathbf{z}(t+h) = \mathbf{z}(t) + \frac{h}{6}(\boldsymbol{R}_1 + 2\boldsymbol{R}_2 + 2\boldsymbol{R}_3 + \boldsymbol{R}_4) \tag{4.7}$$

in which:

$$\begin{aligned} \boldsymbol{R}_1 &= \mathbf{S}(t,\mathbf{z}) \\ \boldsymbol{R}_2 &= \mathbf{S}\left(t+\frac{1}{2}h,\ \mathbf{z}+\frac{1}{2}h\boldsymbol{K}_1\right) \\ \boldsymbol{R}_3 &= \mathbf{S}\left(t+\frac{1}{2}h,\ \mathbf{z}+\frac{1}{2}h\boldsymbol{K}_2\right) \\ \boldsymbol{R}_4 &= \mathbf{S}(t+h,\ \mathbf{z}+h\boldsymbol{K}_3) \end{aligned} \tag{4.8}$$

and h is the time step size defined by the user. The derivation of the above formulation can be found in standard textbooks [50].

The Runge-Kutta Method has been well developed theoretically and proven to be accurate and efficient. It is a standard component in various mathematical software packages, and many variations exist to cater for users' different priorities and some uncommon problems. In this thesis, MATLAB® is adopted as the platform to carry out time domain analysis. ode45 is the key command used, which implements the above-presented 4^{th} order Runge-Kutta method. In general, this command is the first function to try for most problems [51]. One point needs to be noted: MATLAB® uses variable step size for the calculation. This is achieved by estimating the error at every calculation step, comparing the error with the pre-defined tolerance and altering the step size accordingly. It is of course possible to fix the step size h by the user even though it is not advisable. The danger with applying fixed time step size is that if the oscillation period of the input signal is smaller than the time step, crucial dynamic information would totally be missed in the results. In addition, solving with fixed step size tends to be slower comparing to those with variable step size, because if the input signal changes gently, the step size can be relatively coarse without sacrificing the accuracy.

4.2.2 Other Time-domain Methods

The Runge-Kutta Method is one type of the so-called 'Explicit' numerical methods. The name comes from the fact that the current state of a system is calculated using the information from the state of the system at the previous time step. Other methods in the same category are: Forward Euler Method, Central Difference Methods, Taylor Series Schemes, Predictor-Corrector method, [52, 53] etc. These methods are suitable for small scale problems in terms of the order of the system equation, and problems concerning medium to high frequency range of a structure, like those shockwaves response simulation in impact tests. The stability of these type of methods is the main concern. The time step size needs to be inversely proportional to the highest vibration frequency inherent to the structure, which, if not totally impractical, is extremely small for

a finely meshed FE model. Nevertheless, this type of method is a faster choice, if the model is relatively small.

Contrary to the Explicit Method, the so-called Implicit Method finds the solution of the current state of a system by solving an equation involving both current and previous states of the system. A few notable methods in this category are: Newmark [54], Wilson-θ [55] and Houbolt methods [53, 56, 57]. These methods are more suitable for large scale problems and most effective when the concerned vibration of the structure is characterised by a relatively small number of low frequency modes [56]. Transient Analysis in many commercial FE packages uses this type of method, for both linear and nonlinear problems. The application of these methods becomes much simpler with those user-friendly FE software packages, in which the user is guided through choices of parameters that are relevant to particular types of problem. Of course, the user must understand the fundamentals in the first place.

4.3 Frequency-Domain Analysis

'Frequency-domain' is a term used to describe the analysis of mathematical functions or signals with respect to frequency. A time-domain analysis shows how a signal changes over time, whereas a frequency-domain analysis shows how much of the signal lies within each given frequency band over a range of frequencies. If the described signal is periodic, the frequency-domain representation is much more concise, because it needs only a few values to quantify the signal.

A major shortcoming of the time-domain methods is that they are very time-consuming. The computing time required depends on the scale of the structure and accuracy requirement. A small time step is needed if explicit methods are used, as it is inversely proportional to the highest frequency of the structural model. In addition, if the main concern is to obtain the steady-state solution, the calculation must be carried on until any transient effect has died away. In the case of lightly damped structure, this means consuming a significant computing resource on something which is not intrinsically useful. So alternatively, frequency-domain approximation methods for determining the steady-state

response of structures, particularly to periodic external excitation, should be used, in which there is no need to analyse transient motion [13].

The limitation of the frequency-domain methods is what time-domain analysis is strong at: versatility. Some of the most important frequency-domain methods are presented here, all of which assume steady-state periodic response to periodic external excitation.

4.3.1 Perturbation Method

This method can actually be applied in both time domain and frequency domain. It is included here because it can be used to derive steady-state periodic solutions. Perturbation theory is a century-old, and indeed one of the oldest methods used to find approximate solution to a nonlinear problem that cannot be solved exactly. It starts with the assumption that the nonlinear term adds a slight deviation from the solution of the underlying linear problem, which can be solved exactly with an analytical method. One of the techniques is to express the desired solution in terms of a power series of a small perturbation parameter that quantifies the deviation from the exact solution [58], as shown in the following equation:

$$\begin{aligned} u(t) &= u_0(t) + \varepsilon u_1(t) + \varepsilon^2 u_2(t) + \cdots \\ \omega^2 &= \omega_n^2 + \varepsilon\omega_1 + \varepsilon^2\omega_2 + \cdots \end{aligned} \tag{4.9}$$

in which, ε is the perturbation parameter; $u_0(t)$ and ω_n would be the known solution to the underlying solvable linear problem; $u_1(t), u_2(t), \cdots$ and $\omega_1, \omega_2, \ldots$ are higher order solutions representing small deviations due to the nonlinearity; and they can be found iteratively. The closeness to the exact solution depends on the number of higher order terms included in the calculation.

This method is only valid when the real solution is close to that of the underlying linearised problem, which implies that this method is mainly for systems with weak nonlinearity.

4.3.2 Describing Functions

The describing function method was first developed to solve nonlinear problems in control systems [59]. The similarity of the mathematical expressions of a

control system and a structural dynamic system inspired the application of this method in the modelling of a nonlinear structure. This method linearises the nonlinearity by defining a transfer function that relates the fundamental harmonic components of the input and the output to the nonlinearity [13]. The mathematical derivation is briefly shown below, following the approaches of Tanrikulu et al. [60] and Ferreira [13]. The standard Spatial model is used, with a term representing nonlinear interaction force included:

$$[\mathbf{M}]\{\ddot{\mathbf{u}}(t)\}+[\mathbf{C}]\{\dot{\mathbf{u}}(t)\}+[\mathbf{K}]\{\mathbf{u}(t)\}+\{\mathbf{g}(\mathbf{u}(t),\dot{\mathbf{u}}(t))\}=\{\mathbf{f}(t)\} \tag{4.10}$$

in which, $\{\mathbf{g}(\mathbf{u}(t),\dot{\mathbf{u}}(t))\}$ is the nonlinear interaction force; and $\{\mathbf{f}(t)\}$ is the external periodic excitation. The k^{th} element of the nonlinear interaction force is a combination of the interaction forces between DOF k and all other DOFs. This can be expressed in summation form:

$$g_k=\sum_{j=1}^{N}p_{kj} \tag{4.11}$$

in which p_{kj} is a function of the inter-coordinate displacement, y_{kj}, and its time derivatives, and is expressed as:

$$p_{kj}=p_{kj}\left(y_{kj},\dot{y}_{kj}\right) \tag{4.12}$$

in which:

$$y_{kj}=u_k-u_j \tag{4.13}$$

The external harmonic force with an angular velocity ω can be written as:

$$\{\mathbf{f}(t)\}=\{\bar{\mathbf{F}}e^{i\omega t}\} \tag{4.14}$$

It is assumed that the response to the harmonic excitation is also periodic, and can be expanded in the form of Fourier series:

$$\{\mathbf{u}(t)\}=\sum_{n=1}^{\infty}\{\bar{\mathbf{U}}^n e^{in\omega t}\} \tag{4.15}$$

It should be noticed that both $\bar{\mathbf{F}}$ and $\bar{\mathbf{U}}^n$ are complex vectors with the size of the total number of DOFs.

If the nonlinearity is weak, the fundamental component in the Fourier expansion of the response is a good assumption of the exact solution:

$$\{\mathbf{u}(t)\} \approx \left\{\bar{\mathbf{U}}^1 e^{i\omega t}\right\} \tag{4.16}$$

Convert both (4.12) and (4.13) from the time domain to the frequency domain as:

$$\bar{Y}_{kj} e^{i\omega t} = \left(\bar{U}_k^1 - \bar{U}_j^1\right) e^{i\omega t} \tag{4.17}$$

and

$$\bar{P}_{kj} = \frac{1}{\pi} \int_0^{2\pi} p_{kj} e^{-i\omega t} d(\omega t) \tag{4.18}$$

The ratio between $\bar{P}_{kj}$ and $\bar{Y}_{kj}$ is defined as a describing function:

$$v_{kj} = \bar{P}_{kj} \Big/ \bar{Y}_{kj} \tag{4.19}$$

and the complex amplitude of the nonlinear force vector is represented in the form of the describing function:

$$G_k = \sum_{j=1}^{N} v_{kj} \bar{Y}_{kj} \tag{4.20}$$

Substitute (4.14), (4.16), (4.20) and (4.17) into (4.10), we will have, after cancelling the term $e^{-i\omega t}$:

$$\left(-\omega^2 [\mathbf{M}] + i\omega [\mathbf{C}] + [\mathbf{K}] + [\mathbf{\Delta}]\right)\{\bar{\mathbf{U}}\} = \{\bar{\mathbf{F}}\} \tag{4.21}$$

in which $[\mathbf{\Delta}]$ is defined as the generalised quasilinear matrix [60], and its elements are obtained using the following equations:

$$\begin{aligned} \Delta_{kk} &= \sum_{j=1}^{N} v_{kj} \\ \Delta_{kj} &= -v_{kj} \quad (k \neq j) \end{aligned} \tag{4.22}$$

The superscript *1* for the displacement vector $\{\bar{\mathbf{U}}\}$, indicating the fundamental harmonic is dropped, for clarity. Equation (4.21) can be solved iteratively. When better accuracy is needed, higher order terms in the Fourier expansion can be retained, it will however complicate the computation.

4.3.3 Harmonic Balance Method

The Harmonic Balance Method (HBM) is a well-known tool for studying nonlinear dynamic problems in the frequency domain. It can be applied to the analysis of strongly nonlinear systems, such as the rotor-stator contact problem [61], and structures with friction contact interfaces [62-64]. The working principle of this method is that the frequency components of the internal interaction force must equate to those presented in the response. A set of balanced equations are therefore derived, one for each frequency component, which can be solved to get the amplitude and phase of each frequency component. The implementation is summarised below.

It is first assumed that the steady-state solution is periodic, and can therefore be expanded into a Fourier series. The assumed solution is then inserted into the original system dynamic equation. The sine and cosine coefficients of the same harmonic order are set to zero separately. A set of new equations containing all the unknown coefficients are subsequently solved. The assumed solution is finalised in the form of a Fourier series with all the harmonic coefficients determined. The length of the solution series is determined by the user, and in general, if more terms of the Fourier series are taken into account, the closer the approximated solution will be to the exact one. Of course, it requires more computational effort. The mathematical derivation starts from expressing the system equation as below, which is the same as equation (4.10):

$$\left[\mathbf{M}\right]\left\{\ddot{\mathbf{u}}(t)\right\}+\left[\mathbf{C}\right]\left\{\dot{\mathbf{u}}(t)\right\}+\left[\mathbf{K}\right]\left\{\mathbf{u}(t)\right\}+\left\{\mathbf{g}\left(\mathbf{u}(t),\dot{\mathbf{u}}(t)\right)\right\}=\left\{\mathbf{f}\left(t\right)\right\} \tag{4.23}$$

in which, $\left\{\mathbf{g}\left(\mathbf{u}(t),\dot{\mathbf{u}}(t)\right)\right\}$ is the nonlinear internal reaction force; and $\left\{\mathbf{f}\left(t\right)\right\}$ is the external periodic excitation. For clarity purpose, the brackets that represent matrix and vector are omitted in the following mathematical derivations.

Based on the assumption that the response is also periodic, which can be decomposed with Fourier series as:

$${}_{m}\mathbf{u}(t)={}_{m}\mathbf{U}^{0}+\sum_{n=1}^{N}\left[{}_{m}\mathbf{U}_{C}^{n}\cos\left(\frac{n}{m}\omega t\right)+{}_{m}\mathbf{U}_{S}^{n}\sin\left(\frac{n}{m}\omega t\right)\right] \tag{4.24}$$

In which, ω is the frequency of the external harmonic forcing; and m is an integer corresponding to the ratio of the period of the external forcing to the

period of the response. It is used to count for sub-harmonic responses. m=1 when the dominant harmonic in the response is the same as that of the excitation. ${}_m\mathbf{U}_C^n$ is the amplitude of the n^{th} cosine harmonic term, ${}_m\mathbf{U}_S^n$ is the amplitude of the n^{th} sine harmonic term. N is the total number of harmonic terms included in the Fourier series expansion.

The derivatives of the above equation are:

$$\begin{aligned} {}_m\dot{\mathbf{u}}(t) &= \sum_{n=1}^{N}\left[\left(-\frac{n}{m}\omega\right){}_m\mathbf{U}_C^n\sin\left(\frac{n}{m}\omega t\right)+\left(\frac{n}{m}\omega\right){}_m\mathbf{U}_S^n\cos\left(\frac{n}{m}\omega t\right)\right] \\ {}_m\ddot{\mathbf{u}}(t) &= \sum_{n=1}^{N}\left[-\left(\frac{n}{m}\omega\right)^2{}_m\mathbf{U}_C^n\cos\left(\frac{n}{m}\omega t\right)-\left(\frac{n}{m}\omega\right)^2{}_m\mathbf{U}_S^n\sin\left(\frac{n}{m}\omega t\right)\right] \end{aligned} \tag{4.25}$$

The nonlinear reaction force is also expressed in a Fourier series:

$${}_m\mathbf{g}\left(\mathbf{u}(t),\dot{\mathbf{u}}(t)\right) = {}_m\mathbf{G}^0+\sum_{n=1}^{N}\left[{}_m\mathbf{G}_C^n\cos(\frac{n}{m}\omega t)+{}_m\mathbf{G}_S^n\sin(\frac{n}{m}\omega t)\right] \tag{4.26}$$

in which ${}_m\mathbf{G}^0, {}_m\mathbf{G}_C^n, {}_m\mathbf{G}_S^n$ are the respective harmonic terms.

Substitute equation (4.24), (4.25) and (4.26) into (4.23), with a pure sine external excitation:

$$\begin{aligned} &\mathbf{M}\left\{\sum_{n=1}^{N}\left[-\left(\frac{n}{m}\omega\right)^2{}_m\mathbf{U}_C^n\cos\left(\frac{n}{m}\omega t\right)-\left(\frac{n}{m}\omega\right)^2{}_m\mathbf{U}_S^n\sin\left(\frac{n}{m}\omega t\right)\right]\right\}+ \\ &\mathbf{C}\left\{\sum_{n=1}^{N}\left[\left(-\frac{n}{m}\omega\right){}_m\mathbf{U}_C^n\sin\left(\frac{n}{m}\omega t\right)+\left(\frac{n}{m}\omega\right){}_m\mathbf{U}_S^n\cos\left(\frac{n}{m}\omega t\right)\right]\right\}+ \\ &\mathbf{K}\left\{{}_m\mathbf{U}^0+\sum_{n=1}^{N}\left[{}_m\mathbf{U}_C^n\cos\left(\frac{n}{m}\omega t\right)+{}_m\mathbf{U}_S^n\sin\left(\frac{n}{m}\omega t\right)\right]\right\}+ \\ &{}_m\mathbf{G}^0+\sum_{n=1}^{N}\left[{}_m\mathbf{G}_C^n\cos(\frac{n}{m}\omega t)+{}_m\mathbf{G}_S^n\sin(\frac{n}{m}\omega t)\right]=\mathbf{F}\sin(\omega t) \end{aligned} \tag{4.27}$$

Balance the harmonic terms on both sides of the equation:

$$\begin{aligned} const. \quad &\Rightarrow \quad \mathbf{K}\,{}_m\mathbf{U}^0+{}_m\mathbf{G}^0=0 \\ \cos(\frac{n}{m}\omega t)\Rightarrow \quad &-\mathbf{M}\left(\frac{n}{m}\omega\right)^2{}_m\mathbf{U}_C^n+\mathbf{C}\left(\frac{n}{m}\omega\right){}_m\mathbf{U}_S^n+\mathbf{K}\,{}_m\mathbf{U}_C^n+{}_m\mathbf{G}_C^n=0 \\ \sin(\frac{n}{m}\omega t)\Rightarrow \quad &-\mathbf{M}\left(\frac{n}{m}\omega\right)^2{}_m\mathbf{U}_S^n-\mathbf{C}\left(\frac{n}{m}\omega\right){}_m\mathbf{U}_C^n+\mathbf{K}\,{}_m\mathbf{U}_S^n+{}_m\mathbf{G}_S^n=\begin{cases}\mathbf{F} & n=1\\ 0 & n\succ 1\cdots N\end{cases} \end{aligned} \tag{4.28}$$

It is noticed from equation (4.26) that ${}_m\mathbf{G}_C^n$ and ${}_m\mathbf{G}_S^n$ are directly linked with the response ${}_m\mathbf{U}$; hence they can be expressed as:

$$\begin{aligned} {}_m\mathbf{G}_C^n &= {}_m\mathbf{G}_C^n\left({}_m\mathbf{U}^0, {}_m\mathbf{U}_C^1, {}_m\mathbf{U}_S^1, \ldots, {}_m\mathbf{U}_C^N, {}_m\mathbf{U}_S^N\right) \\ {}_m\mathbf{G}_S^n &= {}_m\mathbf{G}_S^n\left({}_m\mathbf{U}^0, {}_m\mathbf{U}_C^1, {}_m\mathbf{U}_S^1, \ldots, {}_m\mathbf{U}_C^N, {}_m\mathbf{U}_S^N\right) \end{aligned} \tag{4.29}$$

Combine equation (4.28) and (4.29) to get $2N$ algebraic equations with $2N$ unknown Fourier coefficients of the response.

$$\begin{aligned} &const. \quad \Rightarrow \quad \mathbf{K}\,{}_m\mathbf{U}^0 + {}_m\mathbf{G}^0 = 0 \\ &\cos\left(\frac{n}{m}\omega t\right) \Rightarrow \\ &-\mathbf{M}\left(\frac{n}{m}\omega\right)^2 {}_m\mathbf{U}_C^n + \mathbf{C}\left(\frac{n}{m}\omega\right){}_m\mathbf{U}_S^n + \mathbf{K}\,{}_m\mathbf{U}_C^n + {}_m\mathbf{G}_C^n\left({}_m\mathbf{U}^0, {}_m\mathbf{U}_C^1, {}_m\mathbf{U}_S^1, \ldots, {}_m\mathbf{U}_C^N, {}_m\mathbf{U}_S^N\right) = 0 \\ &\sin\left(\frac{n}{m}\omega t\right) \Rightarrow \\ &-\mathbf{M}\left(\frac{n}{m}\omega\right)^2 {}_m\mathbf{U}_S^n - \mathbf{C}\left(\frac{n}{m}\omega\right){}_m\mathbf{U}_C^n + \mathbf{K}\,{}_m\mathbf{U}_S^n + {}_m\mathbf{G}_S^n\left({}_m\mathbf{U}^0, {}_m\mathbf{U}_C^1, {}_m\mathbf{U}_S^1, \ldots, {}_m\mathbf{U}_C^N, {}_m\mathbf{U}_S^N\right) - \mathbf{F} = 0 \end{aligned} \tag{4.30}$$

From (4.23) to (4.30), a nonlinear differential equation has been transformed into a set of nonlinear algebraic equations. With a proper iteration algorithm chosen, these equations are ready to be solved. The purpose is to find $2N$ unknowns, ${}_m\mathbf{U}_C^1, {}_m\mathbf{U}_S^1, \ldots, {}_m\mathbf{U}_C^N, {}_m\mathbf{U}_S^N$, with the $2N$ equations at every frequency point ω. Equation (4.30) is re-written in matrix form by combining all the harmonic terms:

$$\mathbf{R}(\omega) = \mathbf{Z}(\omega)\mathbf{U} - \mathbf{F} - \mathbf{G}(\mathbf{U}) = 0 \tag{4.31}$$

Where $\mathbf{U} = \left\{{}_m\mathbf{U}^0, {}_m\mathbf{U}_C^1, {}_m\mathbf{U}_S^1, \cdots, {}_m\mathbf{U}_C^N, {}_m\mathbf{U}_S^N\right\}^T$ is a vector of harmonic coefficients of the response at all system DOFs; $\mathbf{G}(\mathbf{U}) = \left\{{}_m\mathbf{G}^0, {}_m\mathbf{G}_C^1, {}_m\mathbf{G}_S^1, \ldots, {}_m\mathbf{G}_C^N, {}_m\mathbf{G}_C^N\right\}^T$ is a vector of harmonic coefficients for all the nonlinear internal forces. $\mathbf{Z}(\omega)$ is similar to the dynamic stiffness matrix of the linear part of the system with higher harmonic terms included. It is represented as:

$$\mathbf{Z}(\omega)=\begin{bmatrix} \mathbf{K} & \mathbf{0} & \mathbf{0} & \cdots & \mathbf{0} & \mathbf{0} \\ \mathbf{0} & \mathbf{K}-\left(\frac{1}{m}\omega\right)^2\mathbf{M} & \frac{1}{m}\omega\mathbf{C} & \cdots & \mathbf{0} & \mathbf{0} \\ \mathbf{0} & -\frac{1}{m}\omega\mathbf{C} & \mathbf{K}-\left(\frac{1}{m}\omega\right)^2\mathbf{M} & \cdots & \mathbf{0} & \mathbf{0} \\ \vdots & \vdots & \vdots & \ddots & \vdots & \vdots \\ \mathbf{0} & \mathbf{0} & \mathbf{0} & \cdots & \mathbf{K}-\left(\frac{N}{m}\omega\right)^2\mathbf{M} & \frac{N}{m}\omega\mathbf{C} \\ \mathbf{0} & \mathbf{0} & \mathbf{0} & \cdots & -\frac{N}{m}\omega\mathbf{C} & \mathbf{K}-\left(\frac{N}{m}\omega\right)^2\mathbf{M} \end{bmatrix} \tag{4.32}$$

Equation (4.31) represents a nonlinear set of equations with respect to **U**, and the purpose is to find **U** at every desirable frequency. If the nonlinear structure under study has a DOF of N_s, the whole set of equations will have $N_s\times(2N+1)$ unknowns to be decided. One of the most efficient methods for the solution of a set of nonlinear equations is the Newton-Raphson method which possesses quadratic convergence when an approximation is close enough to the solution. The iteration is conducted with the following formula at every frequency point of interest:

$$\mathbf{U}^{(k+1)}=\mathbf{U}^{(k)}-\left(\frac{\partial\mathbf{R}^{(k)}}{\partial\mathbf{U}}\right)^{-1}\mathbf{R}\left(\mathbf{U}^{(k)}\right) \tag{4.33}$$

The superscript (*k*) indicates the number of the current iteration. Performing differentiation of equation (4.33) with respect to **U**, the recurrence formula can be rewritten in the form:

$$\mathbf{U}^{(k+1)}=\mathbf{U}^{(k)}-\left(\mathbf{Z}(\omega)+\frac{\partial\mathbf{G}\left(\mathbf{U}^{(k)}\right)}{\partial\mathbf{U}}\right)^{-1}\mathbf{R}\left(\mathbf{U}^{(k)}\right) \tag{4.34}$$

The derivatives $\partial\mathbf{G}\left(\mathbf{U}^{(k)}\right)\Big/\partial\mathbf{U}$ are calculated using finite-difference formulae.

One further point needs to be mentioned here is that $\mathbf{G}(\mathbf{U})$ cannot be explicitly expressed. It needs be calculated every time a new **U** is derived, with Fourier coefficient calculation:

$$
\begin{aligned}
{}_m\mathbf{G}^0 &= \frac{1}{T}\int_0^T {}_m\mathbf{g}\left({}_m\mathbf{u}(t), {}_m\dot{\mathbf{u}}(t)\right)dt \\
{}_m\mathbf{G}_C^n &= \frac{1}{T}\int_0^T {}_m\mathbf{g}\left({}_m\mathbf{u}(t), {}_m\dot{\mathbf{u}}(t)\right)\cos\left(\frac{n}{m}\omega t\right)dt \\
{}_m\mathbf{G}_S^n &= \frac{1}{T}\int_0^T {}_m\mathbf{g}\left({}_m\mathbf{u}(t), {}_m\dot{\mathbf{u}}(t)\right)\sin\left(\frac{n}{m}\omega t\right)dt
\end{aligned}
\tag{4.35}
$$

in which T is the external excitation period.

4.4 Case Study

The procedure of using the Harmonic Balance Method to derive steady-state periodic response of a nonlinear system is applicable to a system of any number of DOFs. However, for demonstration purposes, only a 1-DOF nonlinear system is presented in this case study, which is meant to show a special type of nonlinearity and the fact that HBM can cope with it well.

4.4.1 Problem Definition

We study the nonlinear equation of a 1-DOF oscillator:

$$m\ddot{u}(t) + c\dot{u}(t) + k_1 u(t) + k_3 u^3(t) = F\sin(\omega t) \tag{4.36}$$

in which some physical values are assigned for the numerical studies:

$m = 1\text{kg};\ c = 1\text{Ns/m};\ k_1 = \text{-}1000\text{N/m};\ k_3 = 10000\text{N/m}^3;\ F = 2000\text{N}.$

The nonlinearity only exists in the restoring spring force, which, with the assigned physical values, can be visualised with the graph below. It resembles a slightly buckled beam undergoing forced lateral vibration, as shown in Chapter Three. This is actually a Duffing's equation with a negative linear stiffness. A similar system was first systematically studied by Holmes [65], in response to the demand from the study of population dynamics and Earth's magnetic field model. It has since become an interesting subject for mathematicians.

When the static force $F = 0$, there are three static equilibrium points, indicated as O, A and B at $u = 0$ and $u = \pm 0.3162$ respectively as shown in Figure 4 - 1. The non-zero equilibrium points A and B are dynamically stable, while point O is not, because of the existence of negative stiffness around this global centre.

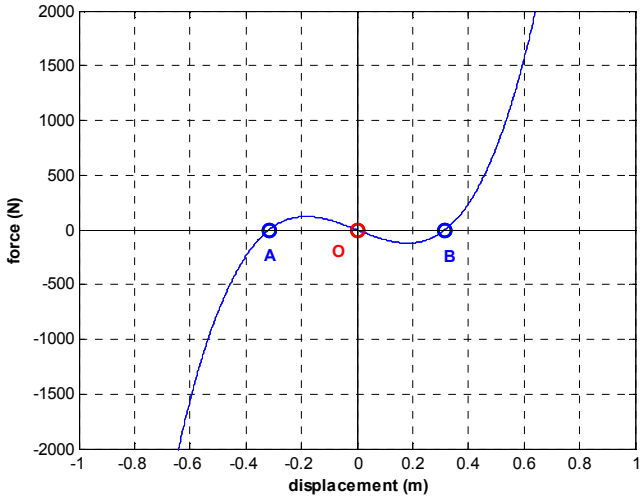

Figure 4 - 1 Force-displacement curve of the nonlinear spring

One of the main purposes of this study is to find as many as possible steady-state periodic solutions for the nonlinear dynamic equation (4.36), and to show that Harmonic Balance Method is a very efficient alternative to the usual time-domain methods.

4.4.2 Time-Domain Calculation

The time integration starts from some initial conditions in terms of displacement u and velocity $\dot{u}$. The differential equations are then integrated over a time interval which is long enough to allow transient effect to disappear and steady-state vibrations to settle down. A fourth-order Runge-Kutta method with variable step scheme is used. Various initial conditions are examined in order to find different steady-state solutions for the same magnitude and frequency of excitation force. The excitation frequency ranges from 1Hz to 80Hz in a step of 0.1Hz. At each frequency point, 200 runs with randomly selected initial conditions are conducted.

The result of this exhaustive study is shown in Figure 4 - 2. The maximum displacement amplitudes over a vibration period of the steady-state response are shown as functions of the excitation frequency. Each 'branch' corresponds to one type of steady-state periodic response of the system, which is characterised by the dominant harmonic components in the response. Some branches have been marked to indicate the dominant harmonics. For example, the branch marked with '1/3, 3/3, …' contains all the 1/3 sub-harmonic responses. In the

frequency range between 18Hz to 32Hz, a cluster of sub-harmonic solutions are found below the branch of main harmonic response. They will be shown with more details in next section.

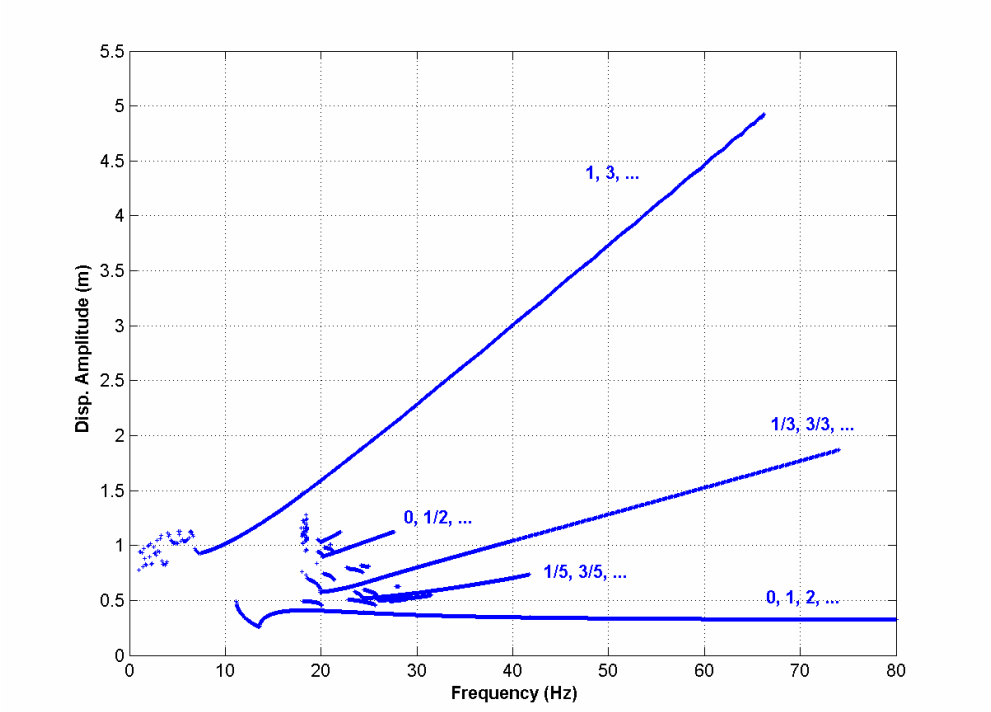

Figure 4 - 2 Steady-state solutions from time-domain integration

4.4.3 Frequency-Domain Calculation

The search for the sub-, super- and major periodic solutions in the frequency domain was performed for different initial approximations of the periodic solutions and for different harmonic numbers kept in the multi-harmonic expansion of the solution. For each calculation, the execution of the algorithm started with a guess for the harmonic coefficients of the forced response. The HBM algorithm with a continuation scheme [66] was used, which ensured that the periodic solutions of the same type were efficiently calculated and traced along the whole frequency range of interest. Both stable and unstable solutions can be determined as a result of these calculations. Owing to these features, the frequency-domain solution process requires only one point close to the trajectory of solutions in order to calculate the whole trajectory. Hence, the number of the frequency-domain calculations is smaller by several orders of magnitude than the number of runs carried out for the time-domain analysis. As a result, the expense required for frequency-domain calculation is a very small fraction of the

time-domain computation expense. The initial approximations for the forced response spectrum were deduced from some steady-state solutions found in the time-domain integration.

The results of all these calculations are plotted in Figure 4 - 3, together with the time-domain calculation results for comparison. The time-domain calculation is represented with blue dots, and the frequency domain calculation with solid black lines. The clustered region is enlarged in Figure 4 - 4 so as to reveal a rich collection of steady-state solutions brought in by the nonlinear stiffness. Each branch has been marked by numbers indicating the dominant harmonics in the response corresponding to the excitation frequency.

The time-domain and frequency-domain results match very closely from the frequency domain comparison. This is further demonstrated by comparing the displacement variations in time domain and the integration curves in phase plane from both calculations. An example is shown in Figure 4 - 5, in which the 1/5 sub-harmonic response at 24.6Hz is examined. In Figure 4 - 5(a), the blue dash line is the force trajectory, for reference purpose. The black solid line is the response trajectory derived from the time integration calculation, which is considered an exact solution to the nonlinear equation. It is easily seen that it is a 1/5 order sub-harmonic response by simply counting the oscillation peaks of the force within one cycle of the response. The dotted line with circles is the response trajectory calculated with HBM when only one harmonic is assumed for the solution. The general trend of the response is followed, but small details are not matching, which is more obvious in the phase plane (Figure 4 - 5(b)). When two more harmonics, 3/5 and 5/5, are added in the HBM calculation, the response, represented by a dotted line with triangles matches the exact solution so well that it is hard to differentiate the two from the graph without the help of the triangles.

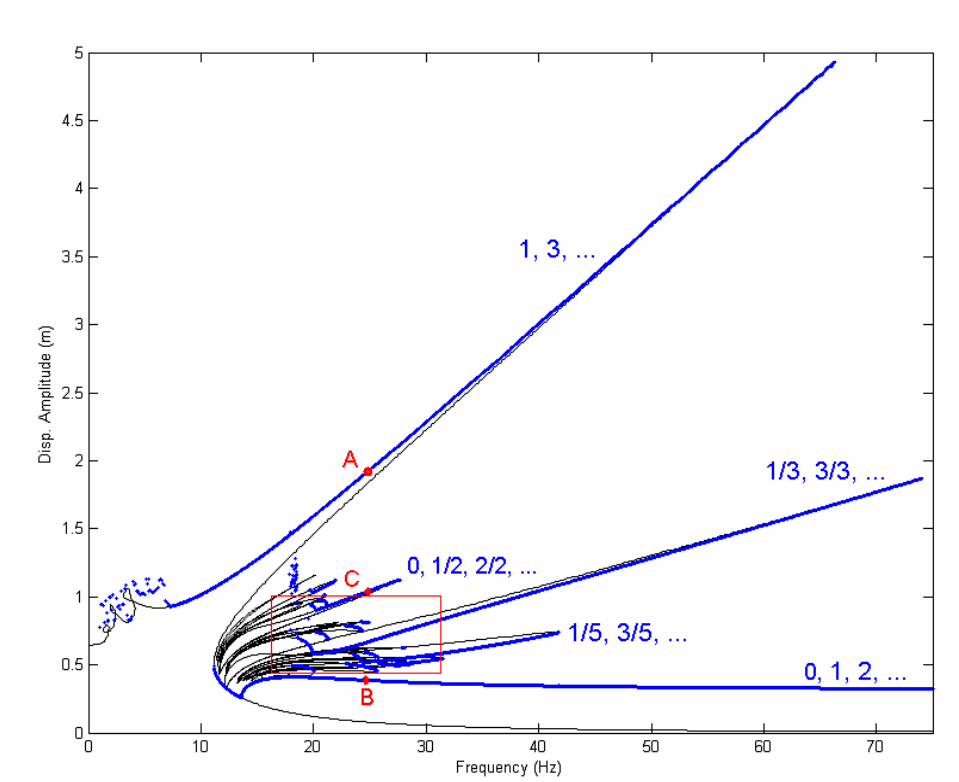

Figure 4 - 3 Results comparison between HBM and time-domain integration

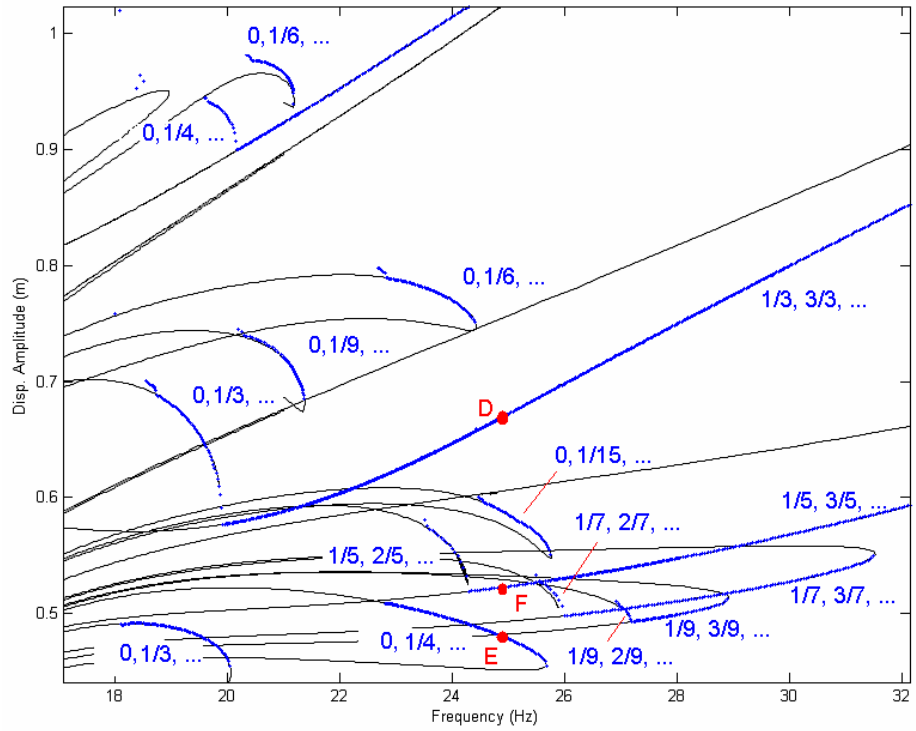

Figure 4 - 4 Results comparison between HBM and time-domain integration – enlarged view

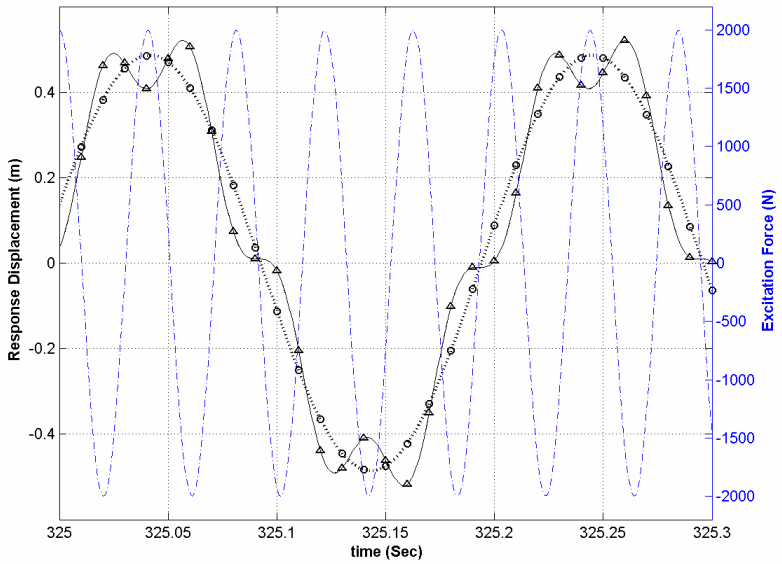

(a)

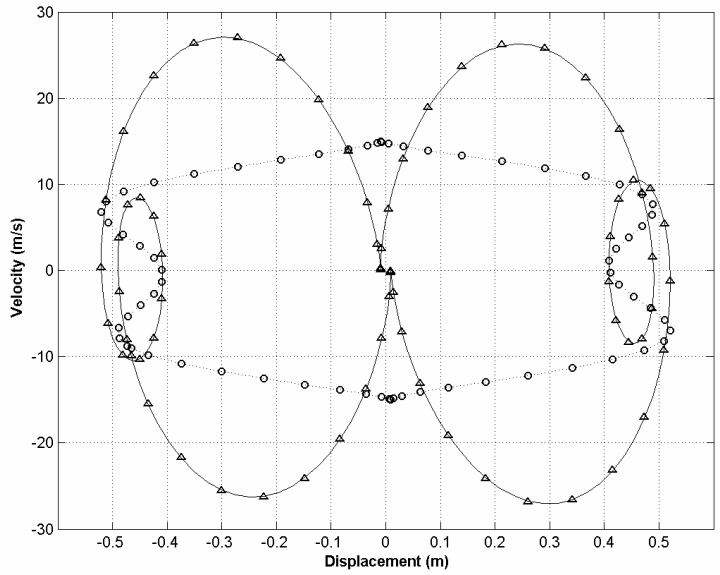

(b)

Figure 4 - 5 (a) displacement variation in time and (b) phase space trajectory of solution corresponding to Point F (1/5 sub-harmonic response) in Figure 4 - 4(b)
('-·-·-·-' external excitation, '——' time integration, '··○··○··○·· ' one harmonic term (1/5) included, '-Δ--Δ--Δ--' three harmonic terms (1/5, 3/5, 5/5) included.)

However, it is in some cases the two results do not match very closely as shown in Figure 4 - 3. The failure is mostly due to three causes: (i) the random nature of the search for solutions in the time domain which, in contrast to the frequency-domain solution, does not guarantee determination of all possible solutions for the branch considered and (ii) close to the region where chaotic vibration dominates, not enough integration time is given for the system to settle down

and (iii) the time-domain solution approach allows us to find only stable steady-state solutions and misses unstable ones.

There are several more interesting discoveries from this exercise, which is somewhat off the main thread of this thesis. More details are shown in Appendix B.

4.5 Concluding Remarks

This chapter focuses on the dynamic analysis of nonlinear structures, and in particular on the periodic response due to external periodic excitation. Nonlinear differential equations that describe the dynamic system can rarely be solved analytically, as concluded by many mathematicians. The approximation methods are good alternatives. Some of them have been presented in this chapter. It is demonstrated in the Case Study that the Harmonic Balance Method is accurate and efficient in solving a problem with strong nonlinearity. A large number of steady-state solutions co-exist at the same excitation frequency and the Harmonic Balance Method is capable of finding them.

Chapter 5

Nonlinear Structural Coupling

5.1 Introduction

Structural coupling methods originated from the demand for efficient analysis of complex structures during a time when high performance computers were still rare. The problem of modelling a complicated structure could be greatly simplified by first dividing the structure into components, each of which could be represented by a smaller, more accurate and refined mathematical model; and then applying some coupling schemes to analyse the dynamic response of the whole assembly from the dynamic properties of individual components [13]. In addition to the savings made in computation time, the concept of structural coupling allows component models to be generated from different sources. It is common in practice that certain component models are better derived from experiment, and the others from direct FE construction. The accuracy and completeness of the assembly model, as well as the dynamic responses obtained, will benefit from optimal component model description.

The linear structural coupling methods are well developed, as discussed in Chapter Two. From an engineering viewpoint [12], there is a need to extend linear coupling methods to nonlinear systems because some engineering

structures are formed by largely linear components with a small number of localised nonlinearities. Thus, a few nonlinear elements cause the whole structural assembly to behave nonlinearly. For example, in a turbine engine, the linear turbine blades are prevented from reaching excessive vibration levels by using the so-called “friction dampers” at the roots connecting to the rotor. The existence of friction dampers makes the linear calculation invalid. Another example can be found in the dynamics of a rotor supported on nonlinear bearings, e.g. squeeze-film bearings or active magnetic bearings. The vibration phenomena of the rotor in this case cannot be described accurately with linear models. In the above two examples, although the overall nonlinear behaviour is significant, the actual number of nonlinear elements is very small. For such cases, there is a need to develop analysis procedures whereby the linear and nonlinear parts can be analysed separately, and combined together with some nonlinear coupling procedures, thus avoiding a nonlinear analysis for the whole structure [12]. It is expected that computation time will be largely reduced by such an approach.

In the literature, the researches carried out to study the dynamic properties of nonlinear structures mostly focused on simple or simplified structures and did not differentiate the extent of nonlinearity in the structure, be it local or global. For time domain analysis, the combination of nonlinearity and large model size causes numerical integration to be impractical, except perhaps for short time transient response calculation. For frequency-domain analysis, even though it is much more efficient than time-domain analysis in finding steady-state solutions, once the model size gets large the iterations can get slower and numerically more unstable. If we can combine frequency-domain methods together with the concept of structural coupling, it is possible to analyse large size structures with localised nonlinearities effectively.

In this chapter, nonlinear structural coupling methods are reviewed and the focus is on frequency domain methods with the FRF coupling approach. Vibration caused by periodic excitation is of major concern in many practical cases; hence a test rig model under periodic external excitation is used to assess the nonlinear coupling method. Different nonlinearities are assigned to the model in order to show the versatility and efficiency of the method.

5.2 Nonlinear Structural Coupling Approaches

There is not much literature available on this topic, even though it is apparently a subject worth more attention. The fundamental idea is to separate the linear and nonlinear part of the assembly. The first stage is the sub-structuring of the original nonlinear system into subsystems, or components, that can be modelled separately: This step achieves two objectives [67]:

- it results in the division of a larger system into smaller subsystems which may be easier to model or to identify from experimental data, and
- it enables the segregation of linear and nonlinear components which will eventually result in an economical analysis procedure.

One of the earliest attempts was made by Dowell [68], who used the Component Mode Synthesis method with Lagrange multiplier to analyse a simply supported beam attached to a nonlinear spring-mass system. Nataraj et al. [67] also used Component Mode Synthesis method and, together with trigonometric collocation method, to calculate periodic solutions of a rotor system with nonlinear support. Watanabe and Sato [69] proposed the so-called Nonlinear Building Block approach to evaluate frequency response characteristics of a structural system with nonlinear springs linking linear components. They used the spatial coupling method and represented the join nonlinearity with its describing function. The use of Guyan reduction [18] on the linear components before applying nonlinear algorithms to calculate the response of the whole assembly has also been tried [70]. The Frequency Response Function (FRF) coupling method has also been explored to obtain steady state periodic response of structural assemblies with localised nonlinearity. This approach is, however, not widely seen in the literature. To the author's knowledge only Petrov [64] and Ferreira [13] have touched on this topic. Ferreira's approach is a direct extension of the linear FRF coupling method, with an additional nonlinear joint matrix added to the assembly FRF matrix. This additional joint matrix is derived using the describing function method. Petrov's approach uses the Harmonic Balance Method and takes the advantage of the fact that omitting internal linear DOFs will not affect the accuracy and completeness of the calculated response if the component models are represented with FRF matrices, and the resultant

assembly model is also in the form of FRF matrix. Iteration is required in both approaches and the Newton-Raphson method is preferred.

5.2.1 Nonlinear FRF Coupling With Describing Function Method

This method was first suggested by Ferreira et. al [13, 71]. It combines the well-developed linear FRF method with linearised description of the nonlinear joints using describing function method. There are different forms of FRF coupling formations, the most basic one has been briefly presented in Chapter Two. A slightly more detailed version is presented below. Two components *A* and *B* are modelled and represented with their respective FRF matrices:

$$\begin{aligned} \{{}_A\mathbf{U}\} &= \left[{}_A\mathbf{H}(\omega)\right]\{{}_A\mathbf{F}\} \\ \{{}_B\mathbf{U}\} &= \left[{}_B\mathbf{H}(\omega)\right]\{{}_B\mathbf{F}\} \end{aligned} \tag{5.1}$$

Each matrix is arranged according to the locations of the DOFs:

$$\begin{aligned} \begin{Bmatrix} {}_A\mathbf{U}_i \\ {}_A\mathbf{U}_c \end{Bmatrix} &= \begin{bmatrix} {}_A\mathbf{H}_{ii} & {}_A\mathbf{H}_{ic} \\ {}_A\mathbf{H}_{ci} & {}_A\mathbf{H}_{cc} \end{bmatrix} \begin{Bmatrix} {}_A\mathbf{F}_i \\ {}_A\mathbf{F}_c \end{Bmatrix} \\ \begin{Bmatrix} {}_B\mathbf{U}_i \\ {}_B\mathbf{U}_c \end{Bmatrix} &= \begin{bmatrix} {}_B\mathbf{H}_{ii} & {}_B\mathbf{H}_{ic} \\ {}_B\mathbf{H}_{ci} & {}_B\mathbf{H}_{cc} \end{bmatrix} \begin{Bmatrix} {}_B\mathbf{F}_i \\ {}_B\mathbf{F}_c \end{Bmatrix} \end{aligned} \tag{5.2}$$

The subscripts *i* and *c* represent the internal and connecting DOFs, respectively. It is assumed that components *A* and *B* are connected rigidly at the interface. By applying the equilibrium and compatibility equations at the interface:

$$\begin{aligned} \{{}_A\mathbf{F}_c\} &= -\{{}_B\mathbf{F}_c\} = \{\mathbf{F}_c\} \\ \{{}_A\mathbf{U}_c\} &= \{{}_B\mathbf{U}_c\} = \{\mathbf{U}_c\} \end{aligned} \tag{5.3}$$

the combined system FRF matrix can be derived and represented as:

$$\begin{aligned} \left[{}_C\mathbf{H}(\omega)\right] &= \left[\left[{}_A\mathbf{H}(\omega)\right]^{-1} \oplus \left[{}_A\mathbf{H}(\omega)\right]^{-1}\right]^{-1} \\ &= \begin{bmatrix} {}_A\mathbf{Z}_{ii} & {}_A\mathbf{Z}_{ic} & \mathbf{0} \\ {}_A\mathbf{Z}_{ci} & {}_A\mathbf{Z}_{cc} + {}_B\mathbf{Z}_{cc} & {}_B\mathbf{Z}_{ci} \\ \mathbf{0} & {}_B\mathbf{Z}_{ic} & {}_B\mathbf{Z}_{ii} \end{bmatrix}^{-1} \end{aligned} \tag{5.4}$$

In which $[\mathbf{Z}]$ is the dynamic stiffness matrix, and derived from the inversion of the FRF matrix as:

$$\left[\mathbf{Z}(\omega)\right]=\left[\mathbf{H}(\omega)\right]^{-1} \tag{5.5}$$

The system equation is therefore expressed as:

$$\begin{Bmatrix} {}_A\mathbf{U}_i \\ \mathbf{U}_c \\ {}_B\mathbf{U}_i \end{Bmatrix}=\begin{bmatrix} {}_A\mathbf{Z}_{ii} & {}_A\mathbf{Z}_{ic} & \mathbf{0} \\ {}_A\mathbf{Z}_{ci} & {}_A\mathbf{Z}_{cc}+{}_B\mathbf{Z}_{cc} & {}_B\mathbf{Z}_{ci} \\ \mathbf{0} & {}_B\mathbf{Z}_{ic} & {}_B\mathbf{Z}_{ii} \end{bmatrix}^{-1}\begin{Bmatrix} {}_C\mathbf{F}_i \\ \mathbf{F}_c \\ {}_C\mathbf{F}_i \end{Bmatrix} \tag{5.6}$$

and in a compact form:

$$\left\{{}_C\mathbf{U}\right\}=\left[{}_C\mathbf{H}(\omega)\right]\left\{{}_C\mathbf{F}\right\} \tag{5.7}$$

The main advantage of the FRF coupling method is that FRFs measured from experiments can be used directly, which means within the frequency range of interest there is no approximation made throughout the derivation of the system FRF matrix. In addition, the assembly model size can be reduced without sacrificing accuracy by including only the connecting DOFs and internal DOFs of interest in the component matrices. The reason is that FRFs derived at any DOF record the dynamic information of the whole structure. Hence, even with the physical DOFs omitted from the FRF matrix, the resultant FRF matrix still truly represents the component. This can significantly reduce the size of the problem since the connecting DOFs normally form only a small portion of the whole structure.

As shown in equation (5.4), three matrix inversions are required to derive the system FRF matrix. This hinders a wider application of this method because of excessive computing time needed and possible ill-conditioned matrices near resonance causing erroneous results [16]. An alternative FRF coupling method introduced by Jetmundsen et al. [14] reduces the number of matrix inversions at each frequency point from three to one. In addition, the size of the matrix to be inverted is restricted to the connecting DOFs only. This further reduces the calculation requirement. The resultant assembly RFR matrix is expressed as:

$$\left[{}_C\mathbf{H}(\omega)\right]=\begin{bmatrix} {}_A\mathbf{H}_{ii} & {}_A\mathbf{H}_{ic} & \mathbf{0} \\ {}_A\mathbf{H}_{ci} & {}_A\mathbf{H}_{cc} & \mathbf{0} \\ \mathbf{0} & \mathbf{0} & {}_B\mathbf{H}_{ii} \end{bmatrix}-\begin{bmatrix} {}_A\mathbf{H}_{ic} \\ {}_A\mathbf{H}_{cc} \\ -{}_B\mathbf{H}_{ic} \end{bmatrix}\left[{}_A\mathbf{H}_{cc}+{}_B\mathbf{H}_{cc}\right]^{-1}\begin{bmatrix} {}_A\mathbf{H}_{ci} \\ {}_A\mathbf{H}_{cc} \\ -{}_B\mathbf{H}_{ci} \end{bmatrix}^T \tag{5.8}$$

Using the same structural coupling concept as described above, Ferreira [13] considered the flexibilities between the connecting DOFs and modelled them with an additional matrix, which, in the presence of nonlinearity, is deduced with describing function method. The derivation starts from defining separately the pre- and post- coupling matrices as:

$$\begin{Bmatrix} \mathbf{U}_i \\ \mathbf{U}_p \\ \mathbf{U}_q \end{Bmatrix} = \begin{bmatrix} \mathbf{H}_{ii} & \mathbf{H}_{ip} & \mathbf{H}_{iq} \\ \mathbf{H}_{pi} & \mathbf{H}_{pp} & \mathbf{H}_{pq} \\ \mathbf{H}_{qi} & \mathbf{H}_{qp} & \mathbf{H}_{qq} \end{bmatrix} \begin{Bmatrix} \mathbf{F}_i \\ \mathbf{F}_p \\ \mathbf{F}_q \end{Bmatrix} \tag{5.9}$$

And

$$\begin{Bmatrix} \mathbf{U}_I \\ \mathbf{U}_P \\ \mathbf{U}_Q \end{Bmatrix} = \begin{bmatrix} \mathbf{H}_{II} & \mathbf{H}_{IP} & \mathbf{H}_{IQ} \\ \mathbf{H}_{PI} & \mathbf{H}_{PP} & \mathbf{H}_{PQ} \\ \mathbf{H}_{QI} & \mathbf{H}_{QP} & \mathbf{H}_{QQ} \end{bmatrix} \begin{Bmatrix} \mathbf{F}_I \\ \mathbf{F}_P \\ \mathbf{F}_Q \end{Bmatrix} \tag{5.10}$$

Here the lower-case subscripts represent the matrices obtained in the pre-coupling condition, and the upper-case subscripts the post-coupling condition, which are to be determined from some mathematical manipulations. All the internal DOFs are grouped together as $\mathbf{U}_i$ and $\mathbf{U}_I$, and the connecting DOFs from the two joining components are expressed as $\mathbf{U}_p$, $\mathbf{U}_P$ and $\mathbf{U}_q$, $\mathbf{U}_Q$. The existence of the flexible joint poses different boundary compatibility and equilibrium conditions, and the joint is expressed as:

$$-\begin{Bmatrix} \mathbf{F}_p \\ \mathbf{F}_q \end{Bmatrix} = \begin{bmatrix} \boldsymbol{G}_{pp} & \boldsymbol{G}_{pq} \\ \boldsymbol{G}_{qp} & \boldsymbol{G}_{qq} \end{bmatrix} \begin{Bmatrix} \mathbf{U}_p \\ \mathbf{U}_q \end{Bmatrix} = [\boldsymbol{G}] \begin{Bmatrix} \mathbf{U}_p \\ \mathbf{U}_q \end{Bmatrix} \tag{5.11}$$

Each entry of the matrix $[\boldsymbol{G}]$ is a main-harmonic describing function for the joint impedance of a connecting pair. The describing function is a quasi-linear representation for a nonlinear element subjected to sinusoidal excitation. The resultant system equation, including the effect of nonlinear joint, is expressed as:

$$\begin{Bmatrix} \mathbf{U}_I \\ \mathbf{U}_P \\ \mathbf{U}_Q \end{Bmatrix} = \left[\begin{bmatrix} \mathbf{H}_{ii} & \mathbf{H}_{ip} & \mathbf{H}_{iq} \\ \mathbf{H}_{pi} & \mathbf{H}_{pp} & \mathbf{H}_{pq} \\ \mathbf{H}_{qi} & \mathbf{H}_{qp} & \mathbf{H}_{qq} \end{bmatrix} - \begin{bmatrix} \mathbf{H}_{ip} - \mathbf{H}_{iq} \\ \mathbf{H}_{pp} - \mathbf{H}_{pq} \\ \mathbf{H}_{qp} - \mathbf{H}_{qq} \end{bmatrix} [\mathbf{B}]^{-1} \begin{bmatrix} \mathbf{H}_{ip} - \mathbf{H}_{iq} \\ \mathbf{H}_{pp} - \mathbf{H}_{pq} \\ \mathbf{H}_{qp} - \mathbf{H}_{qq} \end{bmatrix}^T \right] \begin{Bmatrix} \mathbf{F}_I \\ \mathbf{F}_P \\ \mathbf{F}_Q \end{Bmatrix} \tag{5.12}$$

in which

$$\mathbf{B} = \mathbf{H}_{pp} + \mathbf{H}_{qq} - \mathbf{H}_{pq} - \mathbf{H}_{qp} + \boldsymbol{G}^{-1} \tag{5.13}$$

Each describing function is a function of relative displacements between the connection coordinates; therefore equation (5.12) is a system of nonlinear algebraic equations to be solved iteratively at each frequency point of interest.

The above derivation shows how two component models can be 'joined' mathematically. The same concept can be extended to 'join' more than two component models at one time. This can be achieved by re-arranging the FRF matrix. Additionally, multi-harmonic terms can be included in the describing functions [13, 72]. They will nevertheless multiply the order of the problem, and make this method non-economical.

5.2.3 Nonlinear FRF Coupling with Harmonic Balance Method

For a structural assembly with the equation of motion:

$$[\mathbf{M}]\{\ddot{\mathbf{u}}(t)\} + [\mathbf{C}]\{\dot{\mathbf{u}}(t)\} + [\mathbf{K}]\{\mathbf{u}(t)\} + \{\mathbf{g}(\mathbf{u}(t), \dot{\mathbf{u}}(t))\} = \{\mathbf{f}\} \tag{5.14}$$

the response, excitation and nonlinear internal force are expressed in complex multi-harmonic terms:

$$\begin{aligned}
{}_m\mathbf{u} &= {}_m\mathbf{U}^0 + \sum_{n=1}^{N} {}_m\mathbf{U}^n e^{i\frac{n}{m}\omega t} \\
{}_m\dot{\mathbf{u}} &= \sum_{n=1}^{N} i\left(\frac{n}{m}\omega\right) {}_m\mathbf{U}^n e^{i\frac{n}{m}\omega t} \\
{}_m\ddot{\mathbf{u}} &= -\sum_{n=1}^{N}\left(\frac{n}{m}\omega\right)^2 {}_m\mathbf{U}^n e^{i\frac{n}{m}\omega t} \\
{}_m\mathbf{g}(\mathbf{u}, \dot{\mathbf{u}}) &= {}_m\mathbf{G}^0({}_m\mathbf{U}) + \sum_{n=1}^{N} {}_m\mathbf{G}^n(\mathbf{U}) e^{i\frac{n}{m}\omega t} \\
{}_m\mathbf{f} &= {}_m\mathbf{F}^0 + \sum_{n=1}^{N} {}_m\mathbf{F}^n e^{i\frac{n}{m}\omega t}
\end{aligned} \tag{5.15}$$

in which ω is the frequency of the external harmonic forcing, and m is an integer corresponding to the ratio of the period of the external forcing to the period of the response. It is used to count for sub-harmonic responses; m=1 when the dominant harmonic in the response is the same as that of the excitation; ${}_m\mathbf{U}^n$ is the amplitude of the n^{th} complex harmonic term; N is the total number of harmonic terms included in the Fourier series expansions.

Substitute (5.15) into (5.14) and balance each harmonic term. The subscript *m* is dropped for clarity.

$$\begin{aligned}
&\mathbf{K}\mathbf{U}^0+\mathbf{G}^0\left(\mathbf{U}\right)=\mathbf{Z}^0\left(\omega\right)\mathbf{U}_0+\mathbf{G}^0\left(\mathbf{U}\right)=\mathbf{F}^0\\
&\left[\mathbf{K}-\left(\frac{1}{m}\omega\right)^2\mathbf{M}+\left(i\frac{1}{m}\omega\right)\mathbf{C}\right]\mathbf{U}^1+\mathbf{G}^1\left(\mathbf{U}\right)=\mathbf{Z}^1\left(\omega\right)\mathbf{U}^1+\mathbf{G}^1\left(\mathbf{U}\right)=\mathbf{F}^1\\
&\vdots\\
&\left[\mathbf{K}-\left(\frac{n}{m}\omega\right)^2\mathbf{M}+\left(i\frac{n}{m}\omega\right)\mathbf{C}\right]\mathbf{U}^n+\mathbf{G}^n\left(\mathbf{U}\right)=\mathbf{Z}^n\left(\omega\right)\mathbf{U}^n+\mathbf{G}^n\left(\mathbf{U}\right)=\mathbf{F}^n\\
&\vdots\\
&\left[\mathbf{K}-\left(\frac{N}{m}\omega\right)^2\mathbf{M}+\left(i\frac{N}{m}\omega\right)\mathbf{C}\right]\mathbf{U}^N+\mathbf{G}^N\left(\mathbf{U}\right)=\mathbf{Z}^N\left(\omega\right)\mathbf{U}^N+\mathbf{G}^N\left(\mathbf{U}\right)=\mathbf{F}^N
\end{aligned} \tag{5.16}$$

Combine all these equations into a compact equation:

$$\mathbf{R}\left(\mathbf{U}\right)=\mathbf{Z}\left(\omega\right)\mathbf{U}-\mathbf{F}+\mathbf{G}\left(\mathbf{U}\right)=0 \tag{5.17}$$

Where $\mathbf{U}=\left\{\mathbf{U}^0,\mathbf{U}^1,\cdots,\mathbf{U}^n,\cdots,\mathbf{U}^N\right\}^T$ is a vector of harmonic coefficients of the response at all system DOFs; $\mathbf{F}=\left\{\mathbf{F}^0,\mathbf{F}^1,\cdots,\mathbf{F}^n,\cdots,\mathbf{F}^N\right\}^T$ is a vector of harmonic coefficients of the external excitation force; $\mathbf{G}\left(\mathbf{U}\right)=\left\{\mathbf{G}^0,\mathbf{G}^1,\cdots,\mathbf{G}^n,\cdots,\mathbf{G}^N\right\}^T$ is a vector of harmonic coefficients for all the nonlinear internal forces; $\mathbf{Z}\left(\omega\right)$ is the dynamic stiffness matrix of the linear part of the system, composed of all harmonic components as:

$$\mathbf{Z}\left(\omega\right)=\begin{bmatrix}
\mathbf{K} & \mathbf{0} & \mathbf{0} & \cdots & \mathbf{0} & \mathbf{0}\\
\mathbf{0} & \mathbf{K}-\left(\frac{1}{m}\omega\right)^2\mathbf{M}+i\left(\frac{1}{m}\omega\right)\mathbf{C} & \mathbf{0} & \cdots & \mathbf{0} & \mathbf{0}\\
\mathbf{0} & \mathbf{0} & \ddots & \cdots & \mathbf{0} & \mathbf{0}\\
\vdots & \vdots & \vdots & \mathbf{K}-\left(\frac{n}{m}\omega\right)^2\mathbf{M}+i\left(\frac{n}{m}\omega\right)\mathbf{C} & \vdots & \vdots\\
\mathbf{0} & \mathbf{0} & \mathbf{0} & \cdots & \ddots & \mathbf{0}\\
\mathbf{0} & \mathbf{0} & \mathbf{0} & \cdots & \mathbf{0} & \mathbf{K}-\left(\frac{N}{m}\omega\right)^2\mathbf{M}+i\left(\frac{N}{m}\omega\right)\mathbf{C}
\end{bmatrix} \tag{5.18}$$

This is very similar to equation (4.32), only that this time the entries are in complex form and the size of the matrix is half the original. Multiply (5.17) with

the FRF matrix of the uncoupled assembly, including all the harmonic terms of interest, and we will have:

$$\mathbf{R}(\mathbf{U}) = \mathbf{U} - \mathbf{H}(\omega)[\mathbf{F} - \mathbf{G}(\mathbf{U})] = 0 \tag{5.19}$$

in which:

$$\mathbf{H}(\omega) = \begin{bmatrix} [\mathbf{K}]^{-1} & \mathbf{0} & \mathbf{0} & \cdots & \mathbf{0} & \mathbf{0} \\ \mathbf{0} & \left[\mathbf{K} - \left(\frac{1}{m}\omega\right)^2 \mathbf{M} + i\left(\frac{1}{m}\omega\right)\mathbf{C}\right]^{-1} & \mathbf{0} & \cdots & \mathbf{0} & \mathbf{0} \\ \mathbf{0} & \mathbf{0} & \ddots & \cdots & \mathbf{0} & \mathbf{0} \\ \vdots & \vdots & \vdots & \left[\mathbf{K} - \left(\frac{n}{m}\omega\right)^2 \mathbf{M} + i\left(\frac{n}{m}\omega\right)\mathbf{C}\right]^{-1} & \vdots & \vdots \\ \mathbf{0} & \mathbf{0} & \mathbf{0} & \cdots & \ddots & \mathbf{0} \\ \mathbf{0} & \mathbf{0} & \mathbf{0} & \cdots & \mathbf{0} & \left[\mathbf{K} - \left(\frac{N}{m}\omega\right)^2 \mathbf{M} + i\left(\frac{N}{m}\omega\right)\mathbf{C}\right]^{-1} \end{bmatrix} \tag{5.20}$$

This equation can be solved with the Newton-Raphson iteration method, which has quadratic convergence when an initial approximation is close enough to the exact solution. The attractive bit of this equation is that the FRF matrix, $\mathbf{H}(\omega)$, can be readily formed either from direct experimental measurement or from FE modal calculations of the linear combination of the whole assembly. For the n^{th} harmonic term in the FRF matrix:

$$\mathbf{H}^n(\omega) = \sum_{r=1}^{N_m} \frac{\boldsymbol{\psi}_r \boldsymbol{\psi}_r^*}{(1 - i\eta_r)\omega_r^2 - \left(\frac{n}{m}\omega\right)^2} \tag{5.21}$$

In which, N_m is the number of modes that are used in the modal expansion; ω_r and $\boldsymbol{\psi}_r$ are the corresponding r^{th} natural frequency and mode shape. In many cases, a small number of modes kept in the modal expansion will provide sufficient accuracy in the formation of the FRF matrix.

The use of the FRF matrix to describe the assembly system allows all DOFs where only linear internal interaction forces are applied to be excluded without any loss of accuracy and completeness of the model [64]. The resultant equation only includes DOFs where nonlinear internal interaction forces and external excitation forces are applied, and where the responses are of concern. This will

considerably reduce the size of the equations and the computational cost accordingly.

In order to exclude those linear DOFs, equation (5.19) can be re-written in a form in which the displacement vector of a particular harmonic term $\mathbf{U}^n$ is partitioned into a vector consisting discarded linear DOFs $\mathbf{U}^n_{\text{lin\_d}}$, retained linear DOFs $\mathbf{U}^n_{\text{lin\_r}}$ and nonlinear DOFs $\mathbf{U}^n_{\text{nln}}$.

$$\mathbf{R}\left(\mathbf{U}^n\right)=\begin{Bmatrix}\mathbf{U}^n_{\text{lin\_d}}\\ \mathbf{U}^n_{\text{lin\_r}}\\ \mathbf{U}^n_{\text{nln}}\end{Bmatrix}-\left[\mathbf{H}^n\left(\omega\right)\right]\left[\begin{Bmatrix}\mathbf{F}^n_{\text{lin\_d}}\\ \mathbf{F}^n_{\text{lin\_r}}\\ \mathbf{F}^n_{\text{nln}}\end{Bmatrix}-\begin{Bmatrix}\mathbf{G}^n_{\text{lin\_d}}\\ \mathbf{G}^n_{\text{lin\_r}}\\ \mathbf{G}^n_{\text{nln}}\end{Bmatrix}\right] \tag{5.22}$$

With the fact that $\mathbf{F}^n_{\text{lin\_d}}=\mathbf{0}$ and $\mathbf{G}^n_{\text{lin\_d}}=\mathbf{0}$, this equation is reduced to:

$$\mathbf{R}\left(\mathbf{U}^n_{\text{red}}\right)=\begin{Bmatrix}\mathbf{U}^n_{\text{lin\_r}}\\ \mathbf{U}^n_{\text{nln}}\end{Bmatrix}-\left[\mathbf{H}^n_{\text{red}}\left(\omega\right)\right]\left[\begin{Bmatrix}\mathbf{F}^n_{\text{lin\_r}}\\ \mathbf{F}^n_{\text{nln}}\end{Bmatrix}-\begin{Bmatrix}\mathbf{G}^n_{\text{lin\_r}}\\ \mathbf{G}^n_{\text{nln}}\end{Bmatrix}\right] \tag{5.23}$$

or, in a more compact form:

$$\mathbf{R}\left(\mathbf{U}^n_{\text{red}}\right)=\mathbf{U}^n_{\text{red}}-\mathbf{H}^n_{\text{red}}\left(\omega\right)\left[\mathbf{F}^n_{\text{red}}-\mathbf{G}^n_{\text{red}}\right] \tag{5.24}$$

and with all the harmonics included, equation (5.19) is reduced to:

$$\mathbf{R}\left(\mathbf{U}_{\text{red}}\right)=\mathbf{U}_{\text{red}}-\mathbf{H}_{\text{red}}\left(\omega\right)\left[\mathbf{F}_{\text{red}}-\mathbf{G}_{\text{red}}\left(\mathbf{U}_{\text{red}}\right)\right]=0 \tag{5.25}$$

Equation (5.25) can be solved numerically with the Newton-Raphson method detailed in section 4.3.3.

5.3 Case Studies

In this section, a representative aero-engine test rig model is studied. This single-rotor test rig has one of its two bearing supports specially designed to exhibit considerable nonlinearity, and this results in the whole assembly being studied with nonlinear approaches. The linear parts of the test rig are all flexible; hence adequately detailed FE models are needed to capture even localised flexibilities. This nevertheless leads to large order system equations to be solved.

In the field of structural dynamics involving rotating components, mostly encountered in the literature are those analyses based on simplified models,

which are of course useful in exemplifying the unique properties that only rotating equipments possess. In those analyses, the foundation or casing is generally, or sometimes conveniently, considered rigid, which is not true in practical structures. Large steam turbines, for instance, have foundations which become relatively flexible for the heavy rotors and aircraft engines tend to have very flexible casings [73]. With the development of FE software packages, analyses on models with fairly detailed geometric complexity and with the flexibility of both stator and rotor included is possible [73] even though it is only for linear systems.

When nonlinearity is involved, for example, with a system of linear stator and rotor connected with nonlinear bearings, the analysis normally begins with a 'heavy' simplification of the linear components, in order to efficiently carry out the investigation of the nonlinear phenomenon [74]. A step further in this approach is to perform linear model reduction on the component models first before applying time-domain [75], or frequency-domain calculations.

The first two case studies in this section show the application of the nonlinear FRF coupling with Harmonic Balance Method. The purpose is to show the flexibility and efficiency of this approach in dealing with a complicated nonlinear system. The third case is an impact simulation of the same nonlinear system using a time marching method. Even though good results were obtained, the time spent on the calculation was simply massive.

5.3.1 Description of Test Rig Model

The representative aero-engine test rig has been modelled in SolidWorks®, as shown in Figure 5 - 1. It consists of a flexible rotor-shaft assembly, which is supported on two bearing supports. One of these is specially designed so that it is flexible in the horizontal direction and rigid in the vertical direction. The design details of the bearing will be discussed in Chapter 7. The rotor-shaft assembly is enclosed in a flexible casing, which is set to be semi-transparent in the figure for clarity. The casing is bolted to a steel bar which has one of its end fixed to ground so that the whole assembly mimics an engine hung under a wing. The model is constructed with as much geometric complexity as possible so as to

represent a real structure more accurately. The exact dimensions of each component can be found in Appendix A.

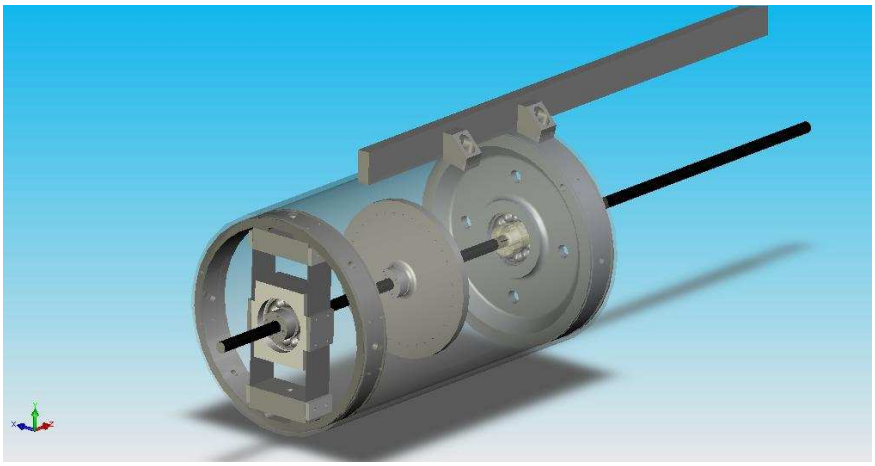

Figure 5 - 1 A schematic view of the test rig in Solidworks®

The 3-D solid model of the test rig was exported to ANSYS®, and the resultant FE model is shown in Figure 5 - 2, in which (b) is a cross-sectional view. Besides the two vertical strips attached to the front bearing block, which are displayed in purple, the bulk structure is formed with element Solid45[1]. The two vertical strips are formed with Shell63[2]. There are a total of 24065 elements and 46055 nodes, which comprise 138165 DOFs when the full system equation is formed. This is of course not comparable to the scale of industrial engine models; nevertheless, such a size of FE model has not been seen applied with various nonlinear methodologies in literature.

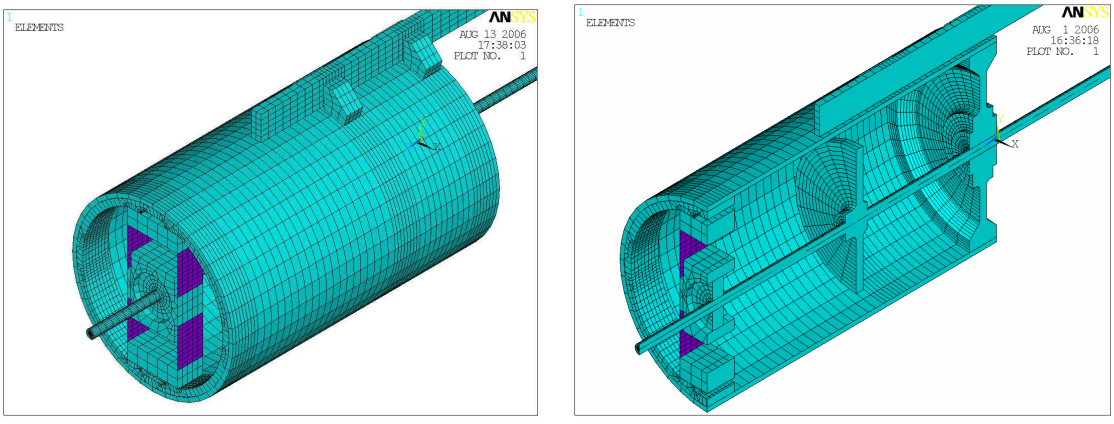

(a) **(b)**

Figure 5 - 2 FE model of the test rig

[1] Solid45 is a 3-D structural solid element in ANSYS®. This element is defined by eight nodes having three translational degrees of freedom at each node.

[2] Shell63 is a 3-D structural Elastic Shell element in ANSYS®. This element is defined by 4 nodes having three translational and three rotational degrees of freedom at each node.

It is assumed that individual components have been validated against real structures via modal testing and analysis. This is extremely important because the components are integral parts of the whole assembly, and mistakes or inaccuracies made at the component level will guarantee a faulty assembly model. Periodic external excitation will be applied to the whole structure and the steady-state response is calculated at any DOF of interest.

5.3.2 Calculation Procedure

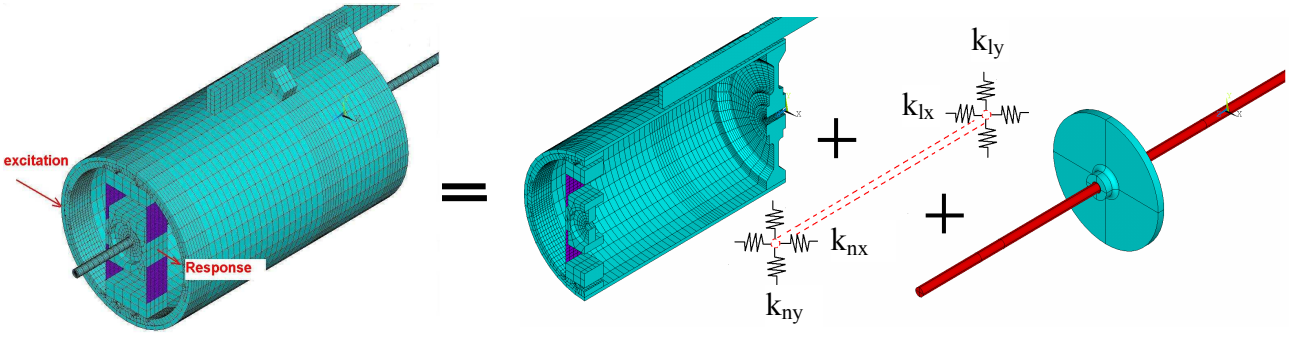

Figure 5 - 3 Separate the test rig for implementing nonlinear coupling method

The test rig is divided into three parts, (i) shaft-rotor assembly, (ii) stator (including bearing supports and all the other structural parts) and (iii) joint, as shown in Figure 5 - 3. The shaft-rotor and stator are joined together by spring elements k_{lx}, k_{ly}, k_{nx} and k_{ny}. The former two link the shaft to the rear bearing support, while the latter two connect the shaft to the front bearing support. It is assumed that $k_{lx}=k_{ly}=k_{ny}=\infty$, which means rigid connections between the shaft and bearing support. k_{nx} represents a flexible connection, which is due to the two vertical stripes that are flexible in the horizontal direction. This horizontal stiffness can be adjusted by changing the length of the strips.

The calculation steps are:

Step 1: Perform modal calculations on both rotor-shaft assembly and stator using FE software to extract modal models of both. The mode shapes are mass normalised.

Step 2: Define DOFs and the number of harmonics to be included in the Harmonic Balance Method calculation. All the interface DOFs, excitation DOFs and DOFs where responses are of interest are included. FRFs at those selected DOFs are calculated using the modal data collected in step 1.

Step 3: Define joint parameters. This also includes providing information of DOF pairs where the connection is made. Both damping and stiffness are used to quantify the joint properties.

Step 4: Apply Harmonic Balance Method with FRF coupling. An internally developed code FORSE [66] is used.

5.3.3 Results

When the two vertical strips are slightly compressed, buckling occurs. The stiffness k_{nx} displays properties as plotted in Figure 5 - 4, which is from a real experiment measurement. O is the global centre, which is an unstable equilibrium point. A and B are two stable local equilibrium points.

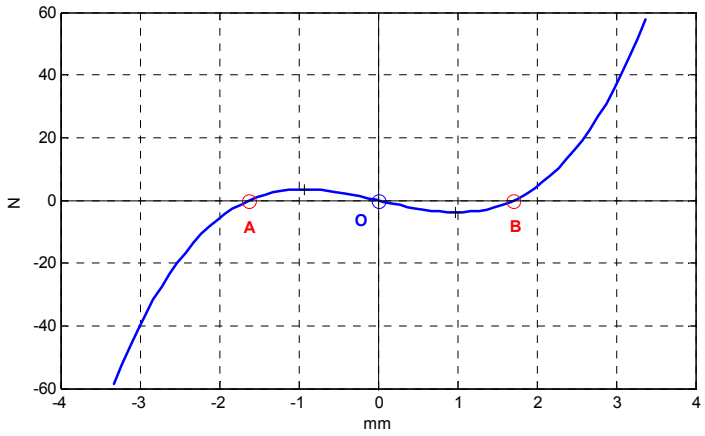

Figure 5 - 4 Force and displacement relation of the stiffness k_{nx}

5.3.3.1 Case one – joint with weakening stiffness property

Small periodic excitation force is used in this case. The excitation and response nodes and directions are shown in Figure 5 - 3. It is expected that the DOFs connected with spring k_{nx} vibrate locally around either point A or B along the stiffness property line as shown in Figure 5 - 4. This is indeed a case of weakening stiffness. The resultant Frequency Response Function plot is shown in Figure 5 - 5. Four calculation runs were carried out, using different excitation force levels as marked in the drawing. The mode at 27Hz is prominently affected by the joint nonlinearity. The FRF curves bend towards lower frequency as the excitation force increases. This manifests a weakening stiffness. Figure 5 - 6 shows a closer look of the FRF curves nearby 27Hz. The mode at 75Hz is not affected by the nonlinearity. It is observed in the FE simulation that this is the

second bending mode of the whole test rig in the horizontal direction, which is not influenced by the nonlinear stiffness we have set.

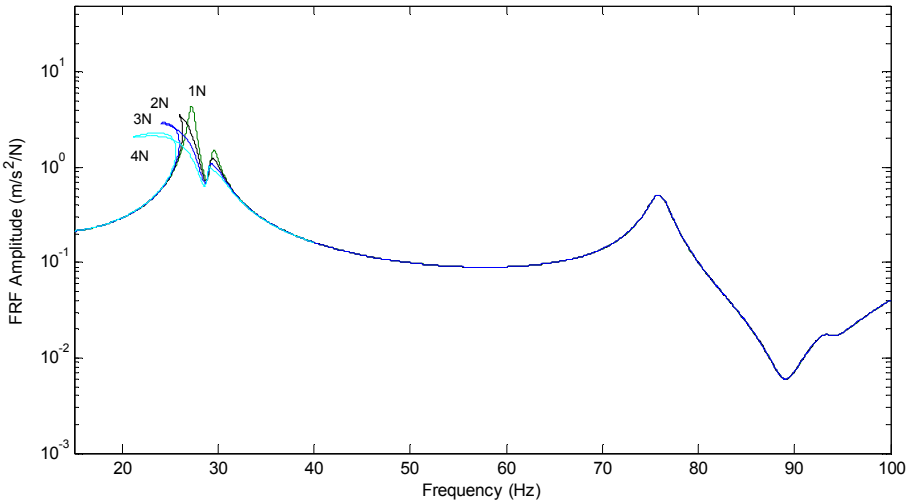

Figure 5 - 5 Frequency response function curves based on Harmonic Balance Method calculation for a system with joint of weakening stiffness property

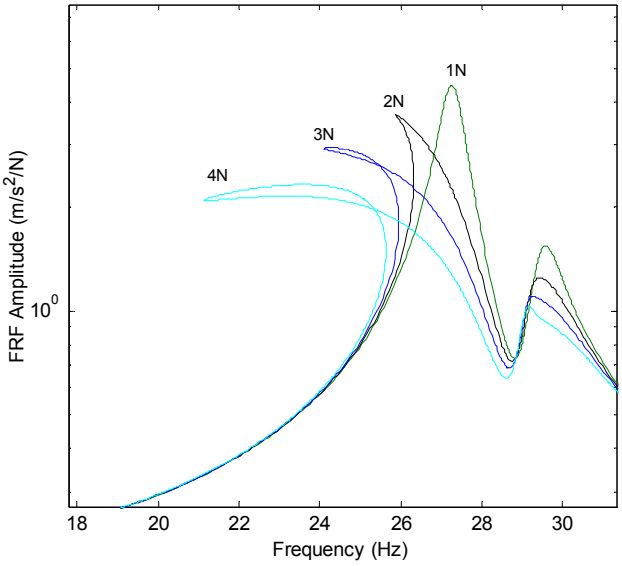

Figure 5 - 6 A close look of the frequency response function curves nearby 27.5Hz

5.3.3.2 Case two – joint with polynomial stiffness property

Large periodic excitation force is used in this case. The excitation and response nodes and directions are shown in Figure 5 - 3. It is expected that the DOFs connected with spring k_{nx} vibrate globally around point O along the stiffness property line in Figure 5 - 4.

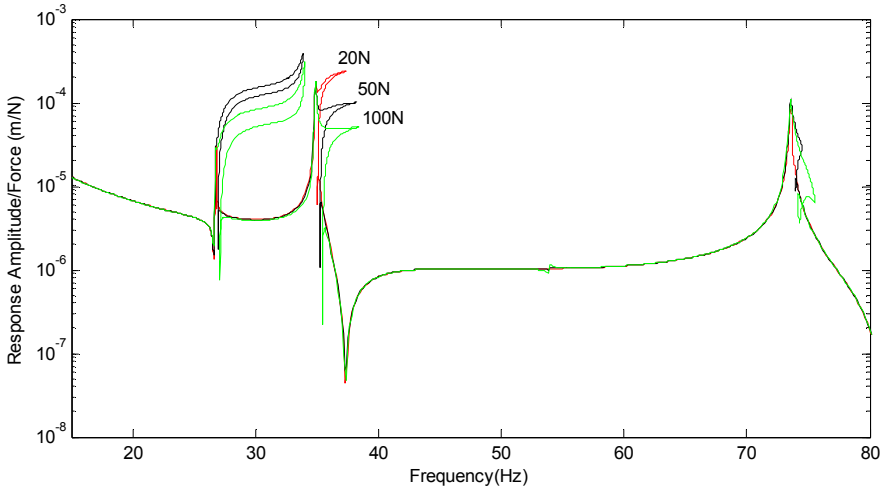

Figure 5 - 7 Frequency response function curves based on Harmonic Balance Method Calculation for system with joint of polynomial stiffness property

Figure 5 - 7 shows the results of three runs of calculation at different force levels, as marked. It is difficult to verify such a result with other types of simulation. It is however evident to see from the graph the characteristic of hardening stiffness effect. The FRF curves at each mode bend towards higher frequency as the excitation force increases. Globally speaking, k_{nx} is a hardening stiffness.

5.3.3.3 Case Three – Impact Simulation

Each run in the previous two cases took 2-5 minutes of computing time on a normal PC with Pentium4 processor, depending on the frequency span and the number of harmonics to be included in the harmonic balance calculation. It is very difficult, if not totally impossible, to simulate a nonlinear system of 138165 number of DOFs to get the steady state periodic solution. To demonstrate the efficiency of the Harmonic Balance Method, a time marching calculation of the same system has been carried out. An impact was applied at the excitation point and the time signature was read at the response point shown in Figure 5 - 3.

Figure 5 - 8 shows the time marching calculation result of the test rig experiencing an impact. This is indeed a transient analysis, carried out in ANSYS®. A Total of 245 time steps with variable sizes were used in the calculation, amounting to 1.9 seconds of real time. 72 minutes of CPU time was consumed. It is imaginable that much more CPU time is required if the steady state solution is of concern; and if the results over the whole spectrum are needed, it may possibly take a few weeks. Considering this is a fairly simple rig

model comparing to the industrial ones, it apparently shows the advantage of the Harmonic Balance Method in cutting down the calculation time for such a nonlinear system.

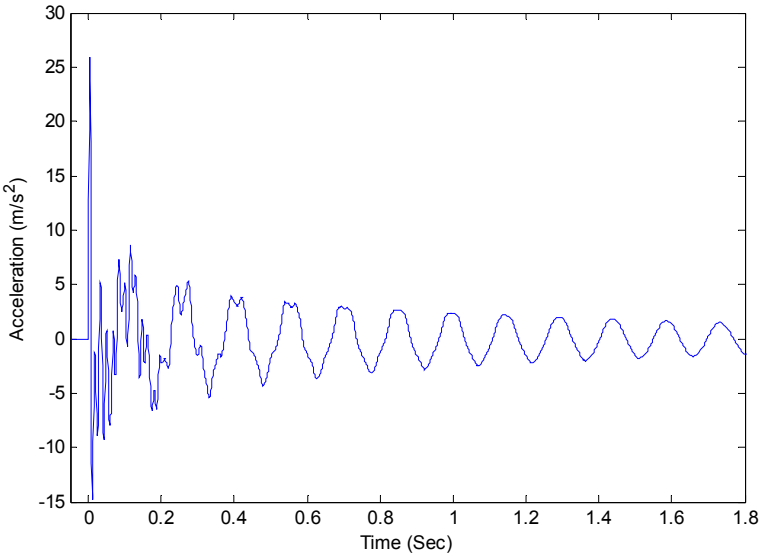

Figure 5 - 8 Time marching calculation result

This impact simulation result has actually been compared with an impact test [76]. It showed good agreement as demonstrated in the following plot, in which the red line is the experimental measurement data.

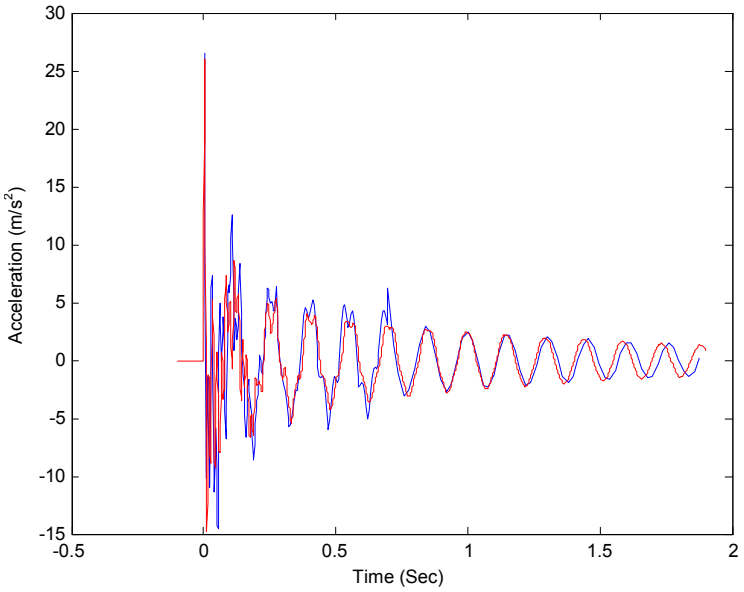

Figure 5 - 9 Time marching calculation result comparison

5.4 Concluding Remarks

Examples in the above case study shows how efficient the FRF coupling with Harmonic Balance Method is in dealing with a large scale structural assembly with localised nonlinearity. It takes no more than a few minutes to find steady state solutions across the spectrum. If a conventional time domain method is used, it will take hours of CPU time just to calculate a transient response for such a system.

There are other nonlinear structural coupling methods available and were discussed in this chapter. In general, they are using linear coupling methods to firstly reduce the size of the problem and then apply different nonlinear methods on the reduced model. The accuracy of the response calculation for the assembly depends on how well the linear model is reduced, which normally has some approximation implied in the process. FRF coupling method, on the other hand, is an exact method, which is of course preferred if it can be integrated with certain nonlinear methods.

Chapter 6

Structural Dynamic Testing and FRF Measurement Techniques

6.1 Introduction

Structural dynamic testing is a very broad topic. Depending on its purpose, there are two types of dynamic test we normally encounter. The first type involves the test structure being subjected to a real or simulated environment in which it operates. By doing so, we can assess the test structure's dynamic behaviour under working conditions. This type of test is also called an operational test, which is especially widely used when a product is at its final design stages. Information, such as how or whether it will survive extreme working conditions, or whether its performance satisfies the design criterion, is collected. This type of test normally only requires the measurement of the response level to understand the behaviour of the test structure. The second type of dynamic test is meant to establish more detailed knowledge of the structure by linking the excitation and response. By doing so, it is possible to build a mathematical model to represent the structure. The same type of mathematic model can also be derived from theoretical analysis, mainly with the help of Finite Element based software. Hence, we can link design with test, aiming to update and validate the FE models, and to make design modifications more predictable. This type of test

is widely known as Modal Testing, in which measuring the Frequency Response Functions and extracting the modal properties are the main objectives. This chapter focuses on modal testing and its extension into nonlinear territory, in which the relation between the response and excitation are still sought after.

With the advancement of computing technology and the Finite Element methods, it is suggested that tests can be substituted with simulations of computer-generated mathematical models. It is never unreasonable to imagine so, but at the moment dynamic testing is not replaceable, simply because:

- Some important physical parameters still cannot be modelled correctly due to our limited understanding, e.g. friction, which sometimes has a big influence on the dynamic behaviour of the whole structure;
- Even if it is possible to model the structure correctly, variability between products of the same design will induce different dynamic behaviour;
- Not all working conditions can be simulated. Either it is too complicated to describe or simply not economical to be put into calculation;
- Human error during the modelling stage are difficult to discover;
- Last but not least, in the process of developing and validating new simulation algorithms, comparison with test results of a physical item is essential.

Being able to understand the necessity of a dynamic test helps to appreciate the importance of good test practice. A physical test is just like a mathematical modelling and simulation job. It involves a chain of operations, mistakes at any one of which will cause errors in the results. This is particularly dangerous because people tend to have more confidence in the test results than in computer simulated ones and trust more what they can observe physically. Therefore, a deep understanding of the test itself is very important: from test setup to data processing, from test structure preparation to catering for physical limitations of test system.

In this chapter, the basic measurement chain in Modal Testing is introduced first, and is followed by detailed descriptions of test equipment used in those tests involved in this thesis work. FRF measurement techniques are presented afterwards. They are grouped according to different types of excitation signals used, with the understanding that FRF derivation varies depending on the signal

form. The advantages and disadvantages of each type of signal are also discussed. This leads to the discussion of FRF measurement on nonlinear structures. Special treatment is required to identify nonlinearity in a structure, or to validate predictions from nonlinear calculation algorithms. The amplitude of either excitation or response must be controlled. An algorithm is presented mathematically on how it is done. This algorithm has been implemented in a LabVIEW-based code.

It should be noted that dynamic testing can be a topic of a whole book [77, 78]. It is not the author's intention to display here every bit of it, rather, only those relevant to this thesis work are touched upon.

6.2 Basic Measurement Chain

We expect to obtain the dynamic properties of a structure, in terms of natural frequencies, damping ratios and mode shapes, by conducting dynamic tests. Those properties can be deduced from the Frequency Response Function, which is obtained by taking the ratio between the response and excitation in the frequency domain; hence it is natural to design an experiment that enables both excitation and response to be measured simultaneously.

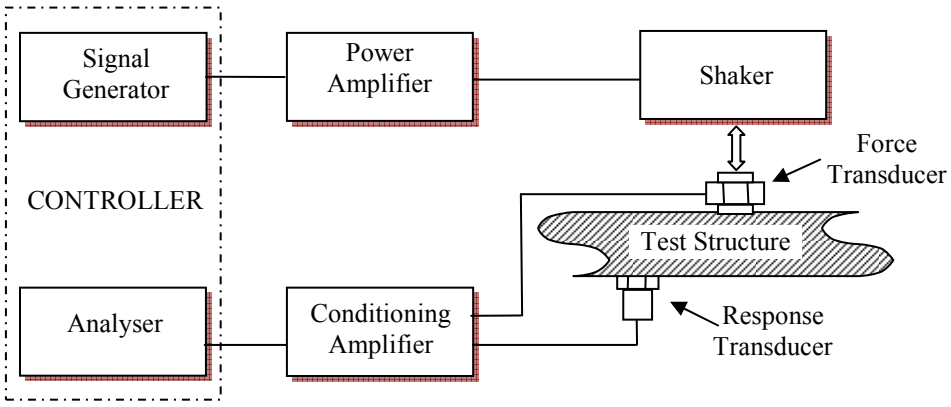

Figure 6 - 10 Schematic representation of basic measurement chain for modal testing

Figure 6 - 10 shows a typical experimental setup used for FRF measurement. There are many variations in terms of the exact hardware used and the way data processed. Nevertheless, all the setups consist the following major items [1]:

- Excitation system: Signal Generator, Power Amplifier, Shaker, Impact Hammer, etc;
- Sensing system: Transducers, Conditioning Amplifier, etc;

- Analysing System: FFT Analyser, etc.

The various tests conducted within this thesis used the above basic measurement chain. The excitation to the test structure is provided by the shaker, which generates a motion following the pattern of the electric current signal it receives from the power amplifier. The excitation signal originates from the signal generator, which is capable of creating a variety of different signals to match the requirements of the structure under test, but it is usually sinusoidal. When an Impact Hammer is used as the excitation device, Signal Generator and Power Amplifier will not be used. The sensing system converts mechanical signals, e.g. force and acceleration, into electronic signals, which are easier to handle. After both excitation and response signals are collected and fed into the analyzer, in the form of time-domain analogue signals, the analyser converts them into frequency domain, and computes the Frequency Response Function hereafter.

It is a common practice nowadays that the signal generator and the analyser are combined into a single unit, which not only makes the test setup more compact, but also improves the controllability of the test itself. Controlled-level dynamic testing, which will be discussed in detail in later sections, is made possible by linking the output from the analyser to the creation of excitation signal from the signal generator; and this is easily accomplished in a single controller unit.

The test structure is also an integral part of the experimental setup. It influences the selection of hardware and excitation type to be used in order to maximise the data quality in a most economical way. The treatment of the test structure can affect the test results prominently. Topics that concern, for example, boundary conditions and optimised location of transducers, are themselves worth in-depth research effort.

6.3 Excitation and Measurement System

This section focuses on individual hardware used in various modal tests conducted within the scope of this thesis. Sound knowledge of the hardware's functionalities is the first step towards achieving reliable test results.

6.3.1 Excitation

The purpose of having an excitation source is to inject kinetic energy into the test structure, and by observing the behaviour of the structure, we can quantify its inherited dynamic properties. Many different types of excitation schemes are employed in vibration testing. Some examples are [77]: a sudden release of a static load; an impact force; mechanical exciter based on either direct-drive or rotating unbalance; electrohydraulic exciter and the most popular one: electromagnetic exciter, commonly known as a shaker. This section elaborates on the two excitation methods used in this thesis' experimental work. One is with the application of an impact hammer, and one with a shaker.

Vibration tests with the application of an impact hammer have some advantages that allow it to be used widely in structural dynamic testing. Firstly, the test setup is simple. The equipment consists of no more than a hammer with a set of different tips, which allow the excitation frequency range to be varied for different test structures. Secondly, hammer test is the fastest method when a preliminary result is needed. Thirdly, it is a much more economical tool comparing to shakers. Nevertheless, the impact hammer has shortcomings that make the use of the other types of exciter is a must in some cases. Firstly, it is an open-loop test. The applied force level is not controlled. This limits its application to linear test only. Secondly, the frequency range that the test structure can be excited is limited and restricted to the type of impact header used. It may possibly happen that some important vibration modes cannot be captured. Thirdly, though the test setup is simple, the requirement for the operator is actually quite high. He/she has to select the right types of impact tip, apply the right window functions to the signals, and be consistent in the way the impact is applied: the point of hitting should be precise, and the impact direction should be normal to the surface.

The electromagnetic shaker is perhaps the most common type of exciter. The supplied input signal is converted to an alternative magnetic field in which is placed a coil which is attached to the drive part of the device, and to the structure. Some of its advantages are: the frequency and amplitude of excitation can be controlled independently, giving more operational flexibility; a large frequency range can be applied, and the variety of excitation pattern is virtually limitless,

which solely depends on the capability of the signal generator; by linking the analyser and the signal generator, it is possible to implement a control system to conduct nonlinear test.

The choice of the exciter to be used depends on many factors, e.g., purpose of the test, time constraint, accuracy requirement, and physical constraint of the test structure. In this thesis, impact test is conducted for identifying the dynamic properties of linear structures with simple geometry. The shaker is used in the test to identify the nonlinearity, as well as validate the assembly algorithm. That will be presented in Chapter 7.

6.3.2 Sensing

It is shown from the basic measurement chain that both excitation and response of the structure need to be captured and quantified properly in order to construct the Frequency Response Functions to extract the dynamic properties. The mechanical response of a structure may be defined in terms of displacement, velocity or acceleration. Any one of these parameters can be used to derive the fundamental response function. The most commonly used response transducer is the piezoelectric accelerometer, and indeed the most common force transducer used is also piezo-material based.

Inside these piezoelectric transducers, piezoelectric materials, such as quartz or man-made ceramics are stressed in a controlled fashion by the input force or acceleration. This stress “squeezes” a quantity of electrical charge from the piezoelectric material in direct proportion to the input stress, creating analogue electrical output signal. Because of the high stiffness of those piezoelectric materials, the piezoelectric transducers have very high resonant frequencies, which enable them work very well across a large frequency range.

The electric charge released by the piezoelectric element is measured in the unit of picocoulomb. It is necessary to utilise amplifiers to couple information, contained within the tiny amount of electric charge, to the physical parameters without dissipating it or otherwise changing it. The output from the amplifier is a voltage signal, which is proportional to the electric charge, and in turn proportional to either force or acceleration being measured. Bruel&Kjaer Type 2626 Condition Amplifiers were used for this purpose.

Before doing any test, the transducers must be calibrated. The use of the manufacturers' quoted transducer sensitivities may not be accurate enough because they can change with time and environment conditions. Both force and motion transducers must be calibrated individually if they are to be used in a controlled-level nonlinear test. When only linear test is involved, the calibration can be conducted in pair, because the ratio of motion to force, not the individual values of each parameter is used to form the Frequency Response Function.

Figure 6 - 11 shows the calibration setup for a Brüel&Kjaer Type 4393 Piezoelectric Accelerometer. A PCB portable handshaker (Model 394C06) delivers a calibrating vibration signal at 159.2Hz with 1g RMS acceleration output. The electric charge is amplified by the conditioning amplifier and converted into a voltage signal, which is readable on the oscilloscope. The sensitivity of the accelerometer is calculated by comparing the amplitude from the readout of the oscilloscope and the calibrating signal. The resultant sensitivity is 3.26pC/g.

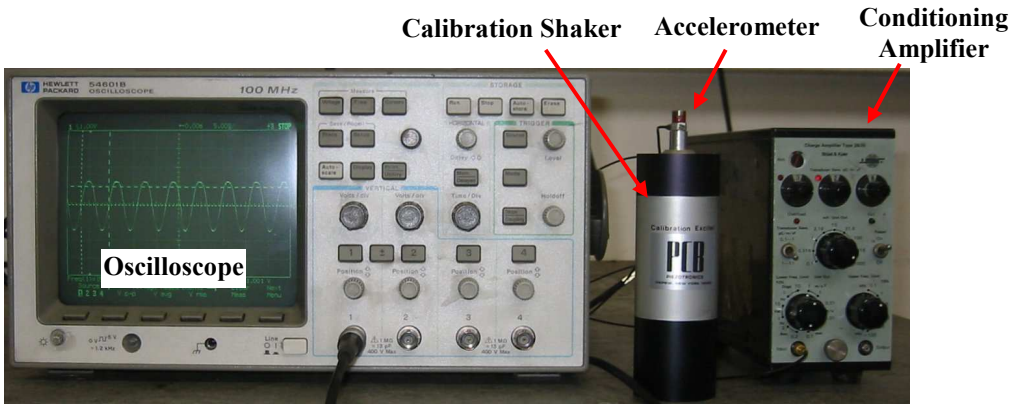

Figure 6 - 11 Calibration for the accelerometer

Figure 6 - 12 shows the calibration setup for a Brüel&Kjaer Type 8200 Piezoelectric force transducer. It is a reverse process to the normal modal testing. With the calibrated accelerometer and a solid mass of known weight, the resultant frequency response function is a straight line according to the following equation.

$$A(\omega) = \frac{\ddot{u}}{f} = \frac{1}{m} \tag{6.1}$$

The shaker generates a pure tone excitation at 159.2Hz. By reading out the acceleration and force signal in terms of voltage from the oscilloscope, and using

the above equation, the sensitivity of the force transducer can be calculated, which is 3.96pC/N.

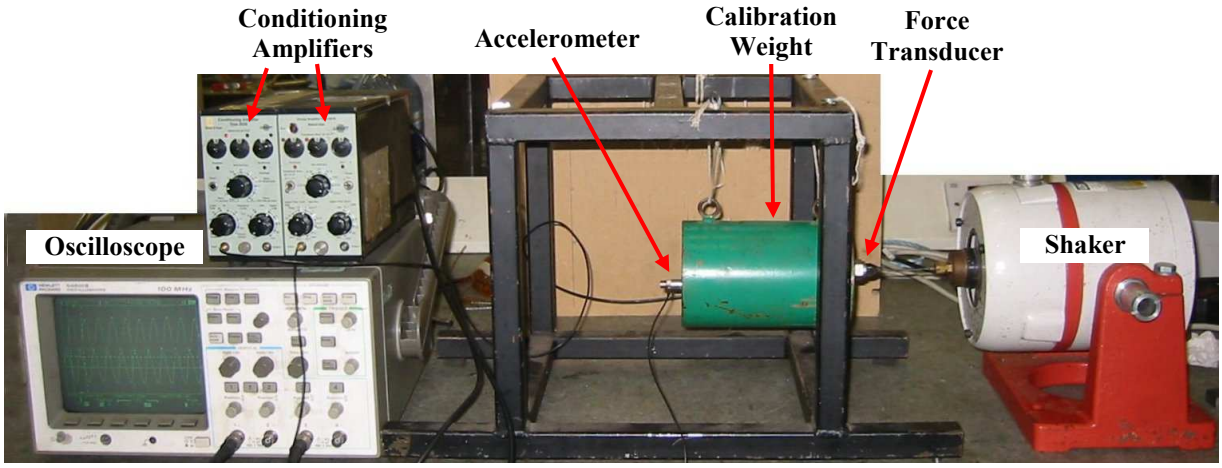

Figure 6 - 12 Calibration for the force transducer

6.3.3 Data Acquisition and Processing

The excitation and response signals from the transducers need to be acquired and processed in order to extract useful information to represent the tested structure. A fairly complicated device for such a purpose is called analyser. The most common type is based on Fast Fourier Transform (FFT) algorithm. It converts analogue time domain signal into digital frequency domain information that can be processed to produce FRFs. It is known as Spectrum Analyser or FFT Analyser. It is best for linear dynamic test, and an example of it is the PULSE™ system from Brüel & Kjaer.

Besides the stand-alone type of analysers like PULSE™, an analyser that consists of a data acquisition card and a PC based software code is also often seen. This is mainly due to the increasing PC computing power that allows the digital signal processing using software to be comparable to a hard-wired analyser in terms of speed and accuracy. This type of analyser also gives the user more control over the data.

Data acquisition and processing is a mature topic and the analysers have been developed for a few decades; however, it is still far from being automatic when operating them. Appropriate parameters need to be set for the analyser before starting a test. Problems, such as aliasing and leakage, must be avoided. Thorough discussions can be found in references [1, 16, 79].

6.4 FRF Measurement Techniques

The Frequency Response Function (FRF) is derived by converting time-domain data from measurement into frequency-domain and taking the ratio of response to excitation. Though similar hardwares are used, different calculation schemes are employed to obtain FRFs, depending on the type of excitation signal used. Different types of signal needs different treatment when frequency domain information is extracted. The selection of excitation type governs the type of transducers, digital signal processing procedures, i.e. the different FRF measurement techniques. In this section, the categorisation is based on the excitation signals used and we aim to choose the most suitable one according to the applicability and other practical considerations.

6.4.1 Sine Excitation

Sine excitation test is one of the most common methods to obtain FRFs. The commanding signal supplied to the exciter is a sinusoid with a fixed amplitude and frequency. A prime advantage of using sine excitation is the large signal-to-noise ratio for all the force and response measurements. This is a consequence of the single excitation frequency for each measurement – there are no other significant sources of excitation to contaminate the results [16]. Equally important for this type of excitation is that the input force level to or response level from the test structure can be accurately controlled by adjusting the excitation signal strength at any frequency point of interest. This is crucial in the successful evaluation of nonlinear structure due to the fact that the FRF curve in the resonance region is distorted at a constant force level, and the resonance frequency is shifted at different response levels.

The FRF is formed over the frequency range of interest. Therefore, the sine excitation needs to be carried out at frequency points within the range. There are two ways to do so. The excitation signal can be stepped from one discrete value to another in such a way [1] as to provide the necessary density of points on the frequency response plot. Alternatively, the excitation signal can be in the form of a continuous sinusoid, the frequency of which is varied slowly but continuously through the range of interest. The former method tends to be slower, but it allows more control over the signal's behaviour, which is crucial in nonlinear

test. The latter is much faster, but it requires extra care on the sweep rate, a wrong setting of which will introduce errors in the derived FRFs. Only step-sine excitation is used in this research.

One paramount drawback of this type of excitation is the time required to obtain an FRF is much more than other excitation methods, provided the other methods are applicable to the same task. In sine excitation, at each frequency step, adequate time must be allowed for the transients to die away before the force and acceleration signals are sampled and processed. Depending on the test algorithm, the delay can be in the form of time or number of vibration cycles or linked with some delay-time estimation algorithm [80]. It is a trade-off sometimes when selecting an excitation method, as which one is more important, accuracy or efficiency. If the purpose is to validate a simulation algorithm, a more rigorous and precise test scheme should be adopted.

6.4.2 Random Excitation

A random excitation signal is defined by a time history of random values at any given instant. It cannot be expressed by a simple mathematical equation, like the other types of excitation signals do, and it must be modelled probabilistically. It is widely used in linear dynamic test because it is a fast approach to obtain accurate estimation of a structure's response over a broad range of frequencies. A noticeable significance of the random signal is that it is a reasonable approximation to the type of excitation found in many typical installations in real life [16]. Random excitation is applied by an electromagnetic shaker driven with a signal from a random signal generator. The versatileness of the signal generator allows different definitions of probability distribution of the excitation to suit different purposes.

The application of random excitation in dynamic testing involves a great understanding of signal processing in order to avoid errors that are not so easily spotted. Some of the concerns are:

- a window function must be applied to the collected time-domain force and response data before the FFT is performed, because periodicity is a prerequisite of valid performance of converting time domain data to frequency domain;

- measurement duration and sample rate need to be well selected to avoid or minimise the leakage effect.

6.4.3 Impact Excitation

Impact excitation, also known as transient excitation is a very popular and convenient excitation technique to produce FRFs. In normal practice, this type of excitation is applied by an impact hammer, which includes a load cell, or force transducer, that detects the impact force applied to the test structure. The FRF measurement starts from sampling the time history of force and response signals, which are then converted into frequency domain by applying Fourier analysis. The force signal, a very short sharp excitation pulse in the time domain, has a flat spectrum over a wide frequency range. Because of this unique property, it is possible to excite all the vibration modes at one go. This makes impact excitation method very attractive when time is the main concern.

The resultant response signal contains all the activated resonance frequency components. Due to the existence of damping, the response signal will decay as the kinetic energy dissipates. The decay rate depends on the extent of damping in the test structure. It should be ensured that an exponential window is applied if the sampling period cannot cover the whole decay span. This is to avoid the leakage problem. The FRF is hence obtained by dividing the spectrum of the response by the spectrum of the excitation.

Unfortunately, impact excitation can rarely be used for nonlinear structural dynamic test. It is because, firstly, the duration and force level the impact executes is of no consistency. This makes it difficult to apply control on them. Secondly, the force applied is very localised. The kinetic energy at the nonlinear region can be too small to trigger any nonlinear behaviour.

6.4.4 Considerations of Measuring FRF Properties of Nonlinear Structures

For a linear structure, the measured FRFs are unique and independent of excitation strength, so all the above-mentioned excitation types can be used, and the choice depends only on the time, physical constraints and accuracy requirements. In the case of identifying or modelling a structure with nonlinear elements, it is widely accepted that one of the best ways is to exercise a degree of amplitude control on the vibration levels during measurement [1]. For doing

so, the stepped sine excitation is preferred because of its controllability, precision and good signal-to-noise ratio with which the structure can be excited [81].

Common stepped sine based FRF measurements require the attachment of an electro-dynamic shaker to the structure under test. The excitation mechanism unavoidably interferes with the test structure [82], and due to the mismatch of impedance between the shaker and test structure, the excitation force is not necessarily proportional to the input excitation signal strength. A phenomenon called 'force drop-out' is observed at the resonances. A simulation is shown in Figure 6 - 13 with parameters of a typical electromagnetic shaker taken from [83]. The simulation is conducted at a constant voltage input to the shaker. The red line represents the force experienced by the structure. It drops significantly as the excitation frequency approaches resonance at 100rad/sec. And it bounces back as the excitation moves away from the resonance. The response level, represented in green line, is also not proportional to the input signal across the frequency range. Despite these, the FRF of a linear structure still can be accurately derived as shown with the blue line. In the nonlinear dynamic test, the variation of the force or response signal must be controlled.

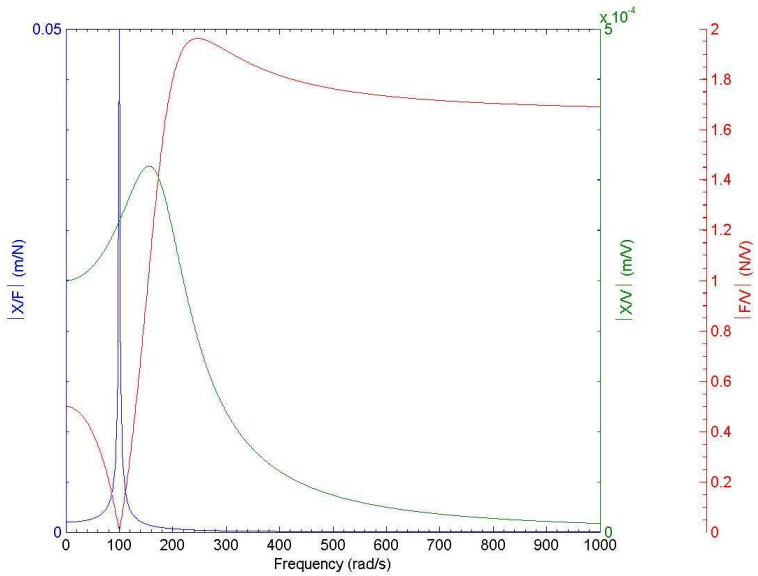

Figure 6 - 13 Observation of 'force drop-out' phenomenon

Another problem with the electromagnetic shaker is that when the vibration amplitude is large, even at the same frequency, the input voltage is not

proportional to the force level applied to the structure. This is because of the inherent nonlinearity of the magnetic field that generates the vibration. This nonlinearity must be coped as well.

6.5 Amplitude Controlled Nonlinear Dynamic Testing Code

Most structural nonlinearities are amplitude-dependent [1], so if the response is kept at a constant level across the whole frequency range, the behaviour of the structure would exhibit the characteristics of a linear system; hence, to keep the response level constant is essential when linearization analysis of a nonlinear structure is required.

Another motivation to have a controllable test is that the theoretical analysis of a nonlinear structure often involves the assumption of a constant amplitude periodic external excitation. In order to validate the theoretical model, as well as the analysis, the test is best conducted as close to the theoretical calculation as possible. Keeping the excitation amplitude constant in the experiment is a way to compare with the calculation.

The control is achieved by adjusting the strength of the input signal to the shaker according to the force or response levels measured. This problem can be classified as an inverse problem [84]. The exact relation between the excitation input signal and excitation force or response varies, depending on the shaker used and the structure tested. It is apparent from the discussion in the previous section that there is no simple mathematical expression linking the input signal strength to the force or response; hence iteration schemes are the best choice, because they depend less on the test setup, and still can produce good results.

An amplitude-controlled nonlinear dynamic testing code has been developed, based on the stepped sine excitation scheme, with the addition of a feedback loop to control either the force or response at each excitation frequency.

6.5.1 Control Algorithm

The controlled parameter is either excitation force or response, which is in the form of acceleration, velocity or displacement, depending on the transducer used. It is governed by the voltage input to the shaker's coil v and the excitation frequency ω, provided no change for all other parameters in the measurement.

From the mathematical point of view, force and response can be controlled in a similar fashion, so only the force control algorithm is presented here.

The desired force measured by the transducer, *f*, can be expressed in terms of v and ω described by an unknown function G:

$$f = \mathbf{G}(v, \omega) \tag{6.2}$$

f and v can be expressed in Fourier Series:

$$f = \sum_{n=1}^{\infty} \bar{f}^n = \sum_{n=1}^{\infty} \bar{F}^n e^{in\Phi} \tag{6.3}$$

$$v = \sum_{n=1}^{\infty} \bar{v}^n = \sum_{n=1}^{\infty} \bar{V}^n e^{in\Phi} \tag{6.4}$$

In which $\bar{F}^n$ and $\bar{V}^n$ are the coefficients of the n^{th} harmonic terms after the force and voltage signals are decomposed. Both $\bar{F}^n$ and $\bar{V}^n$ are complex terms. If a number, *m,* of harmonics is considered, the force and voltage can be represented by vectors of harmonic coefficients as:

$$\bar{v} = \begin{Bmatrix} \bar{V}^1 \\ \bar{V}^2 \\ \vdots \\ \bar{V}^m \end{Bmatrix} \qquad \bar{f} = \begin{Bmatrix} \bar{F}^1 \\ \bar{F}^2 \\ \vdots \\ \bar{F}^m \end{Bmatrix} \tag{6.5}$$

Equation (6.2) cannot be solved analytically because of the unknown nature of the function **G**; however, it can be solved iteratively by converting to the following equation:

$$\bar{f} = \mathbf{G}'(\bar{v}, \omega) \tag{6.6}$$

In which $\mathbf{G}'$ is a transfer function linking two vectors. This equation can be further expressed as:

$$\mathbf{N}(\bar{v}, \omega) = \bar{f} - \mathbf{G}'(\bar{v}, \omega) = 0 \tag{6.7}$$

Equation (6.7) is solved with Newton-Raphson method, which is chosen because of its efficiency in convergence and ease of implementation. In practice, $\bar{f}$ is predetermined as the desired excitation force amplitude, and the purpose of the

iteration is to find the right value of $\overline{v}$ to satisfy equation (6.7). At a particular excitation frequency, the resultant $\overline{v}$ after *n* iterations is:

$$\overline{v}^{(n+1)} = \overline{v}^{(n)} - [\mathbf{N}'(\overline{v}^{(n)})]^{-1}\mathbf{N}(\overline{v}^{(n)}) \tag{6.8}$$

in which $\mathbf{N}'(\overline{v}^{(n)})$ is the Jacobian matrix, which is defined as:

$$\mathbf{N}'(\overline{v}^{(n)}) = \begin{bmatrix} \frac{\partial \mathbf{N}^1}{\partial \overline{V}^1} & \cdots & \frac{\partial \mathbf{N}^1}{\partial \overline{V}^m} \\ \vdots & \ddots & \vdots \\ \frac{\partial \mathbf{N}^m}{\partial \overline{V}^1} & \cdots & \frac{\partial \mathbf{N}^m}{\partial \overline{V}^m} \end{bmatrix} \tag{6.9}$$

Here, all the partial derivatives are evaluated at $\overline{v}^{(n)}$, namely,

$$\frac{\partial \mathbf{N}^i}{\partial \overline{V}^j} = \frac{\partial \mathbf{N}^i(\overline{v}^{(n)})}{\partial \overline{V}^j} \tag{6.10}$$

It should be noticed that the Jacobian matrix here is non-singular so that its inverse exists.

The function **N** is not known analytically, so its partial derivative can only be approximated with a finite difference approach:

$$\frac{\partial \mathbf{N}^i}{\partial \overline{V}^j} = \frac{\partial \mathbf{N}^i(\overline{v}^{(n)})}{\partial \overline{V}^j} \approx \frac{1}{2H^j}(\mathbf{N}^i(\overline{v}^{(n)} + h) - \mathbf{N}^i(\overline{v}^{(n)} - h)) \tag{6.11}$$

in which H^j is a small deviation from $\overline{V}^j$, and h is a column vector of length *m*, with the j^{th} element as H^j and all the other elements zero.

Though mathematically a sound approach, experimentally it is difficult to get the Jacobian matrix with equation (6.11) due to the following reasons:

- In order to get a very close approximation of the partial derivatives, the step H^j should be as small as possible; however, in experimental conditions, a small change in $\overline{V}^j$ may not induce a noticeable change in **N**, because of unavoidable measurement limitations. In a worse case, the finite difference approach with very small step size may give totally erroneous approximation of the Jacobian matrix;

- The unknown nature of the function **N** makes it difficult to define the best step size H_j;
- 2*m* number of measurements are required at every frequency point in order to determine the full Jacobian matrix. This is not practical if the number of harmonics to be controlled is large.

In order to increase the speed of the control algorithm, mainly, to avoid the direct calculation of partial derivatives, the Secant method [49] is used, which is expressed as:

$$\mathbf{N}'(\overline{v}^{(n)}) \approx \frac{\mathbf{N}(\overline{v}^{(n)}) - \mathbf{N}(\overline{v}^{(n-1)})}{\overline{v}^{(n)} - \overline{v}^{(n-1)}} \tag{6.12}$$

With the approximated Jacobian Matrix $\mathbf{N}'(\overline{v}^{(n)})$ calculated, the voltage input to the shaker $\overline{v}^{(n+1)}$ is updated; so is the driving force to the nonlinear system.

As a starting point, and without losing the essence of Newton-Raphson based algorithm described above, a main-harmonic amplitude controlled nonlinear dynamic testing code has been developed in LabView. Figure 6 - 14 displays a flowchart that the code is based on.

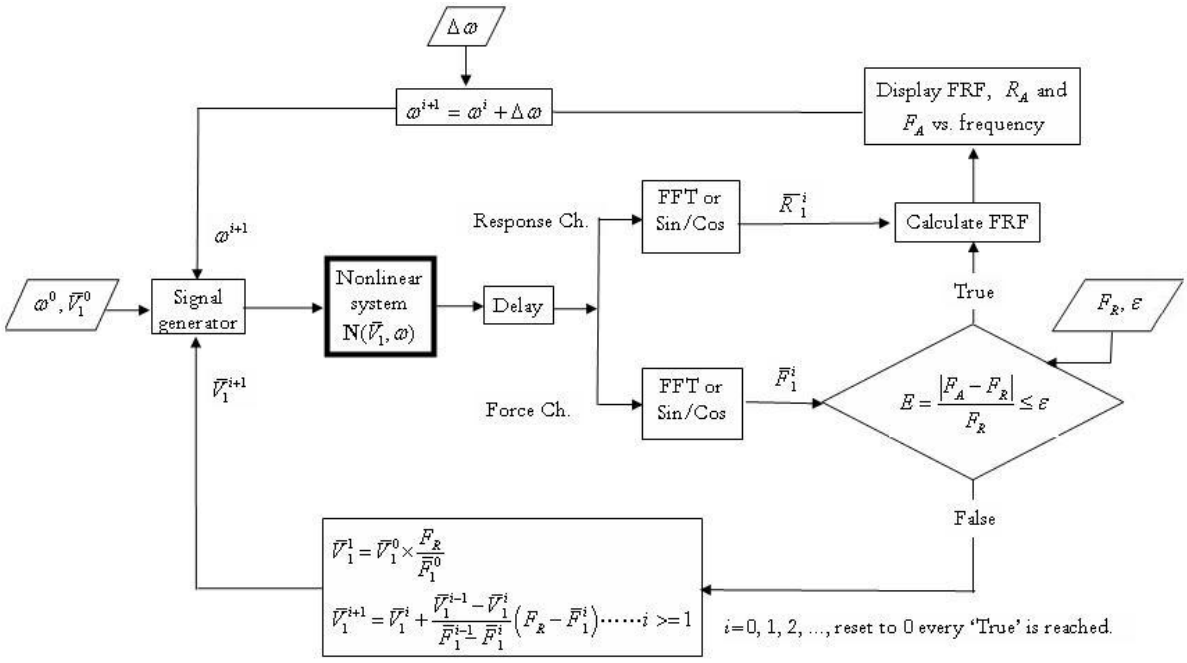

Figure 6 - 14 Schematic representation of nonlinear force control algorithm

The user defines the following parameters beforehand: ω^0 - starting excitation frequency; $\Delta\omega$ - frequency step; $\bar{V}_1^0$ - starting voltage of the driving signal; F_R - desired driving force; ε - error ratio. The nonlinear system in the above figure physically includes the shaker, power amplifier, transducers and the testing structure. Once the cyclic driving signal is released from the signal generator, the force and response signals are recorded after a delay to allow settling, and both signals go through an FFT or other Fourier decomposition to get the main harmonic components. In this force-controlled case, the amplitude of the force signal is compared with the desired force level. If the resultant error is within tolerance, the FRF point is calculated and plotted. The driving signal will go to the next excitation frequency.

If the error ratio limit is exceeded, the iteration process starts. The Secant method requires inputs from the last two iterations, so for the first loop, a proportional interpretation is used to derive the new driving signal amplitude. The reason behind this is that normally the structure is tested starting from a frequency away from any resonances, and at that frequency point, the nonlinear structure displays properties close to linear ones; so the driving signal corresponds with the force in a fairly linear fashion, and a proportional interpretation is suitable. The signal generator is updated with a new amplitude at the same frequency. The resultant force is compared with the desired value again to decide whether a further iteration loop is needed or the FRF point should be calculated. In the case that another iteration is needed, the Secant method interpretation is used. The above described process is repeated until all the FRF points within the frequency range have been obtained.

Besides the control algorithm, there are other points to be taken care of, which are difficult to present in the above flow chart.

- The strength of the driving signal must be capped in order not to damage the whole system accidentally;
- There are possibilities that the Newton-Raphson method fails to locate the root, which is mathematically proven; hence, there must be a cap on the number of loops the program is allowed to run at each frequency point;

- The delay time should be set according to the properties of the tested structure. For flexible and lightly damped structures, the delay time must be set long enough to avoid any transient effect being counted;
- The transition from one frequency point to another, and from one amplitude to another must be smooth. This is due to the fact that at around the resonance, there are possibly more than one stable vibration states. If the transition is abrupt, one steady state may not be captured completely in the frequency range before the vibration jumps to another steady state. This will cause incompletion in the FRF.

6.5.2 LabView Program for the Nonlinear Testing Code

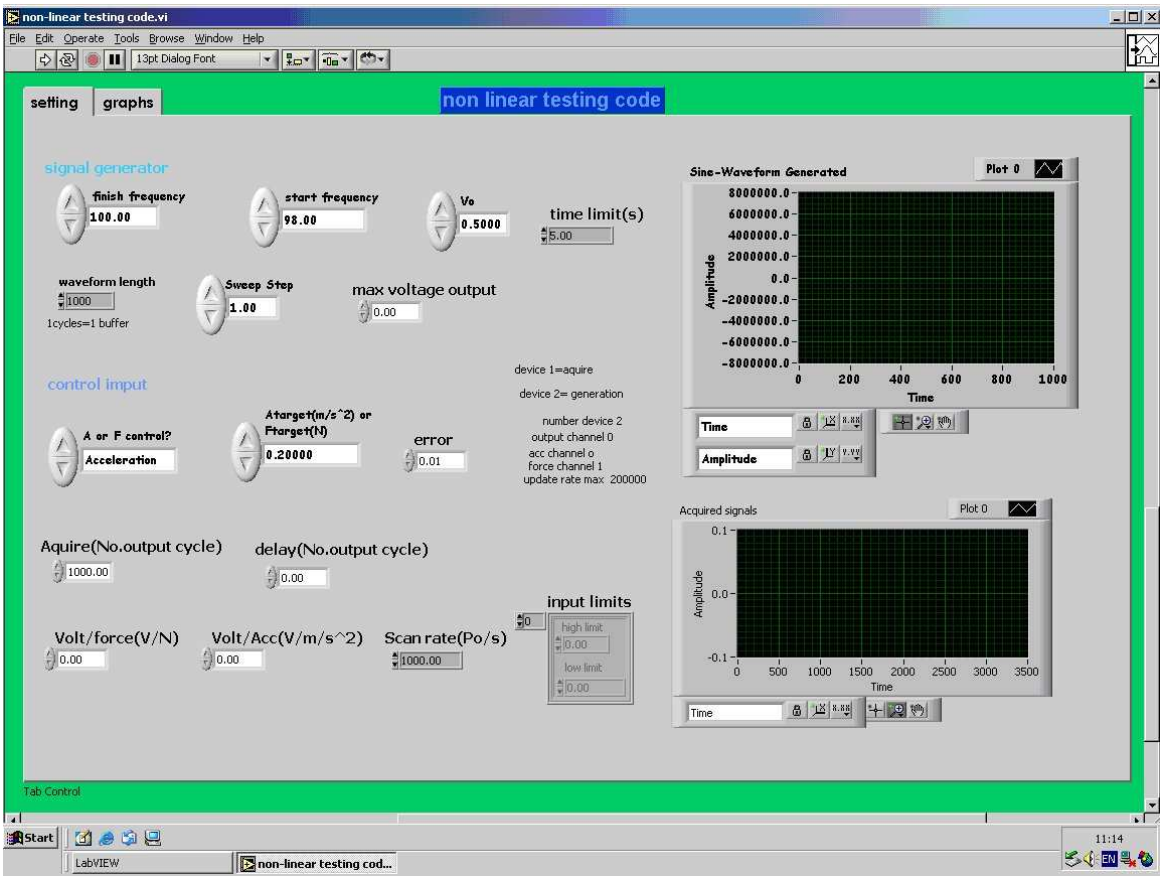

Figure 6 - 15 Control panel of the nonlinear testing code in LabView

The above control algorithm was implemented in LabView, a software development environment based on graphical programming from National Instrument. Figure 6 - 15 shows the design control panel, on which the user can adjust parameters to suit test requirement. One Hewlett Packard 33120A Waveform Generator was used to generate driving signals and one National

Instrument NI4472 Dynamic Signal Acquisition Card was used to acquire force and response signals.

6.5.3 Further Improvement

Though the nonlinear testing code has been successfully implemented and showed its reliability and accuracy in various applications, improvement is still required. The main points are listed below:

- Instead of only the main-harmonic component being monitored and controlled, super-harmonic and sub-harmonic components should also be included in the code. The mathematical foundation has been laid down in section 6.5.1;
- Newton-Raphson iteration can sometime fail to converge if the starting point of the iteration is not well placed. Additional algorithm should be included in the code so as to avoid this from happening;
- Structural dynamic testing, especially when nonlinearity is of concern, requires a very good understanding of the theory and the test specimen itself in order to achieve an efficient and error-free test. This requires the expertise of a specialist. However, things can be made easier if the code can be made smarter, e.g. the delay time can be automatically adjusted based on the vibration data acquired.

6.6 Concluding Remarks

The basic knowledge involved in structural dynamic testing is examined in the first half of this chapter. The fundamental message addressed is that it is important and necessary to conduct dynamic tests, and to do so correctly. The accuracy and correctness of the experiment measurements are dictated by the capabilities of the transducers, data processing equipment and experimental setup. Almost all methods for applying the structural excitation will have some unwanted modification effects on the structure, as well, almost all the response measurement transducers and support fixtures will have an unwanted influence on the structure. Furthermore, many of the potential problems with dynamic tests only become apparent during the actual tests. We should be aware of these problems and strive to select methods to minimise these effects. In many

respects the practice of vibration testing is more of an art than a science. There is no single right way to perform a vibration test, as described by Maia etc. [16].

An amplitude controlled nonlinear dynamic testing code is introduced in the second half. It is a natural extension to a linear one. Though relative simple in concept, the implementation of the algorithm is rather troublesome. Some achievements have been made, in terms of improving the reliability and safety measures, reducing the test time and most importantly, fulfilling its purpose. Nonetheless, more effort should be poured into this field, to develop it up to a level of competency comparable to what linear dynamic test enjoys now.

Chapter 7

Experimental Case Studies

7.1 Introduction

The theoretical background behind the construction of analytical models of a complex structure with a localised nonlinearity has been laid out in previous chapters. It has been shown step-by-step how this is achieved through perfecting component models, incorporating joint models and applying a frequency-domain based nonlinear calculation algorithm. It is now time to demonstrate that all this theoretical build-up and numerical prediction is valid when compared against experiments. Physical experiments and tests have always played a vital role in the field of science and engineering, even after numerical simulations have been greatly improved with the introduction of computers, to ensure that all the relevant physical effects are included. The purpose is simple: we need to assure ourselves that new approaches and algorithms can actually reflect physical nature correctly by directly assessing the physical parameters.

The first part of this chapter describes the construction of the test rig, with emphasis on the design of the nonlinear element and rotor-to-stator joint arrangement. There have been some references to this test rig in previous chapters. This section will provide a full picture. It is followed by modal testing of a component and a linear assembly, which illustrates how experiments help to

improve the analytical models. Last but not least, amplitude controlled stepped-sine sweep tests are presented to accurately measure the non-linearity, the results of which are compared with numerical simulations.

It is worth mentioning here that constructing a test rig and conducting experiments is not an easy and straightforward business. It might only be worth a few pages of presentation in this thesis, but the time and effort involved is well over its fair share.

7.2 Description of the Test Rig

Some considerations for the test rig at the design stage are:

- The test rig should have a reasonably complex nature in terms of geometry, material properties, flexibility and functionality. It is aimed to be representative of a real world structure. This is to differentiate from many purpose-built and academic test rigs commonly seen in lab environments.
- The test rig should have a prominent and clearly-defined nonlinear element. All the other nonlinear sources shall be minimised.
- The nonlinearity shall be adjustable. In the real world, nonlinearity can change throughout the structure's lifespan due to wear and tear, change of operation conditions etc. The analytical models should be able to cope with that and it is very appealing to have it in the test rig.

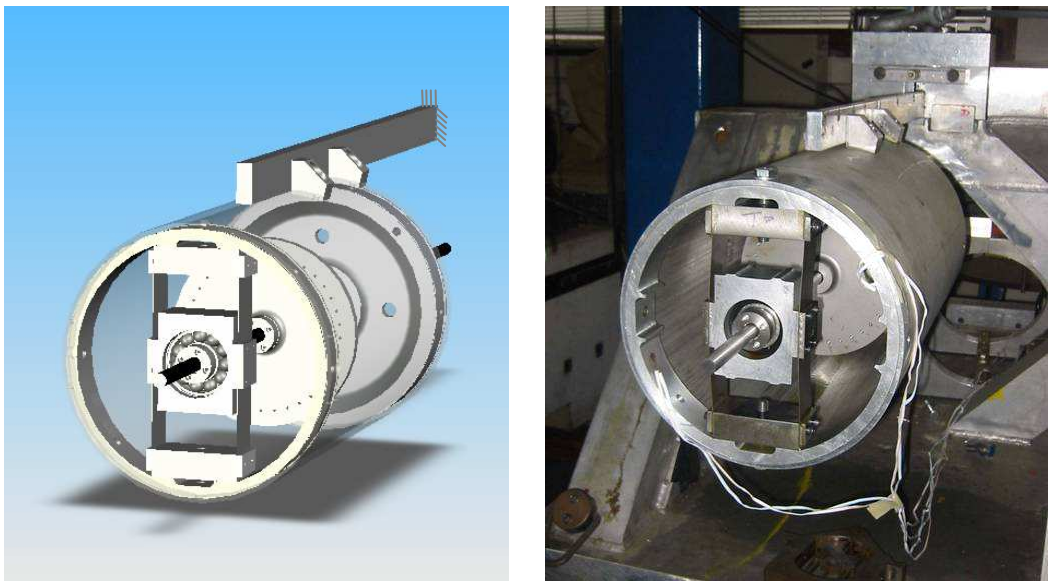

Figure 7 - 1 Overall test rig setup

Figure 7 - 1 shows the computer model and up-and-running test rig as manufactured. The whole rig resembles an aircraft engine that is hung beneath the wing. It neglected all the fine and intricate details that a normal aircraft engine has, but it does consist of key structural components that matter for understanding whole-machine dynamics: flexible support, flexible casing, flexible shaft, rotor and bearing supports. The detailed dimensions and material properties of most of the components can be found in Appendix A. The construction of the nonlinear element, as well as the joint between rotor and stator will be described in more detail in the following two sections.

7.2.1 Construction of the Nonlinear Bearing Support

The purpose of this whole design exercise is to introduce a nonlinear element into an otherwise linear test rig. Some of the considerations for this nonlinear element are: firstly, the nonlinearity shall be adjustable; secondly, the nonlinear element shall be capable of displaying not only weak but also strong nonlinearity; and thirdly, the construction of it should be easily and economically repeated. The front bearing support of the test rig is chosen to be the nonlinear element, which also takes into consideration that in rotating machinery bearings are one of the most common sources of nonlinearity. Details of the Nonlinear Bearing Support (NBS) are shown in Figure 7 - 2.

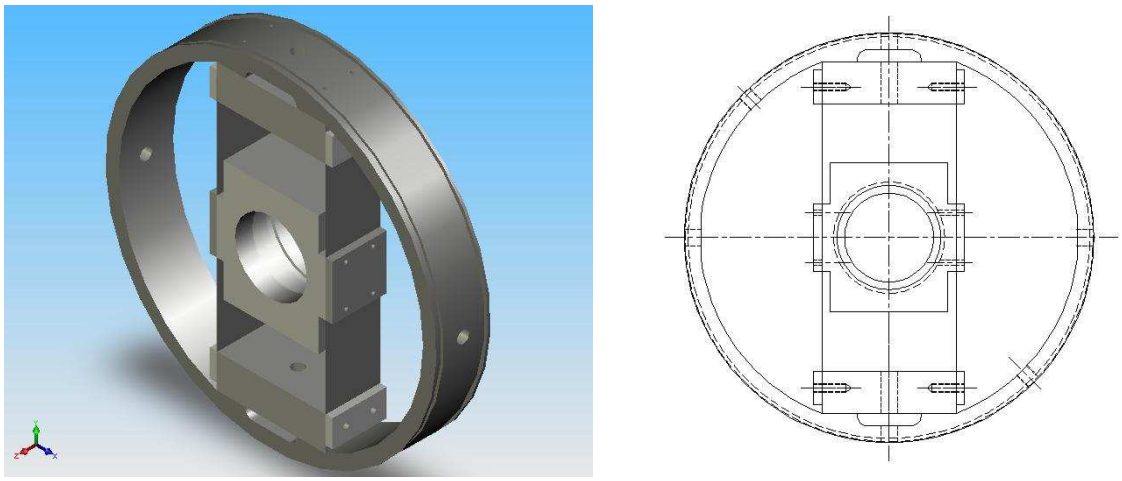

Figure 7 - 2 Schematic models of the nonlinear bearing support

The Nonlinear Bearing Support (NBS) itself is a rather complicated assembly consisting of various joints in the form of bolts and adhesive. Joints are always trouble-makers in structural behaviour modelling and prediction and it is

preferable to reduce the number of joints in the test rig to minimise calculation complexity; nevertheless, they are unavoidable in most practical cases. It is assumed, and later on shown in the experimental results, that the effect of local joints in the NBS on the whole assembly can be neglected.

The whole NBS is first manufactured in pieces as shown in Figure 7 - 3(a). The two 0.5mm spring-steel plates, running parallel (shown vertically in Figure 7 - 3(b)) are then glued to the two fixing blocks as well as the bearing block using Araldite2011®, a multi-purpose epoxy which bonds Ferrous metal and Aluminium excellently. The bearing block is located at the exact mid-span of the spring-steel plates. Some 5mm-thick steel plates are used to sandwich the spring-steel plates to prevent them peeling off. Drilled holes are threaded though the fixing plates and into the fixing blocks as well as the bearing block, to give the spring-steel plates a final security. This part of the NBS is then fastened to the outer rim, with which, a completed NBS is constructed. The final assembly is shown in Figure 7 - 3(c). At a later stage, a bearing will be fitted into the bearing block.

When not stressed, the combination of the spring-steel plates and the bearing block acts as an asymmetric joint to the rotor supported, with different linear stiffness in the vertical and horizontal directions: stiffer in the ‘vertical’ and softer in the ‘horizontal’ direction. Cubic stiffness nonlinearity will be present in the horizontal direction when the displacement is large. The spring-steel plates can be bent slightly by reducing the distance between the two fixing ends. This is achieved by inserting shim plates between the rim and the fixing blocks. A shim plate is basically a thin piece of stainless steel that is normally used to fill small gaps or spaces between objects. In this application, it is used to accurately reduce the distance between the two fixing blocks. As a result of this arrangement, the bearing support displays a stiffness pattern governed by the buckling effect of the spring-steel plates.

The beauty of this assembly, despite the complexity caused by the connections, is the ease of changing the configuration to display different dynamic properties. For example, the spring-steel plates can easily be replaced with other types of plates to produce different patterns of stiffness distribution. Furthermore, the

extent of the nonlinearity can be controlled by the thickness of shim plates inserted.

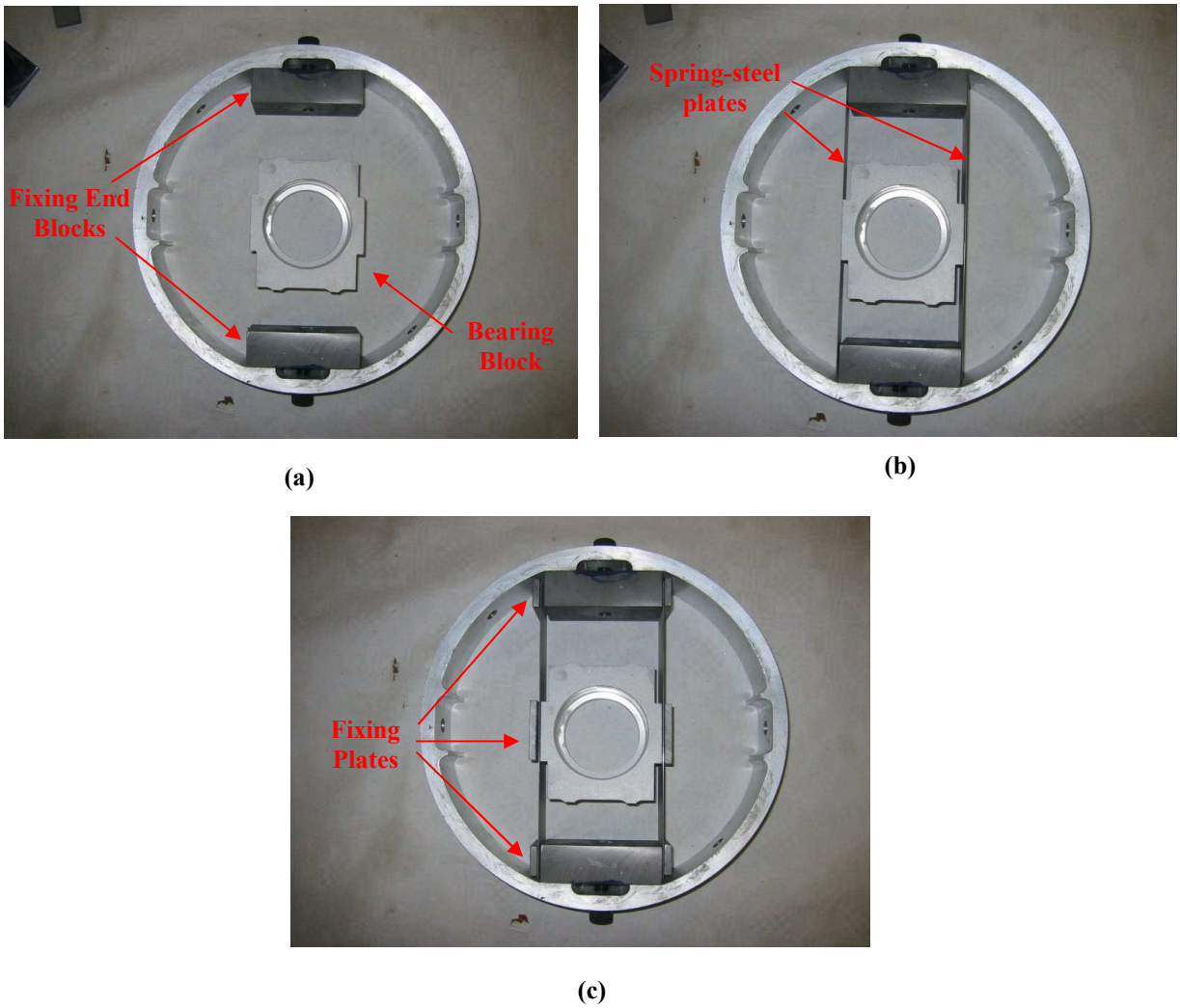

(a) (b)

(c)

Figure 7 - 3 Step-by-step assembly of the nonlinear bearing support

7.2.2 Property of the Nonlinear Bearing Support

The properties of the nonlinear bearing support were measured by conducting a static test, in which the displacement and applied force of the bearing block in the horizontal direction were measured.

It is understood that a negative relationship between the applied force and displacement, as illustrated in Figure 7 - 5, would occur when measuring a buckled beam. In order to obtain a full characteristic curve, compression forces were applied at both sides of the bearing block. Each force was measured independently with a Flexiforce® sensor, which is an ultra-thin and flexible printed circuit. The resistance of this printed circuit is inversely proportional to

the normal force applied. The difference between the two forces applied at both sides of the bearing block is the static force experienced by the nonlinear bearing block at the centre.

When shim plates are not used, the stiffness measured is of typical 3rd order nonlinearity that is encountered when material deformation is large and exceeds the linear assumption of stress and strain relationship. Figure 7 - 4 shows the measurement result, in which the y-axis is the force and the x-axis is the displacement. The red circles are the measurement points, and the blue line is the best fitting curve. The best fitting curve can be expressed with a 3rd order polynomial equation $F_n = k_1 x + k_3 x^3$, in which $k_1 = 2.544 \times 10^4 \text{ N/m}$ and $k_3 = 2.574 \times 10^9 \text{ N/m}^3$.

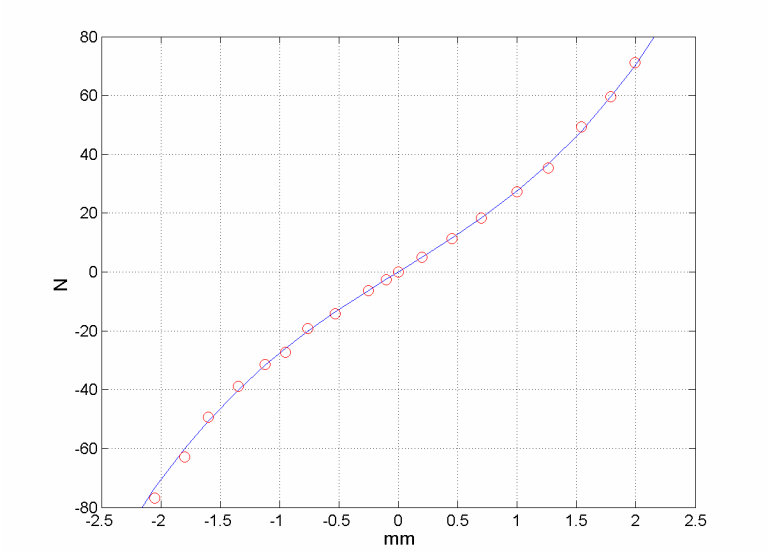

Figure 7 - 4 Nonlinear characteristic of the nonlinear bearing support without shim plate

When shim plates of combined thickness of 0.4mm were used, the spring steel plates were in a buckled state. The measurement results are shown in Figure 7 - 5, The best fitting curve can be mathematically expressed as: $F_n = k_1 x + k_3 x^3$. The stiffness parameters $k_1 = -1.265 \times 10^4 \text{ N/m}$ and $k_3 = 1.381 \times 10^9 \text{ N/m}^3$ were obtained by minimising the discrepancy between measured and approximated values. Point A is the global geometric centre and in this case is an unstable equilibrium point; B and C are two stable equilibrium points.

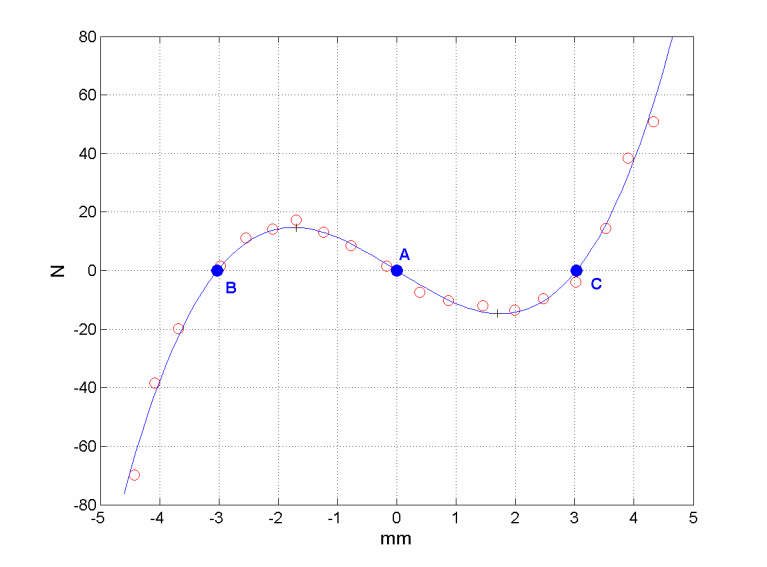

Figure 7 - 5 Nonlinear characteristic of the nonlinear bearing support with 0.4mm shim plates

7.2.3 Construction of the Rotor-Stator Connections

The design of the connection between the rotor and the stator is not insignificant and warrants a special mention here. As the primary purpose of this test rig is to **demonstrate** the analytical modelling capability for a complicated structure with localised nonlinearity, it is useful to have a single and prominent nonlinearity and to minimise any 'side' effects that will complicate the calculation as well as the demonstration. In rotating equipment, the joints between the rotor and stator are often the sources of nonlinearity and uncertainty. This is mainly due to the fact that tight tolerance is difficult to achieve. In normal operation the clearance between the rotor and stator does not cause any problems. However, when performing vibration tests, even a very small amount of clearance can cause rattling and distort the results [61]. One place of major concern is the connection between the shaft and bearing.

A collet and its associated two-piece adaptor shown in Figure 7 - 6 is used to secure the shaft to the bearing. The collet is normally found in a machine tool's rotating spindle as part of a holding device. It has a gentle tapered outer surface and a uniform inner surface which forms a collar around the object to be held. As the two-piece adaptor is tightened, a strong clamping force is exerted onto the object that prevents any gap and sliding movement. Because tightening and securing the collet onto shaft is a gentle and uniform process, it gives good

control in positioning the shaft right at the bearing geometric centre and perfectly perpendicular to each other.

Figure 7 - 6 Bearing-shaft adaptor and collet fixture

7.3 Experimental Studies

This test rig provides the foundation for various types of dynamic test that aim to demonstrate good modelling practice for complex structures. It started from component level rising to the complete assembly.

7.3.1 Modal Testing of Components

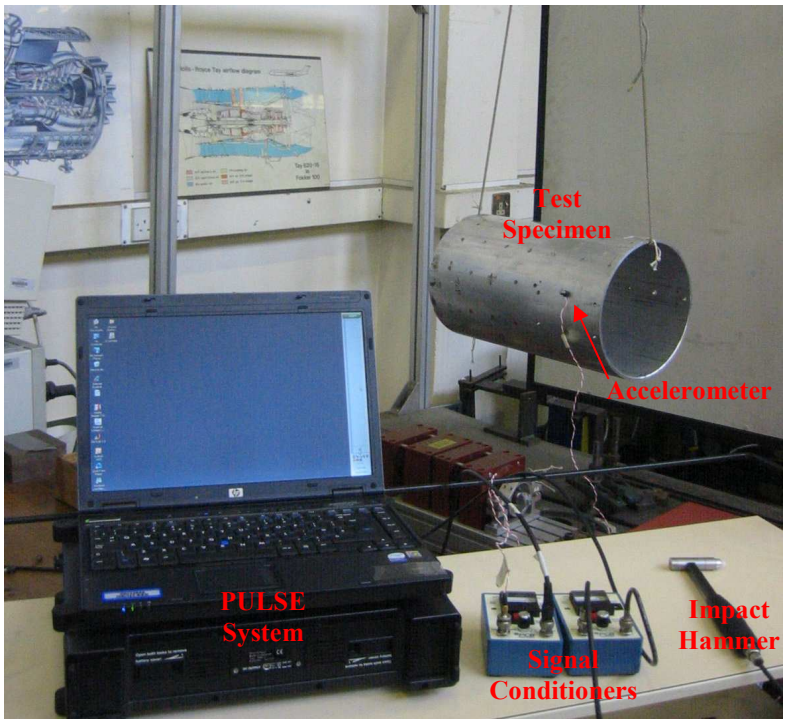

Figure 7 - 7 Modal testing setup for the casing

All the major components of the test rig: casing, rotor, shaft and bearing supports, have been modal tested and validated. This is a very necessary step to achieve a accurate assembly model in the end. Only the modal test on the casing is presented here, while the technique, equipment, data acquisition and processing routine are the same across all the tests.

Figure 7 - 7 shows the setup for impact tests on the casing. The dimensional and material properties of the casing can be found in Appendix A. The casing is suspended at the end of a bungee cord, which adds minimum rigidity to the casing. It is reasonable to assume that the casing is supported at free-free boundary condition. The PCB ICP® Impulse Force Test Hammer 086C02 is used to provide the impulse excitation, which consists of a nearly constant force over a broad frequency range and is capable of exciting all resonances in that range. The size of the hammer, hardness of the tip and velocity at impact determine the amplitude and frequency content of the force impulse. It is from the preliminary FE calculation and good understanding of the experiment itself that the best combination is chosen. The accelerometer used is PCB ICP® Accelerometer 352C67. Both force and acceleration signals are fed through battery-powered PCB ICP® sensor signal conditioners, which amplify the signals to be readable by the analyser. The PULSE™ system from Brüel & Kjær is used for data acquisition and processing. The system consists of a piece of front-end data acquisition system with anti-aliasing filters, which conditions and digitises the transducer signals, and a computer with PULSE operation software that allows real time acquisition, recording and processing of data. Different types of analysers are available. For the impact tests, the FFT analyser is used. Calibration of the transducers followed the similar procedures as in Section 6.3.2.

The modal testing process starts by specifying measurement points on the structure. The number and location of those points chosen affects the resolution of mode shape comparison later on, which is a key factor to determine whether an FE model is valid. In this experiment, 81 grid points on the outer surface of the casing are selected, the location of which is measured and a 3D frame model is constructed using ICATS [85], as shown in Figure 7 - 8. ICATS is a Modal Analysis software package developed in Imperial College London. It extracts

modal properties from experimental data and carries out comparison with FE simulation results.

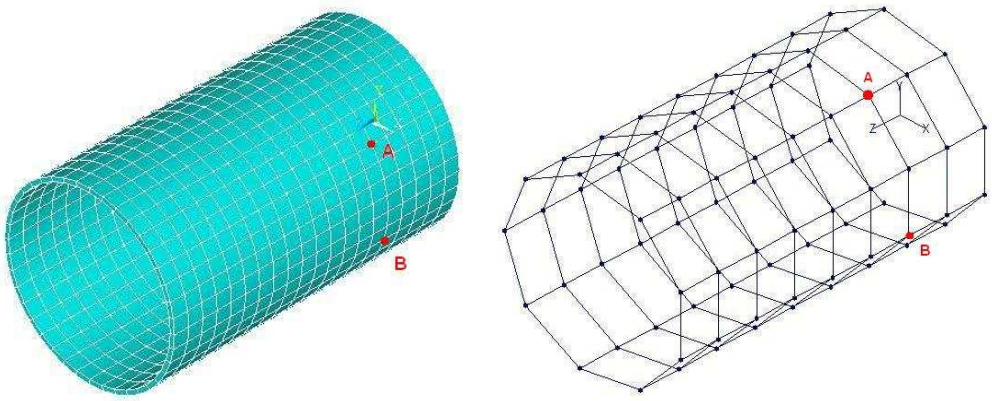

Figure 7 - 8 Finite Element and experimental models of the casing

Only excitations and responses in the radial direction are assessed at each of those grid points. The accelerometer is attached to each grid point in sequence, while the impact hammer excites the freely over-hung casing at a predefined grid point. It is essential to keep each impact the same as the previous one [1], in terms of impacting position and orientation relative to the surface. Double hitting should be strictly avoided in order not to deteriorate the signal quality. The experiment phase is considered complete when all the excitation and response data of each pair of measurement points have been collected.

Table 7 - 1 records the measured natural frequencies and the corresponding analytical ones from the FE analysis. Modal Assurance Criteria (MAC) and Natural Frequency Difference (NFD) of each pair of modes are also listed. The numbering of the modes set is according to the analytical calculation results. There are a few missing modes in the experiment. This is mainly contributed by the small number of divisions along the circumferential direction; nevertheless, the high MAC values of the existing mode pairs are a good indication of a reliable analytical model.

A visual comparison is shown in Figure 7 - 9, in which boxes in red represent highly correlated mode pairs. It can be concluded from here that the analytical casing model represents the physical casing model well within 1600Hz, even though the experimental modal analysis did not identify all modes and the modes do not match perfectly.

Table 7 - 1 Correlation between the experimental and the analytical data

Mode No.	Experimental Frequency (Hz)	Analytical Frequency (Hz)	Modal Assurance Criteria (%)	Natural Frequency Difference (%)
1	275	276.34	95.9	0.4
2	279	276.34	97.3	1.0
3	303	312.88	93.8	3.0
4	311	312.88	95.5	0.3
5	782	792.52	93.9	1.3
6	--	792.52	--	--
7	823	846.28	90.2	2.8
8	--	846.28		--
9	1500	1550.3	91.6	3.3
10	--	1550.3	--	--
11	1515	1558.4	88.5	2.8
12	--	1558.4	--	--
13	1547	1612.6	92.7	4.2
14	--	1612.6	--	--

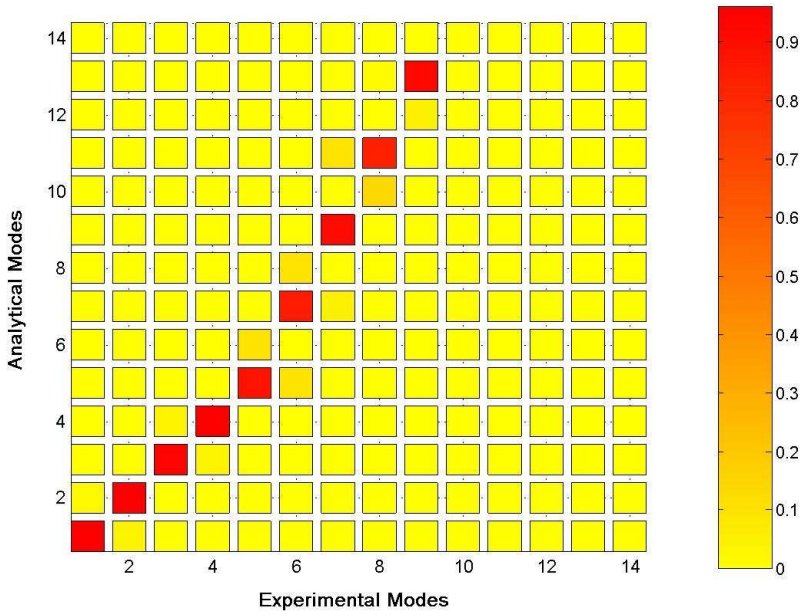

Figure 7 - 9 MAC Correlation between the test and simulation

The casing is modelled as a perfectly axisymmetric structure. Its dynamic properties is characterised by the phenomenon of 'double' modes: two modes with identical natural frequencies and mode shapes which differ only in the

angular orientation of the nodal lines [1, 86]. The first two pairs of double modes are also observed in the experiment, but with splits in their natural frequencies: an indication of the distinctiveness of each mode even though the mode shapes are 'almost' identical. Physically, this is partly caused by the mass of the accelerometer, which destroyed the axisymmetry of the structure, even though only very slightly. Manufacturing deviations such as variable wall thickness can also split real modes.

From a model validation point of view, what matters most is that an analytical model is able to describe the corresponding physical model with sufficient accuracy, so that the user can have the confidence to employ the analytical model in similar applications without referring back to the physical test for further validation. This is one of the most strongly advocated advantages of computerisation in structural dynamic modelling that has been progressed over the past few decades. Confidence is a subjective thing. Rigorous scientific research and the resultant improved methods and procedures help to boost it to a certain degree. However, full confidence still very much depends on intuitive understanding of the application and more importantly, experience. To what extent the analytical model is judged to be accurate and useful is still a subject worth further exploration.

Throughout the model validation process, there are restrictions and uncertainties that prevent a perfect match between the dynamic data obtained from analytical simulations and experiments on physical models. Test setup and instrument limitations, human errors, uncertainty of environmental conditions and unavoidable simplification of analytical models all contribute to the discrepancy. Manufacturing errors will also contribute and the list can be further extended. These effects can be minimised, even though not totally eliminated, if time and cost constraints for such an exercise are not an issue.

The split of double modes due to the added accelerometer can be minimised if the response measurement is of a non-contacting type. One such measurement technique is the Laser Doppler Vibrometer (LDV), which is now gaining popularity in the aerospace industry [87]. It is an optical velocity-measuring device based on the measurement of the Doppler shift in the frequency of laser light scattered by a moving object [88]. Another group of non-contact response

measurement devices are based on principles in electric circuits, e.g. change of inductance, eddy current and capacity etc. due to the change of the gap between the sensor and the object [89]. The unfavourable side of the LDV is the cost of dedicated equipment required is still very high; as well the measurement can only be made in the line of sight. The latter methods require the transducer to be fixed to a frame, which may be moving, hence the transducer measures the relative displacement, whereas an accelerometer measures the absolute acceleration. In addition, the test preparation is much more time-consuming and the operation environment requirement is much more stringent comparing to the tests using traditional piezoelectric-based accelerometers. From the analytical model side, the model can be made as complicated as possible to include all expected test parameters, e.g. considering additional mass and stiffness due to the accelerometer and more realistic boundary conditions.

The analytical model can be further improved by applying model updating methods. The Inverse Eigensensitivity method described in Chapter Two was employed here. Either eigenvectors or eigenvalues can be used; the former tends to be more complicated and used more often in updating local parameters. For a geometrically simple component with homogenous material properties like the casing, global parameters, e.g. physical size, material density and Young's Modulus, are more often of updating value. Another consideration is which one of the two, eigenvalue or eigenvector, is more likely affected by experimental inaccuracy. There is no point to update parameters to a certain level of accuracy while the reference parameter, eigenvalue or eigenvector in this case, cannot be measured with a higher accuracy. The derivation of eigenvectors, or mode shape information, from experiments could suffer imperfection due to slight inaccuracy in marking grid points on the casing surface and non-perfect hammer impact on a curved surface. On the other hand, eigenvalues, or natural frequencies, could usually be measured more accurately; hence they were chosen as the reference parameter.

The natural frequencies after five iterations, with the Young's modulus as the updating parameter, is shown in Table 7 - 2. The iteration aimed to minimise the average Natural Frequency Difference (NFD) . It is reduced from 2.24% to 1.31%.

Table 7 - 2 Model updating result

Exp. Mode No.	Initial value	Iteration number					Measured value
		1	2	3	4	5	
1	276.34	273.42	271.46	269.49	268.49	268.99	275
2	276.34	273.42	271.46	269.49	268.49	268.99	279
3	312.88	309.58	307.36	305.13	304	304.56	303
4	312.88	309.58	307.36	305.13	304	304.56	311
5	792.52	784.16	778.54	772.88	770.03	771.45	780
6	846.28	837.35	831.35	825.3	822.26	823.79	823
7	1550.3	1533.9	1522.9	1511.9	1506.3	1509.1	1500
8	1558.4	1541.9	1530.9	1519.8	1514.2	1517	1515
9	1612.6	1595.6	1584.2	1572.7	1566.9	1569.8	1547
Ave.NFD (%)	2.24	1.63	1.42	1.33	1.32	1.31	

From the above exercise, following the modal validation and updating procedure, we come to the conclusion that the updated analytical model can be further used in the subsequent assembly model, within the frequency range of interest. All the other major components also need to be tested and the analytical models have been updated in a similar manner.

7.3.2 Modal Testing of Linear Assembly

Bolted joints are used in the test rig to link the components. It is assumed that a bolted joint displays linear properties if it is a tight fit and the external excitation is moderate so that there is no relative movement between two connecting surfaces. In this situation, the easiest and most effective way to include the effect of a joint is to model it as a layer of linear elements between the two connecting components in FE analysis. This layer of element shall be able to imitate the stress-strain relationship of the frictional interface between the two components, which execute similar effect on the assembly as the friction force.

Figure 7 - 10 shows an example of a linear assembly: the assembly of the casing and the linear bearing support. These two components are fixed to each other with five evenly spaced bolt joints, which are represented in the FE model by a layer of isotropic elements. It is assumed that there is no slippage at the joints

and the force applied does not exceed the material's limit so that the linear constitutive equations for these elements still hold. Fundamentally, the joints are treated in the same manner as other structural components, with the only difference being that the thin layer element's material properties need to be identified via experiment, the value is initially set to be the same as the components'.

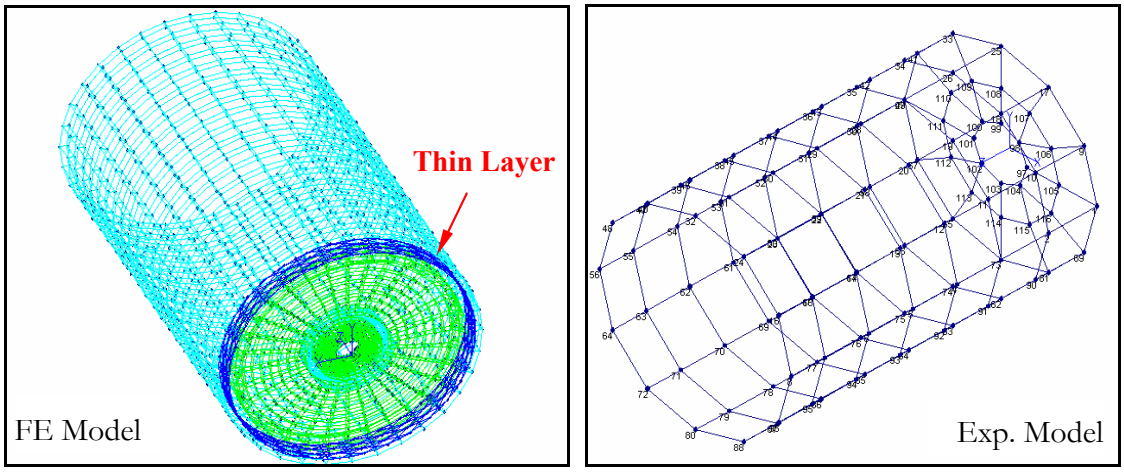

Figure 7 - 10 Finite Element and experimental models of a linear assembly

The experimental setup and analysis procedure are the same as the ones employed for the component tests in the previous section. 118 grid points are chosen as the measurement points as shown in Figure 7 - 10. The test results and comparison are presented in Table 7 - 3. In each case the experimental modal analysis has only located one of the pairs of symmetrical modes.

Table 7 - 3 Correlation between the experimental and the initial analytical data

Mode No.	Experimental Frequency (Hz)	Analytical Frequency (Hz)	Modal Assurance Criteria (%)	Natural Frequency Difference (%)
1	287.7	301.3	95.1	4.73
2	--	301.3	--	--
3	798.2	838.4	89.9	5.04
4	--	838,4	--	--
5	1259.5	1360.6	93.7	8.03
6	--	1360.6	--	--
7	--	1646.1	--	--
8	1515.6	1646.1	87.5	8.61

The Young's modulus E of the thin-layer elements is adjusted to minimise the average Natural Frequency Difference It is found that at E = 15x10^{9}Pa, the average reaches the minimum. The results are shown in Table 7 - 4.

Table 7 - 4 Correlation between the experimental and the updated analytical data

Mode No.	Experimental Frequency (Hz)	Analytical Frequency (Hz)	Modal Assurance Criteria (%)	Natural Frequency Difference (%)
1	287.7	294.57	94.1	2.39
2	--	294.57	--	--
3	798.2	810.77	92.8	1.57
4	--	810.77		--
5	1259.5	1280.67	93.7	1.68
6	--	1280.67	--	--
7	--	1610.10	--	--
8	1515.6	1610.10	89.5	6.24

By comparing Table 7 - 3 and Table 7 - 4, it can be seen that the correlation between experimental and predicted data by the new FE model was improved: the average Natural Frequency Difference is about 3%, although the value for the last mode is greater than 6%. The MAC values were improved slightly as well. The relatively poor agreement for the highest mode, compared with the good agreement for casing alone, suggests that the joint is more complex than a single isotropic element description.

7.3.3 Nonlinear Dynamic Tests

The overall test setup for the rig is shown in Figure 7 - 11. The shaker provides a controlled excitation force to the structure which is measured by a B&K 8200 force transducer. The response is measured at the nonlinear bearing block using a B&K 4393 accelerometer which is attached to the structure via a stud-type fixing.

It is understood from the theoretical studies that nonlinear structures display a unique frequency response property when excitation amplitude is kept constant at any frequency. This property can be used as a guideline to verify whether an analytical model represents its real counterpart accurately or not. The force-control algorithm introduced in Chapter Six is applied here. It ensures that a

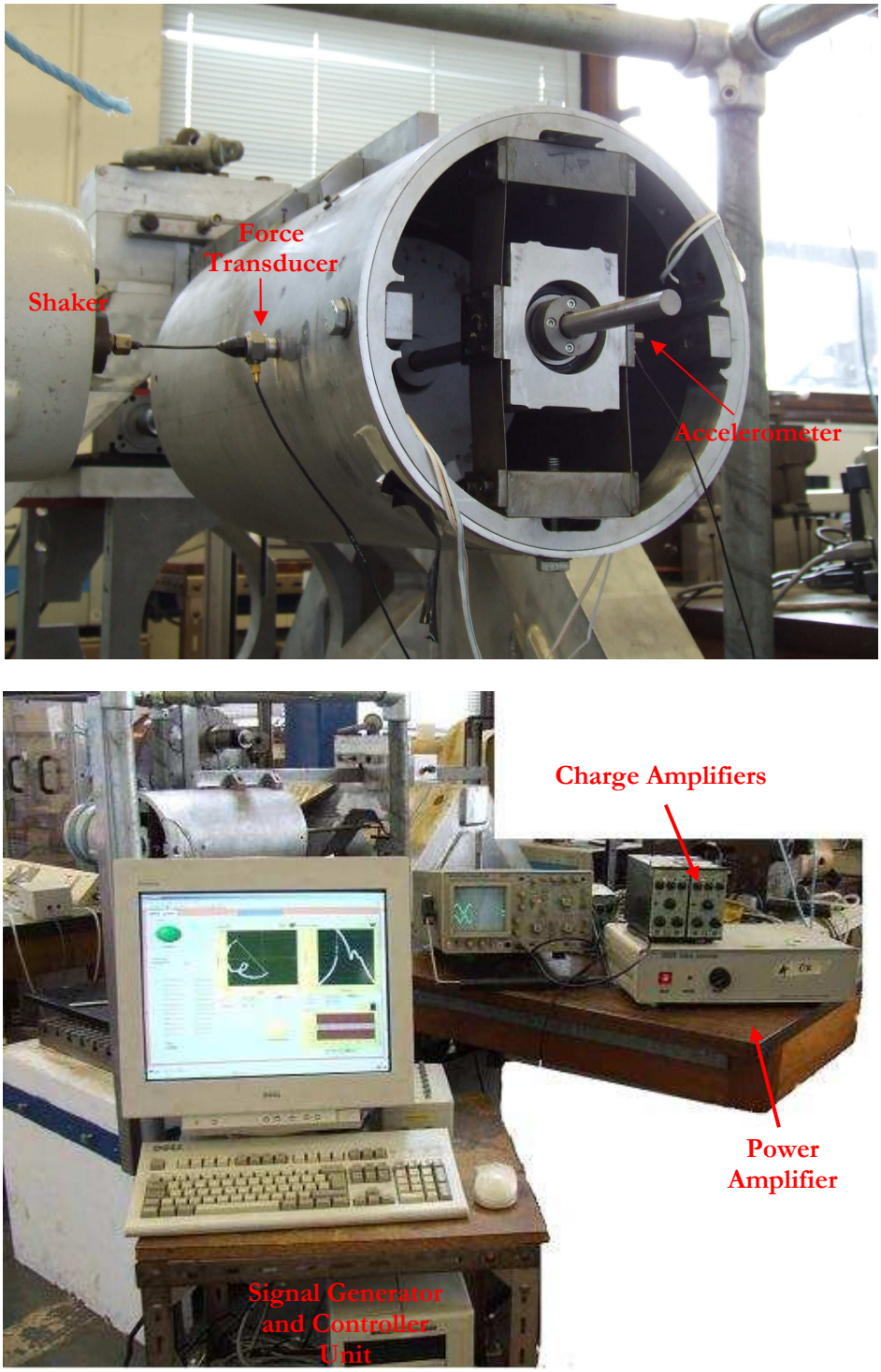

Figure 7 - 11 Overall setup of the test rig and the measurement system

constant excitation force is applied to the structure at every excitation frequency point. The waveform is generated via the HP 33120A function generator which has the capability of changing the clock rate of the output signal without discontinuity. This property is essential because if there is a burst between waveforms when the frequency progresses, a long settling time is required for

the structure to achieve the steady-state condition. In addition, the nonlinear structure is characterised by the possible existence of unstable steady-state responses, which cuases a jump in the stable response amplitude at around the resonance. This will make the control of the excitation force level difficult and reduce the chance of discovering all possible steady-state solutions. A National Instrument NI4472 Dynamic Signal Acquisition Card is used to acquire force and response signals, which are then processed in a LabView based program for displaying and storage. A schematic block diagram of the whole test setup is shown in Figure 7 - 12, in which the casing is omitted to show the internal components.

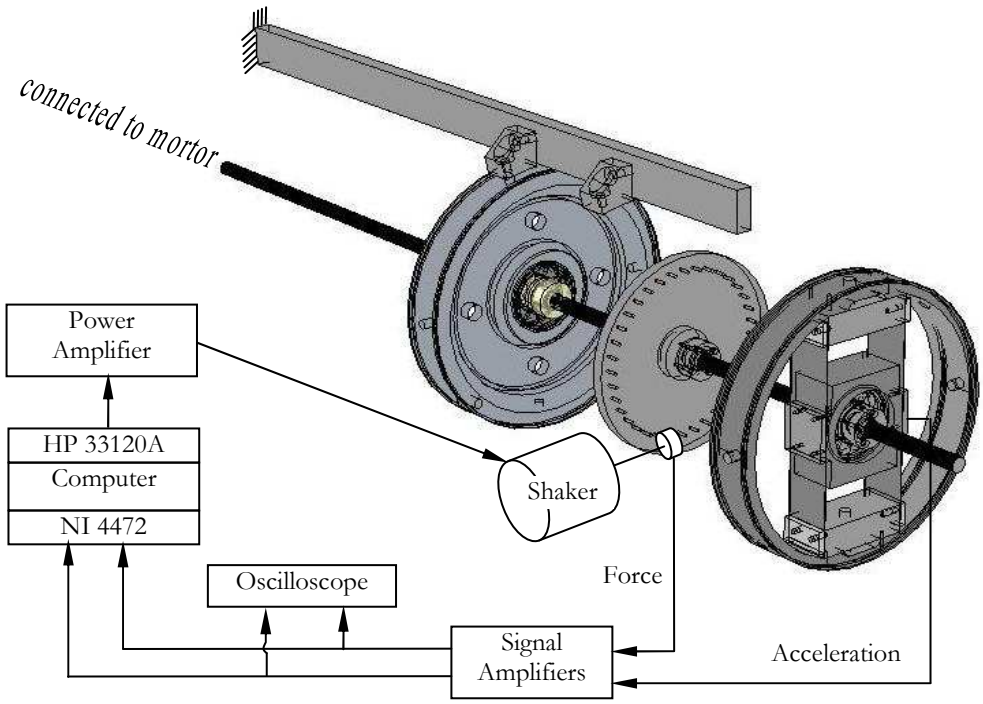

Figure 7 - 12 Block diagram of the nonlinear test rig set up

In the following two sections, two nonlinear cases are studied and put into tests. Test results are compared with simulations that apply the Multi-Harmonic Balance Method to FRF models of linear components.

7.3.3.1 Case study one: third-order nonlinearity

When there are no shim plates inserted between the bearing block and the rim, the measured joint stiffness in the horizontal direction is described by a third order polynomial as shown in Figure 7 - 4. Four runs of stepped-sine sweep tests are carried out with controlled force amplitude set at 0.1N, 2N, 3N and 4N

respectively. The results are presented in Figure 7 - 13. The sweeps started from 5Hz to 80Hz with step size of 0.2Hz. In each run, four modes are clearly identified within the test frequency range. The influence of the nonlinearity is manifested in the slightly distorted FRF curves at mode 2 and 3. The peaks bend over to the higher frequency side as the excitation force level increases, an indication of hardening stiffness as expected. Mode 1 and 4 do not seem to be affected by the joint nonlinearity.

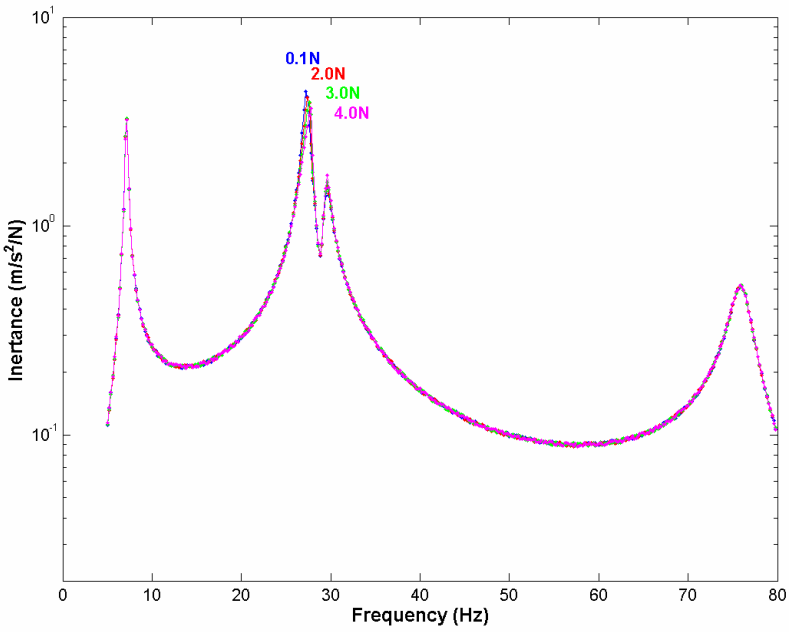

Figure 7 - 13 Measured FRFs for the 3rd order nonlinearity case

Modal analysis carried out on the FE model of the test rig with equivalent linear stiffness at the Nonlinear Bearing Support reveals why mode 1 and 4 are not affected by the nonlinearity. Figure 7 - 14 shows the mode shapes of the four modes. In each plot, the black wireframe model is the rig at rest condition and the blue wireframe model is the maximum deformation at the corresponding natural frequency. The scale of the deformations has been adjusted for clearer presentation.

Modes 1 and 4 are the first and second horizontal bending modes of the whole rig. The relative movement of the nonlinear bearing support is minimum and negligible. Mode 2 is the first bending mode of the spring steel plates supporting the bearing block, at which the nonlinear effect should be most prominent. Mode 3 is the swaying mode of the test rig and it includes deformation of the spring

steel plates supporting the bearing block, suggesting that the nonlinearity will also affect this mode.

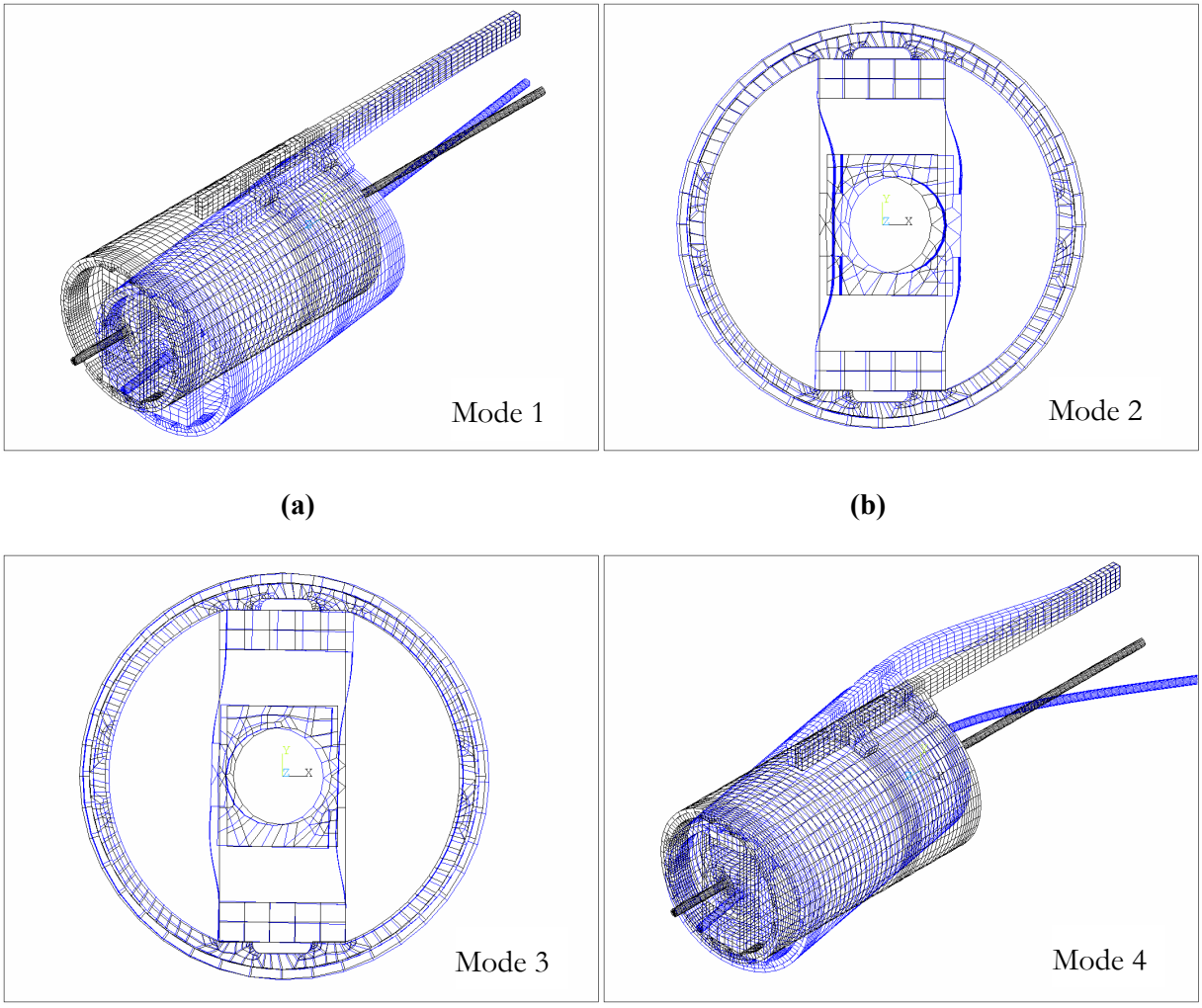

Figure 7 - 14 First four modes of the linearised FE model of the test rig

Finer sweep tests were carried out to identify clearly the shift of the resonant frequency of mode 2. Figure 7 - 15 shows the results of four sweeps with different excitation forces. The solid lines are derived from the simulation using the Multi-Harmonic Balance Method for comparison. The simulation results agree with the test very well.

7.3.3.2 Case study two: second-order nonlinearity

After 0.4mm shim plates have been inserted between the bearing block and the rim of the nonlinear bearing support, the bearing block rests at one of its two off-centre stable points, B or C as indicated in Figure 7 - 5. When the excitation is

small, the vibration of the bearing block is restricted to the local proximity of the stable point. Around the stable point, for example point B along the stiffness characteristic curve, the stiffness has a 2nd order nonlinearity. This property is evident from the plot below, in which a 2nd order polynomial curve in red-dot fits well to the measured characteristic curve in blue line around the stable point B; hence it would be expected that a weakened stiffness characteristics would be shown in the FRF curves.

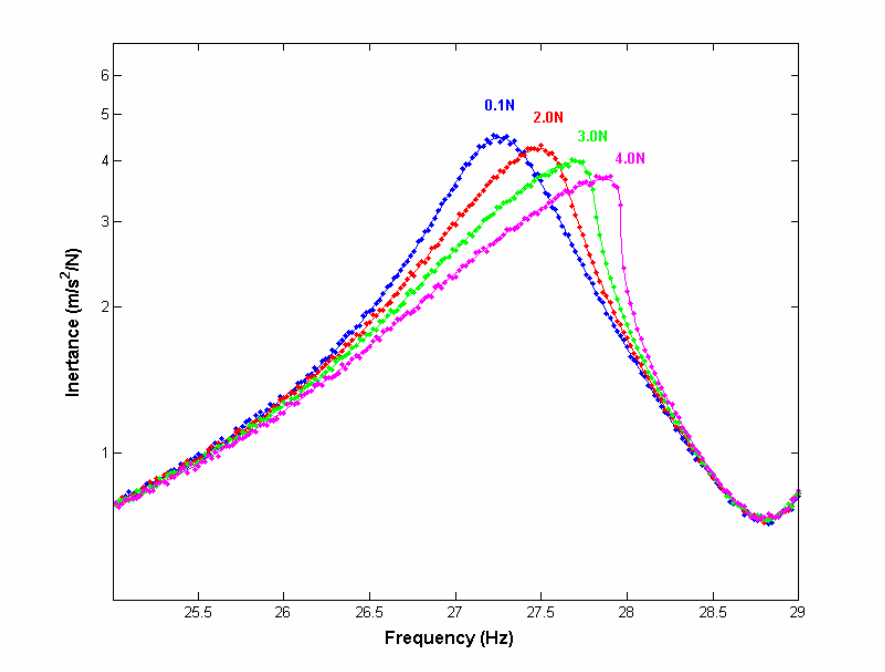

Figure 7 - 15 Comparison of FRFs for the 3rd order nonlinearity case

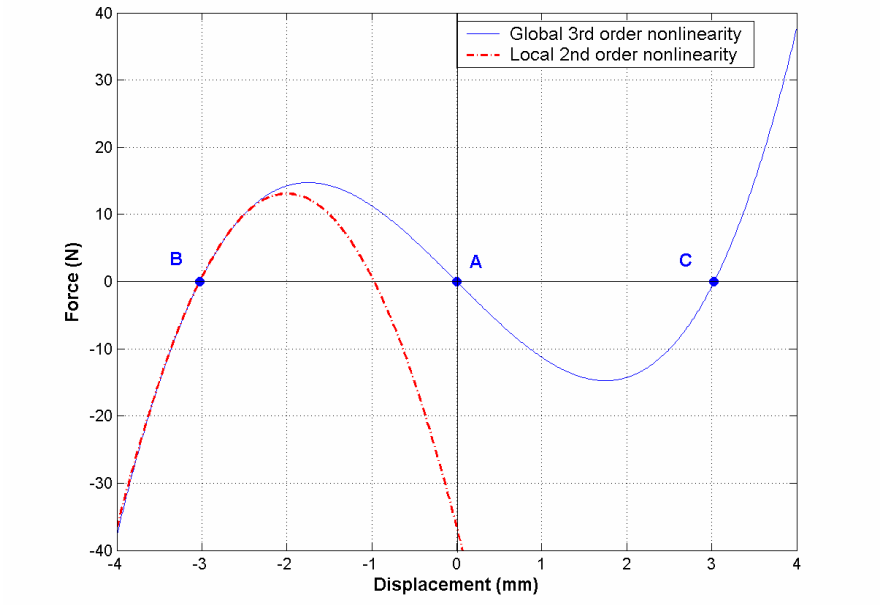

Figure 7 - 16 Indication of the 2nd order nonlinearity

Four runs of stepped-sine sweep tests have been carried out with controlled force amplitude at 0.1N, 2N, 3N and 4N, as indicated in Figure 7 - 17. The sweeps started from 5Hz to 80Hz with step size set at 0.2Hz. In each run, four modes were clearly identified within the frequency range. The influence of the nonlinearity is evident in the distorted FRF curves at modes 2 and 3. The peaks bend over to the lower frequency side as the excitation force level increases, an indication of weakening stiffness as expected. Mode 1 and 4 are the first and second bending modes of the test rig, as shown in Figure 7 - 14, which are not affected by the nonlinearity.

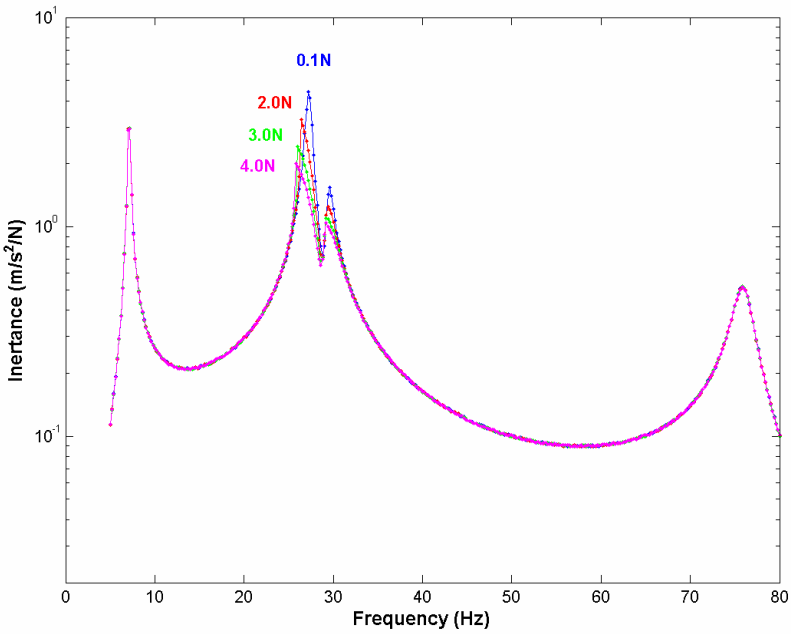

Figure 7 - 17 Measured FRFs for the 2nd order nonlinearity case

Finer sweep tests were carried out between 21Hz and 29Hz with a step size of 0.02Hz. Figure 7 - 18 shows the test results of three sweeps with different excitation forces. The excitation frequencies progressed from 21Hz to 29Hz. The solid lines are derived from the simulation with the Multi-Harmonic Balance Method. The solid lines cover steady-state solutions regardless whether the solution is stable or not. It is not possible to observe the unstable solution in tests unless special conditions are applied. One method was reported in a paper by Stanbridge et. al. [62], in which an additional mass must be added to the system. Also, the design of the force control algorithm was not as straightforward as the method used in this test. Without using the special treatment, the response

amplitude will jump at a frequency at which the steady-state solution becomes unstable. In the stepped-sine sweep test with 4.0N constant excitation force, the response amplitude jumped at 25.7Hz. The response amplitude jump is also observed in Figure 7 - 19, in which the stepped-sine sweeps start from 29Hz, i.e. sweep down in frequency.

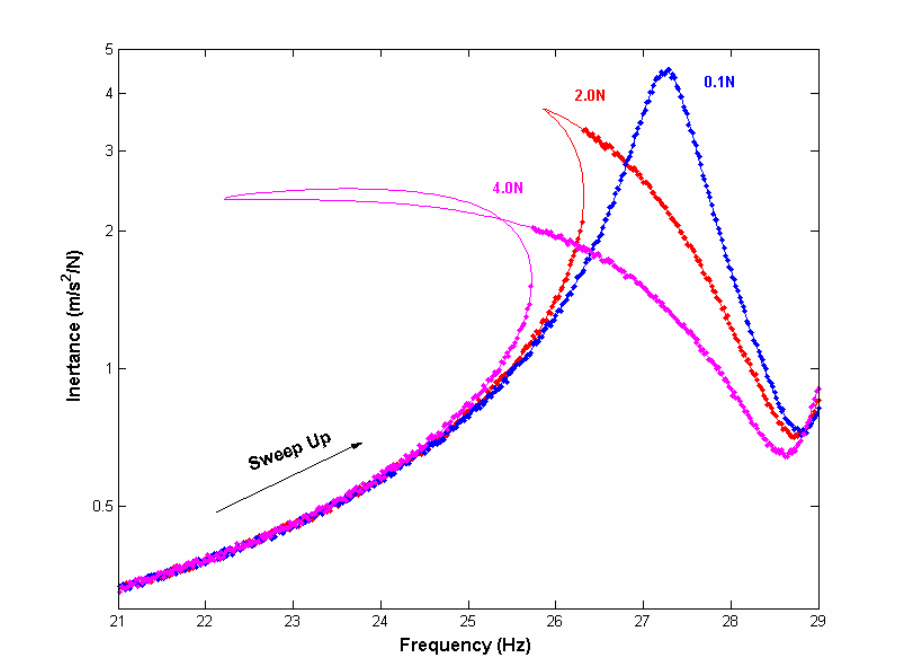

Figure 7 - 18 Comparison of FRFs for the 2nd order nonlinearity case – sweep up

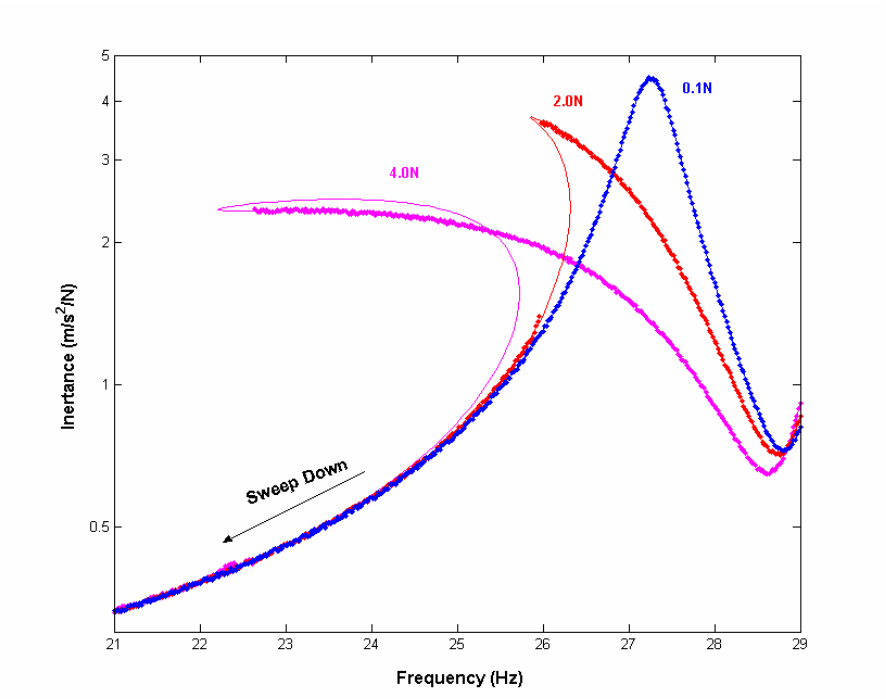

Figure 7 - 19 Comparison of FRFs for the 3rd order nonlinearity case - sweep down

The combination of Figure 7 - 18 and Figure 7 - 19, i.e. the sweep-up and sweep-down tests provides a full picture of steady-state response of such a nonlinear system in a practical situation.

7.3.3.3 Discussion of the nonlinear tests

The original idea behind the design of the Nonlinear Bearing Support was that it could display an adjustable nonlinearity and could be excited over its full operation range. A strong nonlinearity was achieved by compressing the steel strips into a slight buckled state, at which there existed non-stable negative stiffness. Analytically the steady-state solution of a system with such nonlinearity can be worked out using the Multi-Harmonic Balance Method, as demonstrated in Chapter Five; however as experienced by the author the steady-state response of such a system was difficult to achieve in experiment. The reasons, concluded after several failed attempts, are: firstly, large excitation force and shaker stroke are necessary in order to move the nonlinear bearing support over its full operation range. This requires either a large shaker or an additional control algorithm to compensate the force-displacement distortion inherited in the shaker due to the requirement for large stroke. This is especially true near the resonance frequencies. Secondly, there are multiple steady-state solutions at frequencies near the resonance. Initial conditions decide which steady-state solution the system will end up after the transient response decays away. The ‘transient’ stage in this case refers to the stage when the response tries to settle down on one steady-state solution while moving continuously from one steady-state solution to another. This transient response, or rather the ‘undetermined’ stage of the response requires much longer and basically unpredictable time to settle down, if ever it does. The requirement for the control algorithm to cope with such a property is very high.

In the two experimental case studies, the control algorithm showed stable operation and fast convergence when only the main harmonic component in the excitation was controlled. It would be ideal and also technically possible to control and keep the higher harmonics at zero; nevertheless the iteration and calculation would slow down the measurement, and as observed during the experiment, the higher harmonic components contributed only a few percent of

the total amplitude of the vibration at resonance. Therefore, it is reasonable to keep only the main harmonic terms in the experiment.

The damping of the nonlinear bearing support has not been mentioned in this thesis, for the purpose of simplifying the whole problem and focusing only on the nonlinearity in the stiffness. However, it does affect the prediction of the steady-state solutions. In this thesis work, a structural damping ratio of 0.05 was assigned to the joint, and indeed the prediction matches very nicely with the experiment result.

7.4 Concluding Remarks

The main theme of this thesis is about complex structural assembly modelling. It is not only about choosing the best available practices in mathematical modelling but also about carrying out systematic experiments to verify the analytical models. A fairly complicated test rig was designed and manufactured for such a purpose. It consists of key elements typical to complex structural assemblies: flexible components, semi-rigid connections and nonlinear elements. Dynamic tests were carried out on components, linear assemblies and nonlinear assemblies to measure steady-state responses which had good agreement with analytical analysis results.

Chapter 8

Conclusions and Future Work

8.1 Conclusion of the Research Work

The problem studied in this research originated from real life applications: we need a comprehensive methodology to model accurately and efficiently the dynamics of a complex structural assembly, such as a rotating machine, and the predictions from the assembly should be validated against experiments whenever possible. A bottom-up process was used in this thesis. It is similar to a product assembly line. It starts from small parts that have been manufactured to agreed standards. With properly-designed connection mechanisms, it eventually grows in complexity and completeness. The key for a high-quality final product relies on the high quality components and integration scheme. Similarly, in the structural modelling process, we need to take good care of components, linear joints, nonlinear joints and coupling algorithms in order to get a satisfactory final assembly model.

Each of the above topics can be studied relatively separately, and to a depth beyond the reach of a single thesis work. Rather, this thesis takes a step back and looks into how each can be best combined to serve the overall purpose of producing a ‘reliable’ model.

It is believed that in practical situations, 'real' loadings are not really known, material characteristics cannot be exactly predicted, and knowledge of how a structure actually works is imprecise because of the complexity; hence analytical models carrying uncertainty information are best for predicting and explaining the structural behaviour. Uncertainty definitely exists, but the boundary between certainty and uncertainty is not fixed. New techniques, methods and procedures can help to improve our grasp of the definite truth and push the boundary further into previously uncertain territory. It is the author's firm belief that we need to concentrate on perfecting our understanding of the definite world before resort to those uncertainty theories.

8.1.1 Conclusion on the Modelling of Linear Structures

Theories and methods behind linear structural modelling have already been well developed. It might seem to be quite basic nowadays, but it is crucial to get the fundamentals right before we embark on more complicated problems.

The Finite Element Method has been the dominant method to construct the fundamental Spatial model, from which the Modal model and Response model can be derived analytically if the structure can be considered to be linear. Theses three types of model representations are the key in structural dynamics analysis, because they are interrelated and can be derived from experiments on real structures. This provides the basis for validating the analytical model.

Model validation is a necessary step towards achieving an accurate component model. It is a way to minimise the uncertainty at the component level. The casing example discussed in Section 7.3.1 showed that the original value of one of the material properties, Young's Modulus, was not very accurate, possibly due to the uncertainty of the exact alloy used or processing at the manufacturing stage. This value was improved by carrying out a model updating process, after which the dynamic properties from both prediction and test were brought closer to each other. No perfect match was achieved though; this was attributed to the test method used, possible dimension variability in the thickness etc.

8.1.2 Conclusion on Joint Representations

Mechanical joints have all along been a difficult subject to study because of the large amount of variety and the complex physics they involve. If all the fine

details of a joint are included in the model, the resultant assembly model will be very large and efficient analysis of it will be a problem. Therefore some simplifications must be carried out. The aim is to provide manageable but realistic joint models to the whole assembly model at minimum cost.

Linearisation is the first type of simplification. Mechanical joints, even though their behaviour are better described as nonlinear, can sometimes still be considered as linear at normal operation conditions. They can be represented in the same way as other linear structural components, in the form of symmetric system matrices. The direct construction of such matrices can be tedious; hence using an FE model to model a joint is a convenient alternative. The advantage of the FE joint model is that it can be readily integrated with the remaining structural FE models. An example has been shown in Section 7.3.2 with such application. After parameter updating at the joint only, the linear structural assembly model displays dynamic properties that are comparable to the test.

When a nonlinearity must be included in the joint, some physical measurement has to be carried out. It should be noted that a joint is often extremely difficult to model accurately using a purely analytical method. It always relies on experimental data to verify and correct the mathematical models, normally in the form of constitutive equations, either by static loading or dynamic loading methods. The joint property of the nonlinear bearing support was obtained by conducting a static test as shown in Section 7.2.1.

8.1.3 Conclusion on the Modelling of Nonlinear Structures

Calculation efficiency is one of the areas that was assessed in this thesis. It is still a very challenging issue when studying the dynamics of nonlinear structures. Nonlinear differential equations that describe the dynamic system are difficult to solve analytically, as concluded by many mathematicians. Approximation methods are often good alternatives.

Depending on the domain in which the approximation method is conceptualised, nonlinear structural dynamic behaviour can be calculated in the time domain and/or the frequency domain. Most nonlinear problems are tackled in time domain, because it is straightforward and the results are directly comparable to experimental observation. However, time-domain analyses in the literature

mostly involve problems with only one or a few DOFs. They are used more for gaining insight into the physics of a nonlinear system, rather than for prediction purposes. If, however, slightly larger scale systems need to be dealt with, time domain analysis requires extremely large computation resource. It is without doubt that if all the parameters are set correctly, the time-domain calculations provide very accurate solution, but it is definitely not a choice if the prediction results need to be rapidly generated, e.g. if the prediction is used for condition monitoring purposes or for design optimisation procedures where a series of iterative stages are required to improve the initial design.

Frequency-domain methods are another choice, but they are limited to predicting steady-state response. If the transient response is of concern, this type of method cannot be used. Both transient response and steady-state response are important to the understanding of the structure's dynamic behaviour and either or both of them could be used to assess whether the analytical model is constructed correctly by comparing the simulation with experimental data. In addition, as was stated before, steady-state responses are most common for practical structures or machinery in steady operating conditions, so frequency-domain methods were chosen to study the nonlinear structural dynamics.

The Harmonic Balance Method is proven to be an efficient and accurate frequency-domain method. It can handle problems with very strong nonlinearity as shown in Section 4.4. A case study of a one DOF system with the combination of cubic and negative linear stiffness illustrated that a large number of steady-state solutions co-exist at the same excitation frequency at certain frequency range. This is in contrast to a linear system in which only one solution exists at each frequency. The calculation results from the Harmonic Balance Method agree very well with time-domain calculation results, and Harmonic Balance Method consumes much less computational power.

8.1.4 Conclusion on the Modelling of Complex Structures with Localised Nonlinearity

The difficulties relating to modelling a complex structure are mainly due to the existence of nonlinearities. There are two types of nonlinearity distributions in structures, global distribution, e.g. in the case of large displacement, and local

distribution, e.g. in the case of nonlinear joint. It is worth to be mentioned again here that nonlinearity is the underlying truth in describing the dynamic behaviour of engineering structures even though linearisation works very well in many cases.

The most common formation of a complex structure in reality is the combination of many linear components with linear or nonlinear joints, i.e. a largely linear structure with localised nonlinearity. Accurate and efficient modelling techniques for the complex structure are much dependent on the effective use of the dynamic information embedded in the linear part of the structural assembly.

The Frequency Response Function (FRF) coupling method is an accurate and efficient method in linear structural dynamics. The reduction of the problem size comes from the omission of DOFs that are of no interest while retaining the exact dynamic information in the remaining DOFs in the form of Frequency Response Functions. Combining the FRF coupling concept and the Harmonic Balance Method produced satisfactory prediction results for a complex structural assembly with localised nonlinearity, not only efficiently, as shown in Section 5.3.3, but also accurately, as shown in Section 7.3.3. The case study shows that it took no more than a few minutes of CPU time of a typical PC to find steady-state solutions across a large frequency range. If a conventional time domain method is used however, it would take hours of CPU time just to calculate a few seconds of response for the same system.

It was concluded after the whole exercise that FRF coupling together with Harmonic Balance Method is a very efficient and accurate way to model complex structures with localised nonlinearity, provided we have good component models and joint models and are interested in steady-state response conditions.

8.1.5 Conclusion on Experimental Verification of the Modelling Process

The main theme of this thesis is about complex structural assembly modelling. It is not only about choosing the best available practices in mathematical modelling but also about carrying out systematic experiments to verify the analytical models. A fairly complicated test rig was designed and manufactured for such a

purpose. It consists of key elements typical to complex structural assemblies: flexible components, semi-rigid connections and nonlinear elements.

In many respects the practice of vibration testing is a mixture of art and science. It requires experience, deep understanding of the subject and latest measurement technology available. There are too many variables in a test and there is no single right way to perform a vibration test.

The accuracy of the experimental measurements is dictated by the capabilities of the transducers, data processing equipment, test structure preparation and human involvement. Almost all methods for applying the structural excitation will have some unwanted modification effects on the structure, as well almost all the response measurement transducers and support fixtures will have an unwanted influence on the structure too. Many of the potential problems with dynamic tests only become apparent during the actual tests. We should be aware of these problems and strive to select appropriate methods to minimise these effects. On the other hand, we should accept the limitations caused by other more uncontrollable factors, e.g. time and cost limitation. Instead of pursuing the best test practices, we may have to settle on the best available practices.

To accomplish the verification of the nonlinear calculation algorithm, an amplitude- controlled nonlinear dynamic testing code was introduced. It was to some degree, the application of the Harmonic Balance Method in test. Though relatively simple in concept, the implementation of the algorithm was rather troublesome. Some achievements have been made, in terms of improving the reliability, safety measures and reducing the test time.

8.2 Contributions

A summary of major contributions of this research work is reported below:

- The single most important contribution of this thesis work to the field of structural dynamics is that for the first time the issue of both accuracy and efficiency regarding the dynamic modelling of complex structural assembly is addressed, examined in detail and more importantly, verified successfully against a series of experiments conducted on a relatively complicated structural assembly. FRF coupling combined with the Harmonic Balance

Method is demonstrated to be capable of accurately predicting the steady-state response of nonlinear structural assembly in a very timely fashion;

- The Harmonic Balance Method has been applied successfully on a 1-DOF nonlinear system in finding a large number of steady-state solutions: major-, sub- and super- harmonic responses upon the same external excitation. It not only shows the effectiveness of frequency-domain method comparing to time-domain method, but also shows the effect of nonlinearity on the structural's dynamic behaviour;
- A test rig was designed and manufactured. It has a prominent and adjustable nonlinear element built in, as well as the key structural elements that can be found in typical rotating equipment, which make it a very versatile test specimen that can be used beyond this project;
- A robust amplitude-controlled nonlinear dynamic testing code was developed, which has been successfully tested out.

8.3 Future Work

Here is a list of topics that author finds interesting and would like to suggest pursuing further:

- One of the characteristics of analytical steady-state response of nonlinear structure is the possible existence of non-stable solutions. Harmonic Balance Method can not produce results that differentiate these two types of solution, without referring to classical time-domain methods. It will be very useful to further develop the frequency-domain methods that can efficiently differentiate these two;
- Nonlinearity identification is another area to be explored with the application of the calculation algorithm for complex structural assembly. It is not an easy task because being an inverse problem, there are much more unknown variables than the known ones. However this can be potentially very valuable, especially in damage detection, because damage is often the source of nonlinearities and can alter the steady-state dynamic properties during normal operation, which could be picked up as an indication of its existence;

- The amplitude-controlled nonlinear dynamic testing code should be further developed. It should include more harmonics in its control loop so that it is possible to handle more severe nonlinear cases.

8.4 Papers and Reports Related to the Thesis Work

Some publications attributed to this thesis work are listed below.

8.4.1 Conference Publications

2. S. Huang, D. A. Robb, D. J. Ewins and E. Petrov, “Dynamic Modelling and Testing of a Representative Aeroengine Test Rig with Adjustable Nonlinear Bearing Supports”, presented at ISMA2006 International Conference on Noise and Vibration Engineering, Leuven, Belgium, 2006.

1. S. Huang, E. Petrov, and D. J. Ewins, "Comprehensive Analysis of Periodic Regimes of Forced Vibration for Structures with Nonlinear Snap-Through Springs," presented at 6th International Conference on Modern Practice in Stress and Vibration Analysis, Bath, UK, 2006.

8.4.2 Reports

Europe Union Project – GROWTH – MagFly (GRD1-2001-40191)

6. S. Huang and D. A. Robb, “Structural Damage Sensitivity Investigation with the Application of Modal Data”.

5. S. Huang and D. A. Robb, “Integrated Dynamic Model of Complete System”.

4. S. Huang and D. A. Robb, “Development of validated component modelling techniques for casing, bearing supports and rotor to provide representative characteristics”.

3. W. Liu, S. Huang, and D. A. Robb, “Sensor Placement Optimisation for Damage Detection”.

2. S. Huang, W. Liu and D. A. Robb, “Development of Reliable Model Reduction Techniques for the Whole System”.

1. S. Huang, and D. A. Robb, ”Alternative Design of Load-Sharing Bearings”.

References

[1] D. J. Ewins, *Modal Testing: Theory, Practice and Application*, 2nd ed: Research Studies Press Ltd, 2000.

[2] R. W. Clough and J. Penzien, *Dynamics of Structures*: McGraw-Hill, Inc., 1993.

[3] R. W. Clough, "The Finite Element Method in Plane Stress Analysis," presented at 2nd ASCE Conference on Eletronic Computation, Pittsburgh, PA, 1960.

[4] A. Hrenikoff, "Solution of Problems in Elasticity by the Framework Method," *Journal of Applied Mechanics*, vol. 8, pp. 169-175, 1941.

[5] K. H. Huebner, D. L. Dewhirst, D. E. Smith, and T. G. Byrom, *The Finite Element Method for Engineers*, 4th ed: Wiley, 2001.

[6] G. Chen, "FE Model Validation for Structural Dynamics," PhD Thesis, Department of Mechanical Engineering, Imperial College London, 2001.

[7] D. J. Ewins, "Model Validation: Correlation for Updating," *Proc. of Indian Academy Sciences, Sadhana*, vol. 25, pp. 221-234, 2001.

[8] M. I. Friswell and J. E. Mottershead, *Finite Element Model Updating and Structural Dynamics*: Kluwer Academic Publishers, 1995.

[9] D. J. Ewins, "Adjustment or Updating of Models," *Proc. of Indian Academy Sciences, Sadhana*, vol. 25, pp. 235-245, 2001.

[10] M. Imregun and W. J. Visser, "A Review of Model Updating Techniques," *Shock and Vibration Digest*, vol. 3, pp. 9-20, 1991.

[11] J. E. Mottershead and M. I. Friswell, "Model Updating in Structure Dynamics: a Survey," *Journal of Sound and Vibration*, vol. 167, pp. 347-376, 1993.

[12] Y. H. Chong and M. Imregun, "Coupling of Non-linear Substructures using Variable Modal Parameters," *Mechanical Systems and Signal Processing*, vol. 14, pp. 731-746, 2000.

[13] J. V. Ferreira, "Dynamic Response Analysis of Structures with Nonlinear Components," PhD Thesis, Department of Mechanical Engineering, Imperial College London, 1998.

[14] B. Jetmundsen, R. L. Bielawa, and W. G. Flannelly, "Generalized Frequency Domain Substructure Synthesis," *Journal of the American Helicopter Society*, vol. 33, pp. 55-64, 1988.

[15] W. C. Hurty, "Vibrations of Structural Systems by Component Mode Synthesis," *Journal of Engineering Mechanics*, vol. 86, pp. 51-69, 1960.

[16] N. M. M. Maia, J. M. M. Silva, and etc., *Theoretical and Experimental Modal Analysis*: Research Studies Press Ltd, 1997.

[17] R. R. Craig, "A Review of Time-Domain and Frequency-Domain Component Mode Synthesis Method," *International Journal of Analytical and Experimental Modal Analysis*, vol. 2, pp. 59-72, 1987.

[18] R. J. Guyan, "Reduction of Stiffness and Mass Matrices," *AIAA Journal*, vol. 3, pp. 380, 1965.

[19] R. R. Craig, "Methods of Component Mode Synthesis," *Shock and Vibration Digest*, vol. 9, pp. 3-10, 1977.

[20] M. Misawa and H. Katayama, "Improvement of Boundary Modes in Component Mode Synthesis," presented at IMAC XXI, Kissimmee, Florida, US, 2003.

[21] W. Liu and D. J. Ewins, "Substructure Synthesis Via Elastic Media," *Journal of Sound and Vibration*, vol. 257, pp. 361-379, 2002.

[22] J. Kim, J. C. Yoon, and B. S. Kang, "Finite Element Analysis and Modelling of Structure with Bolted Joints," *Applied Mathematical Modelling*, vol. 31, pp. 895-911, 2007.

[23] J. Mackerle, "Finite Element Analysis of Fastening and Joining: Abibliography (1990-2002)," *International Journal of Pressure Vessels and Piping*, vol. 80, pp. 253-271, 2003.

[24] B. J. Hamrock, B. O. Jacobson, and S. R. Schmid, *Fundamental of Machine Elements*: Mcgraw Hill, 1999.

[25] J. G. Maloney, M. T. Shelton, and D. A. Underhill, "Structural Dynamic Properties of Tactical Missile Joints," General Dynamics CR-6-384-945-001, 1970.

[26] M. Palmonella, M. I. Friswell, J. E. Mottershead, and A. W. Lees, "Finite Element Models of Spot Welds in Structural Dynamics: Review and Updating," *Computers & Structures*, vol. 83, pp. 648-661, 2005.

[27] B. Horton, H. Gurgenci, M. Veidt, and M. I. Friswell, "Finite Element Model Updating of the Welded Joints in a Tubular H-Frame," presented at 17th International Modal Analysis Conference, Orlando, Florida, USA,, 1999.

[28] W. H. Zhu, S. Stoeck, H. Pape, and S. L. Gan, "Comparative Study On Solder Joint Reliability Using Different FE-Models," presented at Electronics Packaging Technology Ccnference, 2003.

[29] H. Ahmadian, M. Ebrahimi, J. E. Mottershead, and M. I. Friswell, "Identification of Bolted Joint Interface Models," presented at ISMA 27, Leuven, Belgium, 2002.

[30] R. A. Ibrahim and C. L. Pettit, "Uncertainties and Dynamic Problems of Bolted Joints and Other Fasteners " *Journal of Sound and Vibration*, vol. 279, pp. 857-936, 2005.

[31] H. Ahmadian and H. Jalalia, "Generic element formulation for modelling bolted lap joints " *Mechanical Systems and Signal Processing* 2007.

[32] E. J. Berger, "Friction Modeling for Dynamic System Simulation," *Applied Mechanics Reviews*, vol. 55, pp. 495-533, 2002.

[33] L. Gaul and R. Nitsche, "The Role of Friction in Mechanical Joints. ," *Applied Mechanics Reviews*, vol. 52, pp. 93–106, 2001.

[34] D. J. Segalman, "Modelling joint friction in structural dynamics," vol. Structural Control and Health Monitoring, pp. 430-453, 2006.

[35] F. P. Bowden and D. Tabor, *The Friction and Lubrication of Solids*. Oxford: Oxford University Press, 1950.

[36] H. Olsson, K. J. Astrom, C. Canudas de Wit, M. Cafvert, and P. Lischinsky, "Friction models and friction compensation," *European journal of control*, vol. 4, pp. 176-195 1998.

[37] C. Kajdas, S. S. K. Harvey, and E. Wilusz, *Encyclopedia of Tribology*: Elsevier, 1990.

[38] C. Canudas de Wit, H. Olsson, K. J. Astrom, and P. Lischinsky, "A New Model for Control of Systems with Friction," *IEEE Transactions on Automatic Control*, vol. 40, pp. 419-425, 1995.

[39] D. D. Quinn and D. J. Segalman, "Using Series-Series Iwan-Type Models for Understanding Joint Dynamics," *Journal of Applied Mechanics*, vol. 72, pp. 666-673, 2005.

[40] W. D. Iwan, "A Distributed-element Model for Hysteresis and Its Steady-state Dynamic Response," *Journal of Applied Mechanics*, vol. 33, pp. 893-900, 1966.

[41] W. D. Iwan, "On a Class of Models for the Yielding Behavior of Continuous and Composite Systems," *Journal of Applied Mechanics*, vol. 89, pp. 612-617, 1967.

[42] L. Gaul and J. Lenz, "Nonlinear Dynamics of Structures Assembled by Bolted Joints," *Acta Mechanica*, vol. 125, pp. 169-181, 1997.

[43] Y. C. Wang, S. G. Adams, J. S. Thorp, and e. al., "Chaos in MEMS, Parameter Estimation and Its Potential Application," *IEEE Transactions on Circuits and Systems - I: Fundamental Theory and Applications*, vol. 45, pp. 1013-1020, 1998.

[44] M. J. Brennan, S. J. Elliott, P. Bonello, and J. F. V. Vincent, "The "Click" Mechanism in Dipteran Flight: If it Exists, Then What Effect Does it Have?," *Journal of Theoretical Biology*, vol. 224, pp. 205-213, 2003.

[45] M. Boeswald, M. Link, S. Meyer, and M. Weiland, "Investigations on the Non-Linear Behaviour of a Cylindrical Bolted Casing Joint Using High Level Base Excitation Tests," presented at ISMA2002, Leuven, Belgium, 2002.

[46] J. F. Wilson and E. G. Callis, "The Dynamics of Loosely Jointed Structures," *International Journal of Non-Linear Mechanics*, vol. 39, pp. 503-514, 2004.

[47] G. Schmidt and A. Tondl, *Non-Linear Vibrations*: Cambridge University Press, 1986.

[48] C. Hayashi, *Nonlinear Oscillations in Physical Systems*: McGraw-Hill, Inc, 1964.

[49] W. Cheney and D. Kincaid, *Numerical Mathematics and Computing*, 5th ed: Wadsworth, 2004.

[50] A. Ralston, *A first course in numerical analysis*: McGraw-Hill, 1965.

[51] C. Moler, *Numerical Computing with MATLAB*: SIAM, 2004.

[52] P. Henrici, *Discrete Variable Methods in Ordinary Differential Equations*: John Wiley & Sons, 1968.

[53] M. A. Dokainish and K. Subbaraj, "A Survey of Diret Time-Integration Methods in Computational Structural Dynamics - I. Explicit Methods," *Computers & Structures*, vol. 32, pp. 1371-1386, 1989.

[54] N. M. Newmark, "A Method of Computation for Structural Dynamics," *Journal of the Engineering. Mechanics Division, ASCE*, vol. 85, pp. 67-94, 1959.

[55] E. L. Wilson, I. Farhoomand, and K. J. Bathe, "Nonlinear Dynamic Analysis of Complex Structrues," *Earthquack Engineering Structure Dynmaics*, vol. 1, pp. 1519-1528, 1973.

[56] K. Subbaraj and M. A. Dokainish, "A Survey of Direct Time-Integration Methods in Computational Structural Dynamics - II. Implicit Methods," *Computers & Structures*, vol. 32, pp. 1387-1401, 1989.

[57] J. C. Houbolt, "A Recurrence Matrix Solution for the Dynamic Response of Elastic Aircraft," *Journal of Aeronautical Sciences*, vol. 17, pp. 540-550, 1950.

[58] W. T. Thomson, *Theory of Vibration with Applications*, 4th ed: Prentice-Hall, 1993.

[59] N. N. Bogoliubov and J. A. Mitropolsky, *Asymptotic Methods in the Theory of Non-linear Oscillations*: Hindustan Publishing Company, 1963.

[60] O. Tanrikulu, B. Kuran, N. Ozguven, and M. Imregun, "Forced Harmonic Response Analysis of Nonlinear Structures Using Describing Functions," *AIAA*, vol. 31, pp. 1313-1320, 1993.

[61] G. Groll, "Windmilling in Aero-Engines," PhD Thesis, Department of Mechanical Engineering, Imperial College London, 2001.

[62] A. B. Stanbridge, K. Y. Sanliturk, D. J. Ewins, and J. V. Ferreira, "Experimental Investigation of Dry Friction Damping and Cubic Stiffness Nonlinearity," presented at ASME Design Technical Conferences, Pittsburgh, Pennsylvania, 2001.

[63] E. P. Petrov and D. J. Ewins, "Analytical formulation of friction interface elements for analysis of nonlinear multi-harmonic vibrations of bladed discs," *Trans. ASME: J. of Turbomachinery*, vol. 125, pp. 364-371, 2003.

[64] E. P. Petrov, "A Method for Use of Cyclic Symmetry Properties in Analysis of Nonlinear Multiharmoic Vibrations of Bladed Disks," *Journal of Turbomachinery*, vol. 126, pp. 175-183, 2004.

[65] P. Holmes, "A Nonlinear Oscillator with a Strange Attractor," *Philosophical Transactions of the Royal Society of London*, vol. 294, pp. 419-448, 1979.

[66] E. P. Petrov, "Forced Response Suite (FORSE) - Computer code for multi-harmonic balance analysis," Imperial College London.

[67] C. Nataraj and H. D. Nelson, "Periodic Solutions in Rotor Dynamic Systems With Nonlinear Supports: A General Approach," *Journal of Vibration, Acoustics, Stress, and Reliability in Design*, vol. 111, pp. 187-193, 1989.

[68] E. H. Dowell, "Component Mode Analysis of Nonlinear and Nonconservative Systems," *Journal of Applied Mechanics*, vol. 47, pp. 172-176, 1980.

[69] K. Watanabe and H. Sato, "Development of Nonlinear Building Block Approach," *Journal of Vibration, Acoustics, Stress, and Reliability in Design*, vol. 110, pp. 36-41, 1988.

[70] J. Kim and T. D. Burton, "Reduction of Nonlinear Structural Models Having Nonsmooth Nonlinearity," presented at International Modal Analysis Conference, Los Angeles, US, 2002.

[71] J. V. Ferreira and D. J. Ewins, "Nonlinear Receptance Coupling Approach Based on Describing Functions," presented at 14th International Modal Analysis Conference, Dearborn, US, 1996.

[72] J. V. Ferreira and D. J. Ewins, "Multi-Harmonic Nonlinear Receptance Coupling Apprach Based on Describing Functions," presented at 15th International Modal Analysis Conference, Orlando, US, 1997.

[73] J. S. Rao, "Dynamics of a Three Level Rotor System Using Solid Elements," presented at ASEM Turbo Expo 2003, Altanta, US, 2003.

[74] M. Karlberg and J. O. Aidanpaa, "Numerical Investigation of an Unbalanced Rotor System with Bearing Clearance," *Chaos, Solitons and Fractals*, vol. 18, pp. 653-664, 2003.

[75] K. Hu, Z. P. Mourelatos, and N. Vlahopoulos, "Computational Analysis for Dynamic Response of a Rotating Shaft on Flexible Support Structure with Clearances," *Journal of Sound and Vibration*, vol. 267, pp. 1-28, 2003.

[76] S. Huang and D. A. Robb, "Real Time Simulation of Full Engine and Response to Transient Loads," European Community Competitive and Sustainable Growth Programme GRD1-2001-40191, 20th October 2006.

[77] K. G. McConnell, *Vibration Testing: Theory and Practice*: John Wiley & Sons, Inc., 1995.

[78] *Handbook on Modal Testing*: Dynamic Testing Agency, 1993.

[79] R. B. Randall, *Frequency Analysis*: Brüel & Kjaer, 1987.

[80] M. I. Friswell and J. E. T. Penny, "Stepped Sine Testing Using Recursive Estimation," *Mechanical Systems and Signal Processing*, vol. 7, pp. 477-491, 1993.

[81] S. Perinpanayagam, "Modal test Strategy for Early Model Validation of Engineering Strucutres," PhD Thesis, Department of Mechanical Engineering, Imperial College London, 2004.

[82] W. M. To and D. J. Ewins, "A Closed-Loop Model for Single/Multi-shaker Modal Testing," *Mechanical Systems and Signal Processing*, vol. 5, pp. 305-316, 1991.

[83] G. R. Tomlinson, " Force Distortion in Resonance Testing of Structures with Electro-dynamic Vibration Exciters," *Journal of Sound and Vibration*, vol. 63, pp. 337-350, 1979.

[84] I. Bucher, "Exact Adjustment of Dynamic Forces in Presence of Non-Linear Feedback and Singularity - Theory and Algorithm," *Journal of Sound and Vibration*, vol. 218, pp. 1-27, 1998.

[85] "ICATS Suite 2006," Imperial College London, 2006.

[86] D. J. Ewins, "Modal Analysis for Rotating Machinery," presented at Proceedings of 5th International Conference on Rotor Dynamics, Darmstadt, Germany, 1998.

[87] C. Zang, G. Chen, D. J. Ewins, and R. A. Ibrahim, "Review of Current Status of Full-filed Measurement Equipment Hardware and Software, Test Planning and Integration Tools, Suggestions for Future Development," European Union VIVACE Project 2005.

[88] L. E. Drain, *The Laser Doppler Technique*: Wiley & Sons., 1980.

[89] B. Raton, *The Measurement, Instrumentation and Sensors Handbook*: CRC Press Ltd., 2001.

Appendix A

Technical Drawings

A.1 Casing

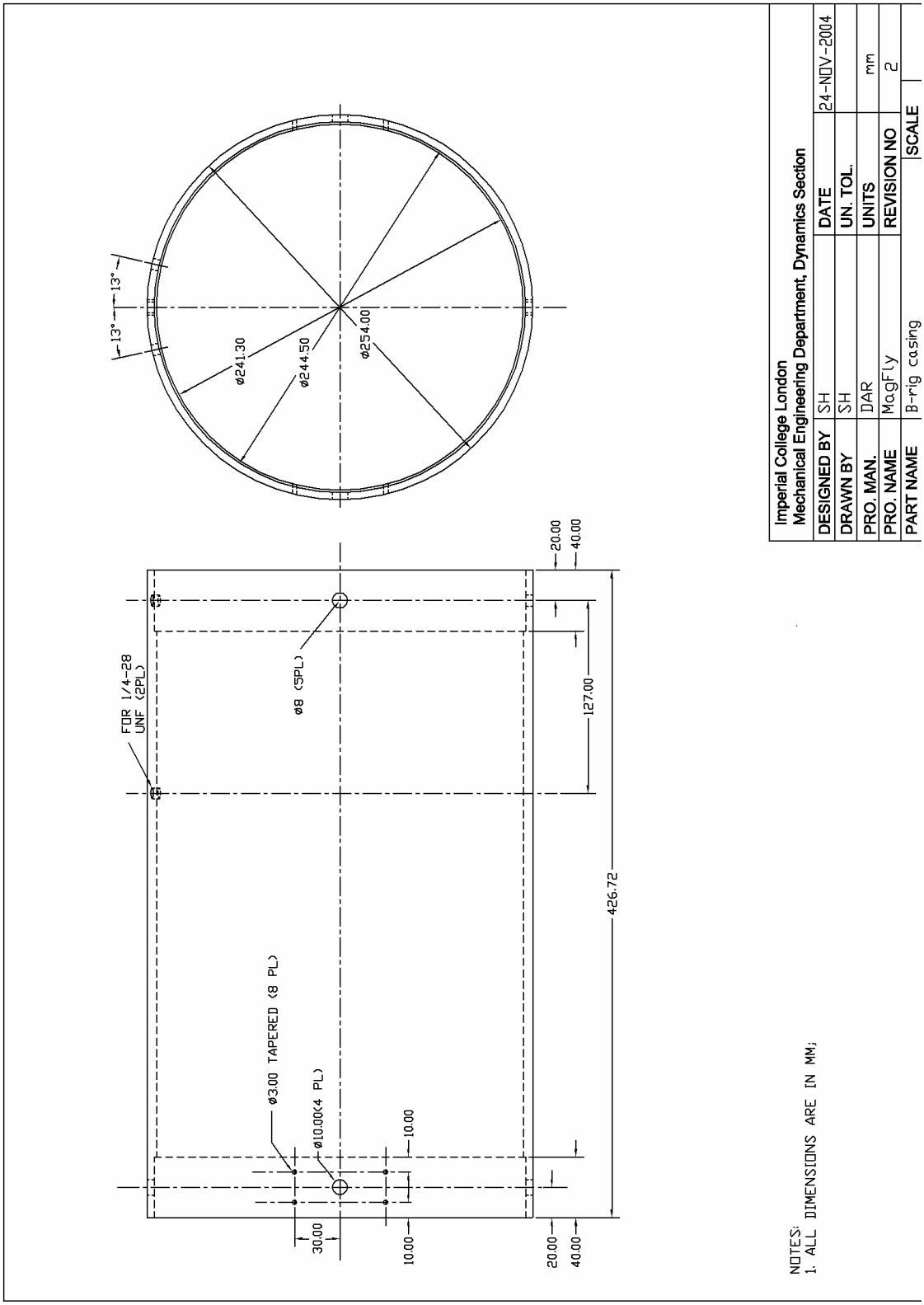
13°
13°
ø241.30
ø244.50
ø254.00
20.00
40.00
FOR 1/4-28 UNF (2PL)
ø8 (5PL)
127.00
426.72
ø3.00 TAPERED (8 PL)
ø10.00(4 PL)
10.00
30.00
10.00
20.00
40.00
NOTES:
1. ALL DIMENSIONS ARE IN MM;
Imperial College London
Mechanical Engineering Department, Dynamics Section
DESIGNED BY SH
DRAWN BY SH
PRO. MAN. DAR
PRO. NAME MagFly
PART NAME B-rig casing
DATE 24-NOV-2004
UN. TOL.
UNITS mm
REVISION NO 2
SCALE

A.2 Linear Bearing Support

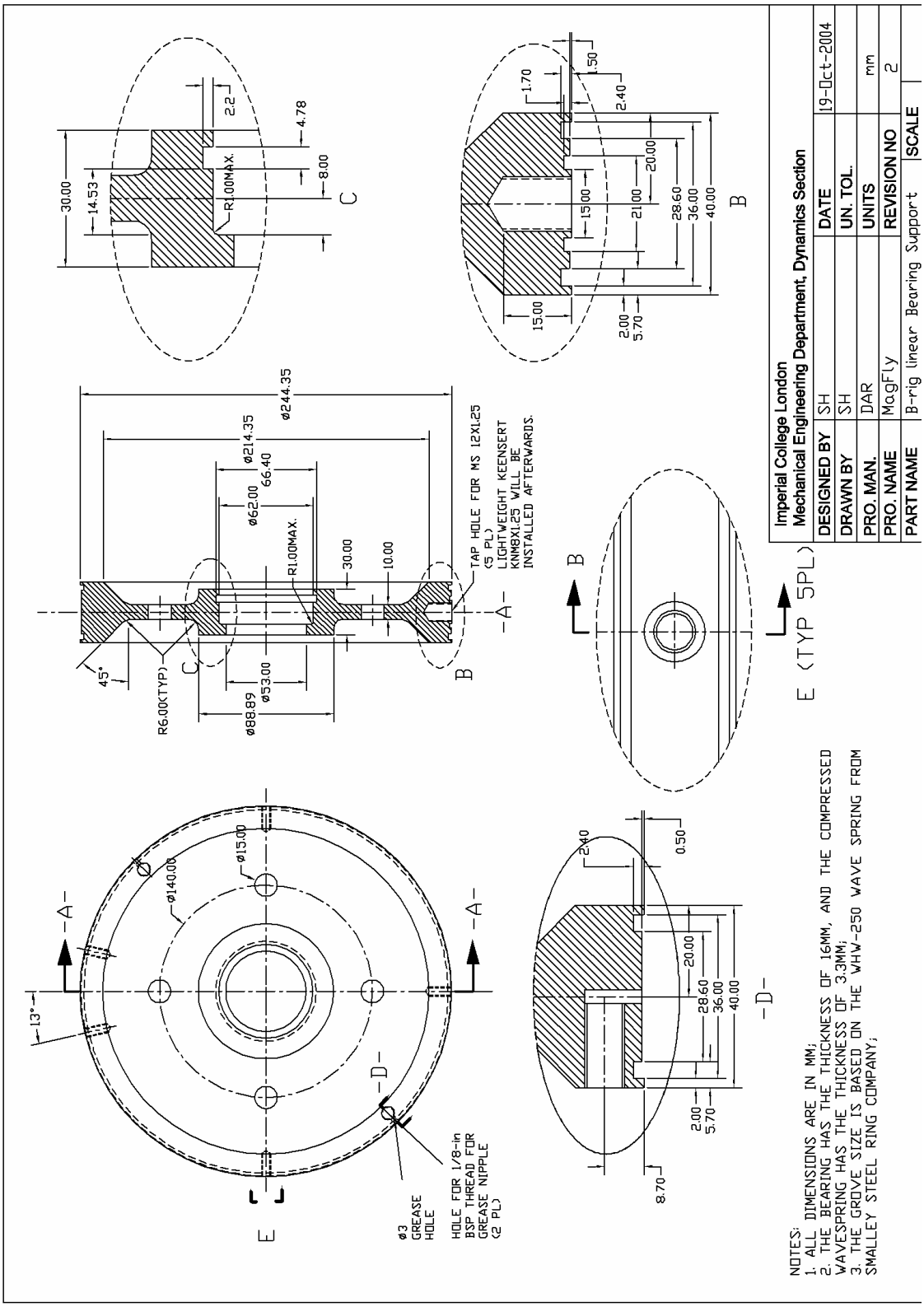

A.3 Nonlinear Bearing Support – Rim

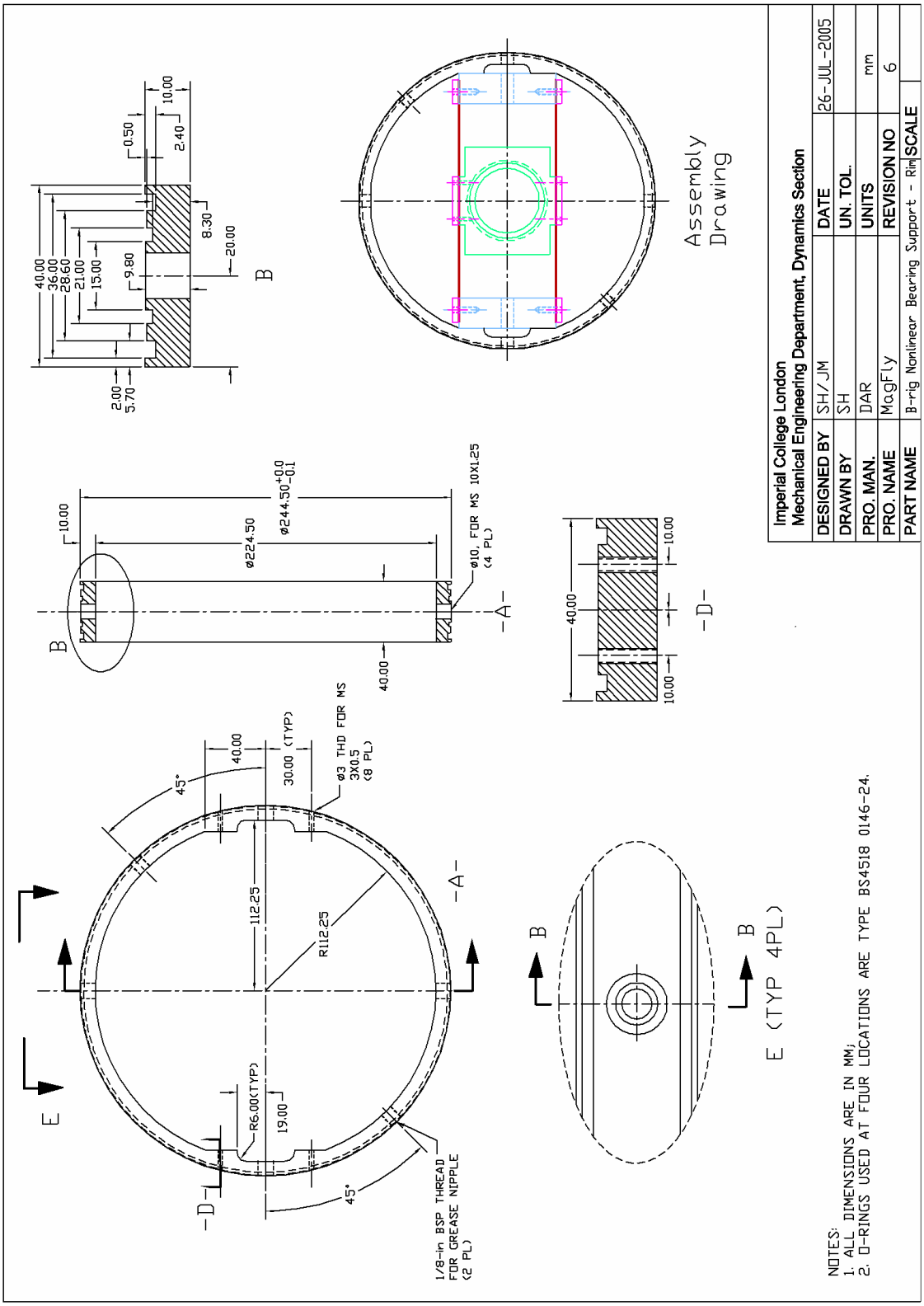

A.4 Nonlinear Bearing Support – Assembly

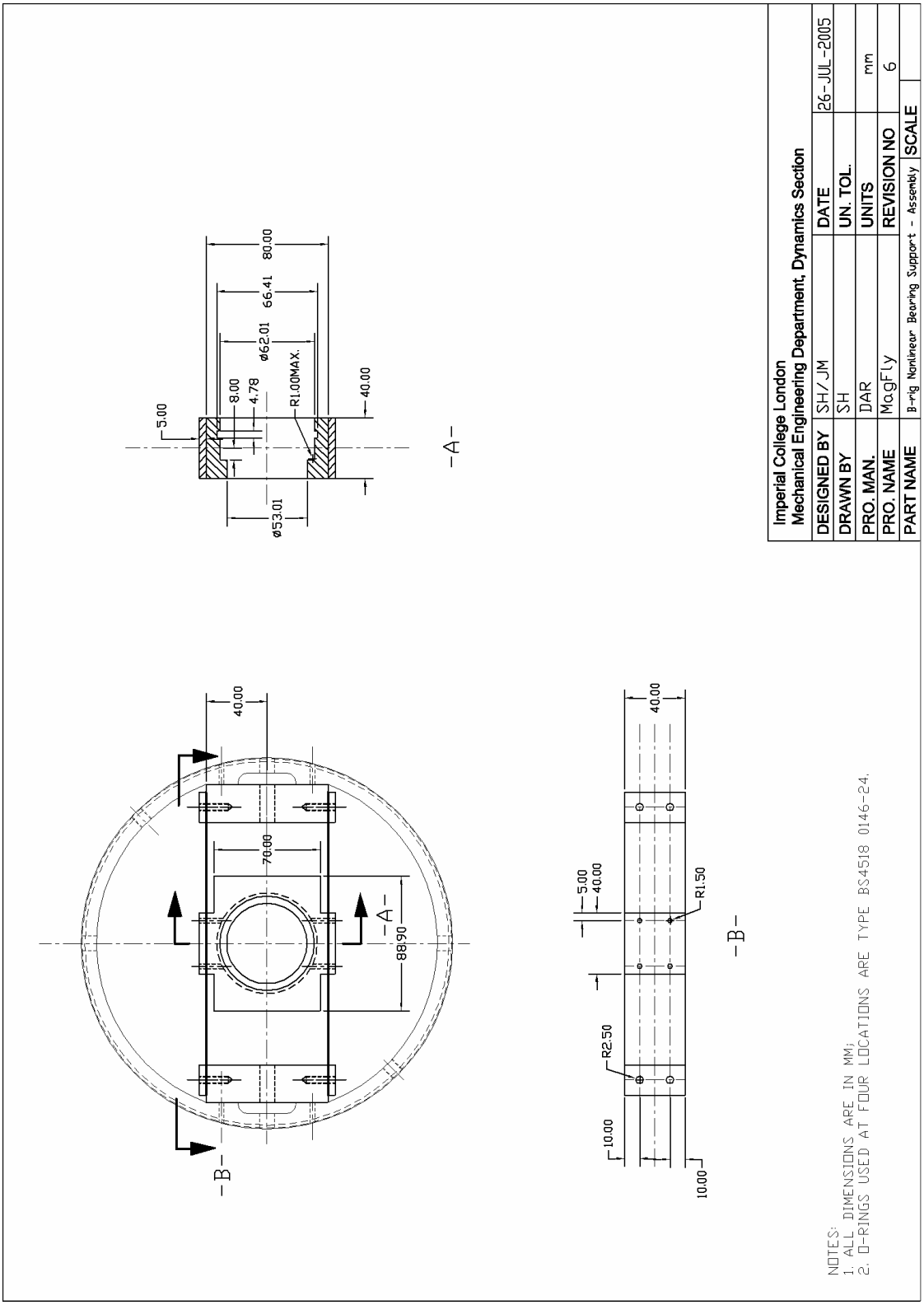

A.5 Shaft Lock

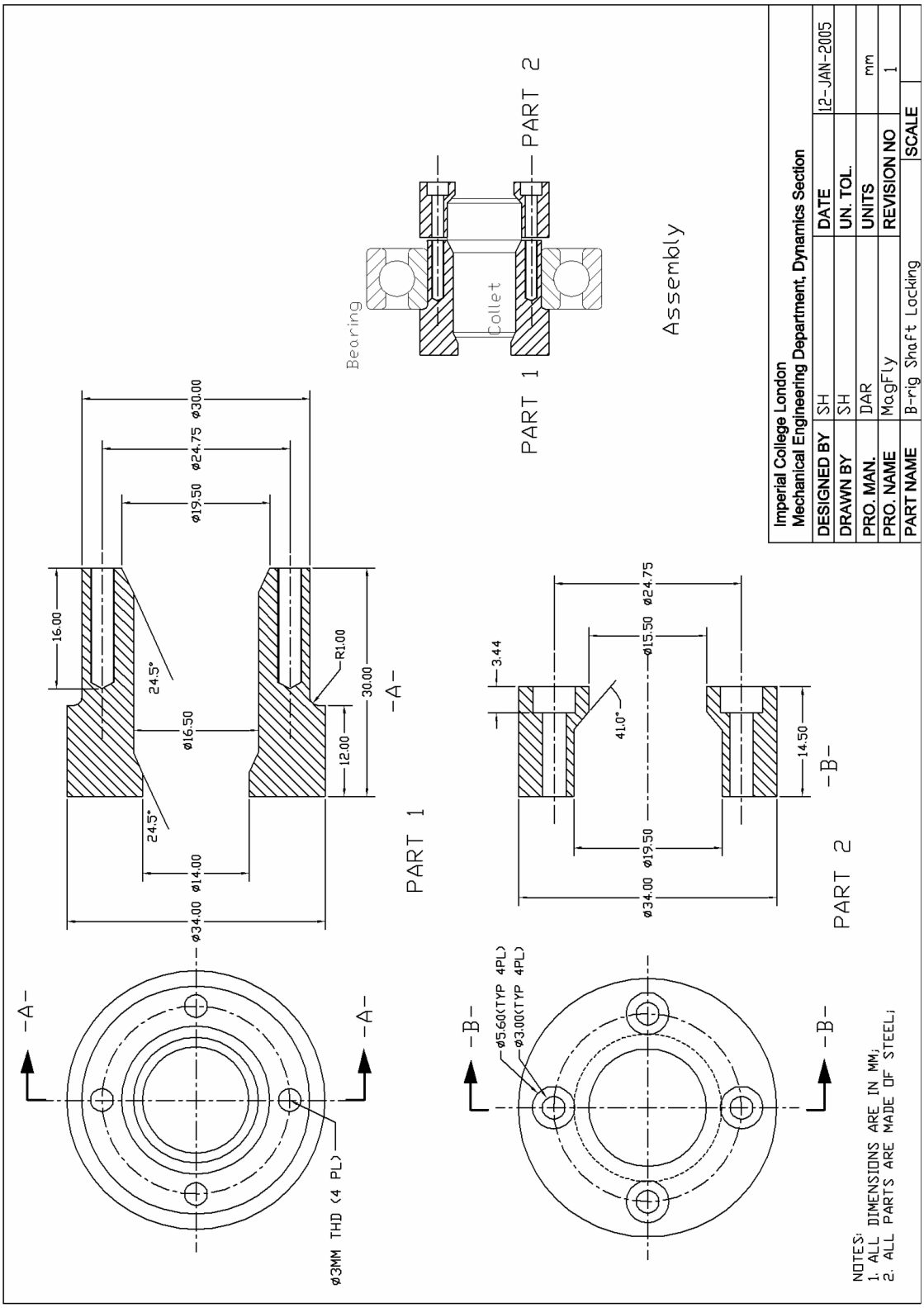

A.6 Rotor

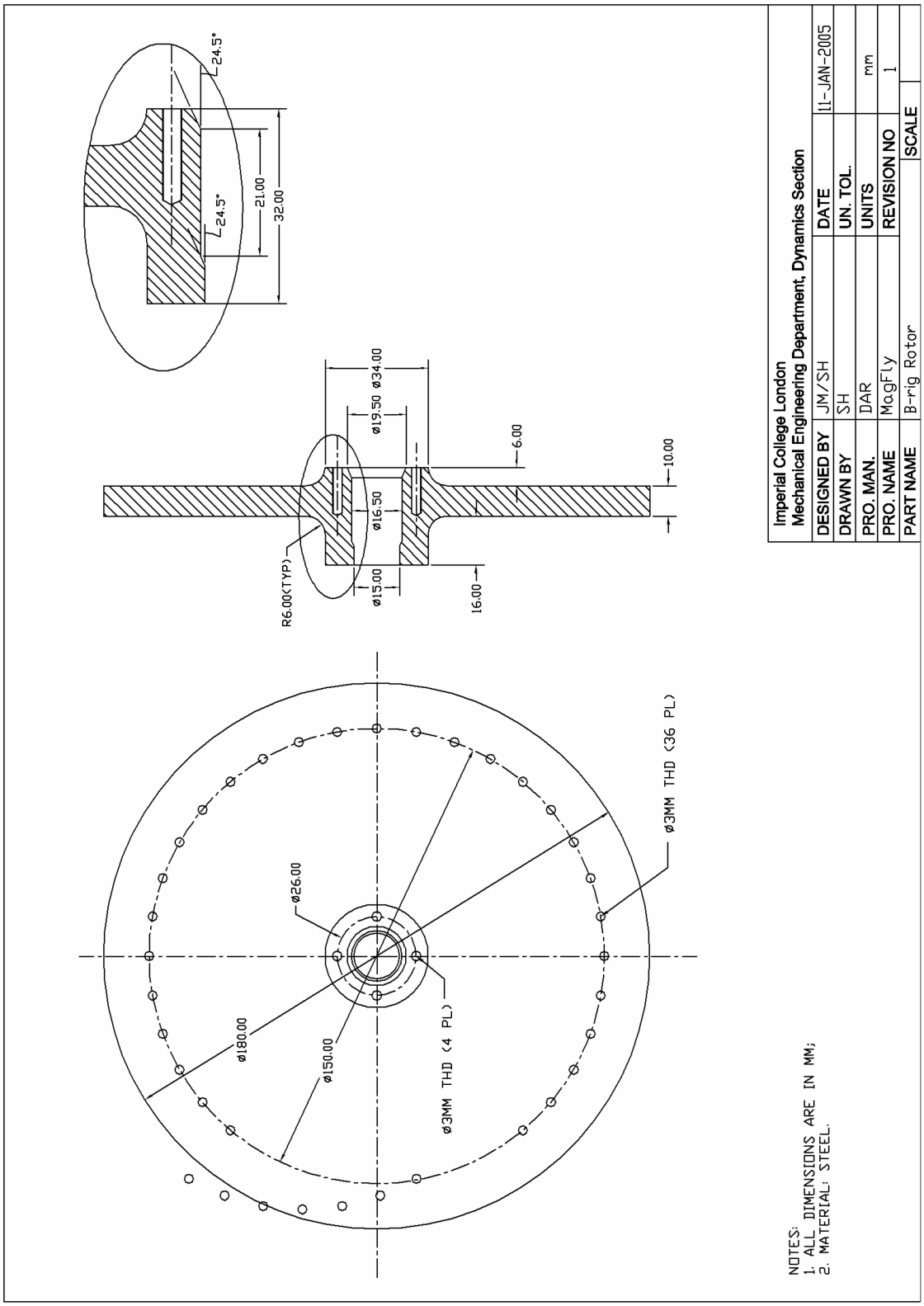
24.5°
24.5°
21.00
32.00
ø19.50 ø34.00
6.00
10.00
ø16.50
ø15.00
16.00
R6.00(TYP)
ø26.00
ø180.00
ø150.00
ø3MM THD (36 PL)
ø3MM THD (4 PL)
NOTES:
1. ALL DIMENSIONS ARE IN MM;
2. MATERIAL: STEEL.
Imperial College London
Mechanical Engineering Department, Dynamics Section
DESIGNED BY JM/SH
DRAWN BY SH
PRO. MAN. DAR
PRO. NAME MagFly
PART NAME B-rig Rotor
DATE 11-JAN-2005
UN. TOL.
UNITS mm
REVISION NO 1
SCALE

A.7 Structural Bar and Miscellaneous Components

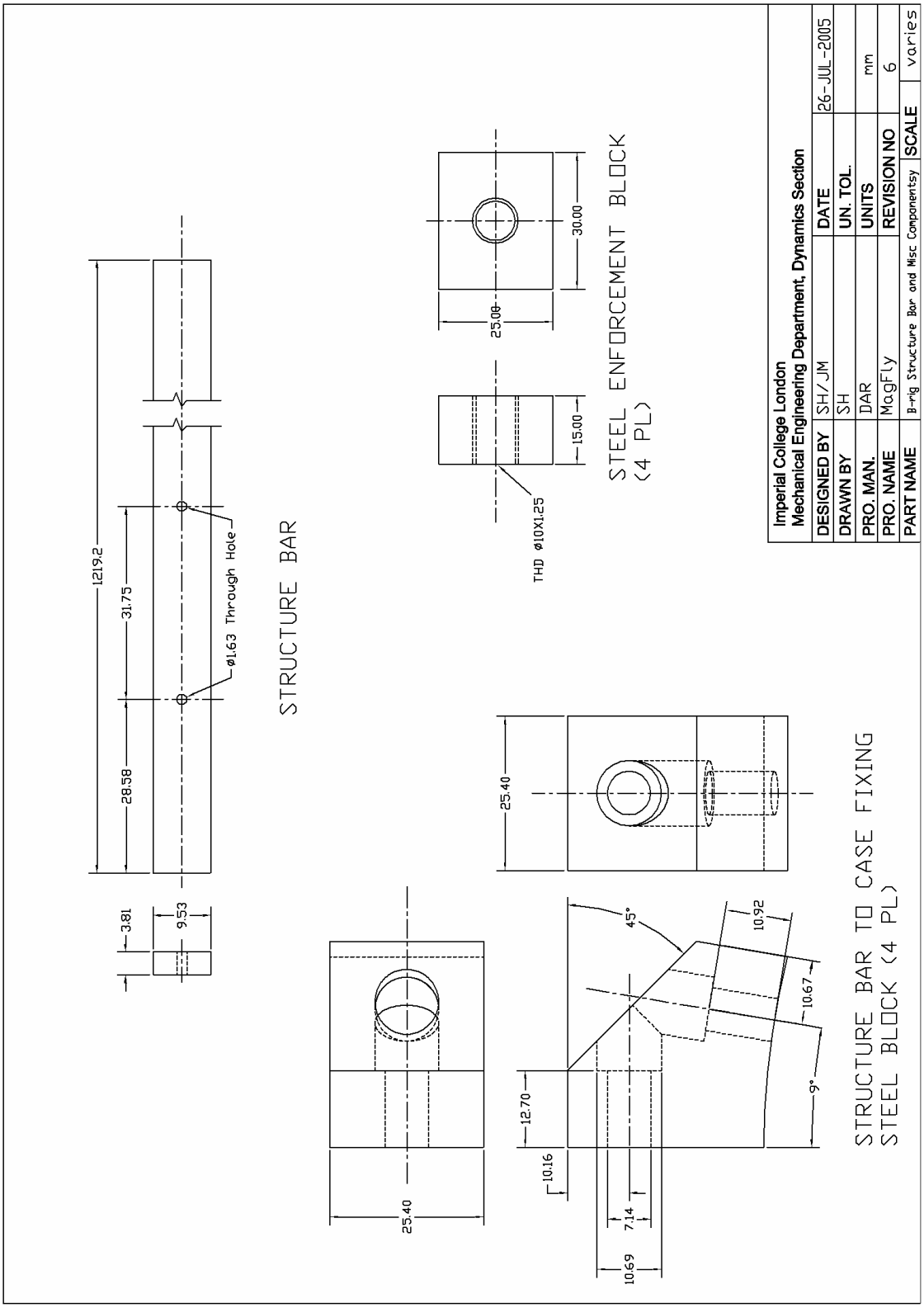

Appendix B

Simulation of a 1-DOF Nonlinear Oscillator

B.1 Comparison of results from time integration and HBM calculation

The Nonlinear Bearing Support of the test rig was designed in such a way that it displays in the horizontal direction a stiffness pattern that is the combination of a negative linear stiffness and a third-order polynomial stiffness. The resultant system governing equation is:

$$m\ddot{u}(t) + c\dot{u}(t) + k_1 u(t) + k_3 u^3(t) = F\sin(\omega t) \tag{B.1}$$

in which $k_1 < 0$ and $k_3 > 0$.

Such equation also appears in population dynamics and Earth's magnetic field model. It was first systematically reported by Holmes [65] in 1979, and has since become an interesting subject, mainly for mathematicians to understand the intricate behaviours of such a nonlinear system. It is understood that multiple steady-state solutions exist in a nonlinear system when it is under periodic excitation. It will be very interesting to see how such kind of nonlinear responses can be captured by frequency-domain calculations. It has been proven from this exercise that HBM can locate steady-state solutions much faster than time-domain method.

The following parameters are chosen for numerical studies: F =2000N; m =1kg; c =1Ns/m; k_1 =-1000N/m k_3 =10000 N/m^3. One of the main purposes of this

study is to find as many as possible steady-state periodic solutions at any given excitation frequency. Time-domain calculation based on Runge-Kutta method was conducted at 24.6Hz. 200 different initial conditions, in terms of velocity and displacement, were applied. Different types of steady-state solutions were observed, manifested in the form of major- and sub- harmonic responses. HBM was applied to the same system at the same excitation frequency. The comparison of some of the steady-state responses are presented in Figure B - 1 to Figure B - 6. The first plot shows the time domain variation of the response and excitation, from which it is possible to judge what is the dominant harmonic term in the response. The second plot is the so-called 'phase diagram' in which a trajectory of motion is plotted over period of the response. The velocity and displacement are the two coordinates.

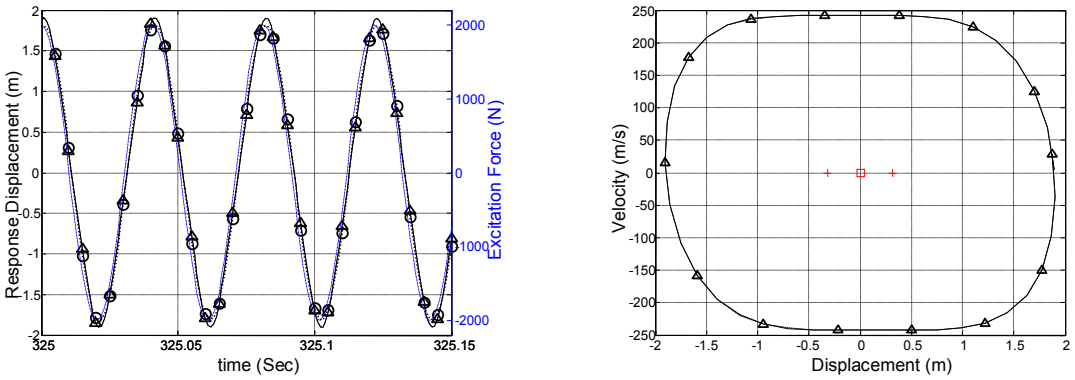

(a) **(b)**

Figure B - 1 (a)Time domain variation of displacement and excitation and (b) phase space trajectory of solution of the major harmonic response with zero constant component in *('-·-·-·-' external excitation, '___' time integration, '··○··○··○·· ' one harmonic term (1) included, '-Δ--Δ--Δ--' two harmonic (1, 3) terms included.)*

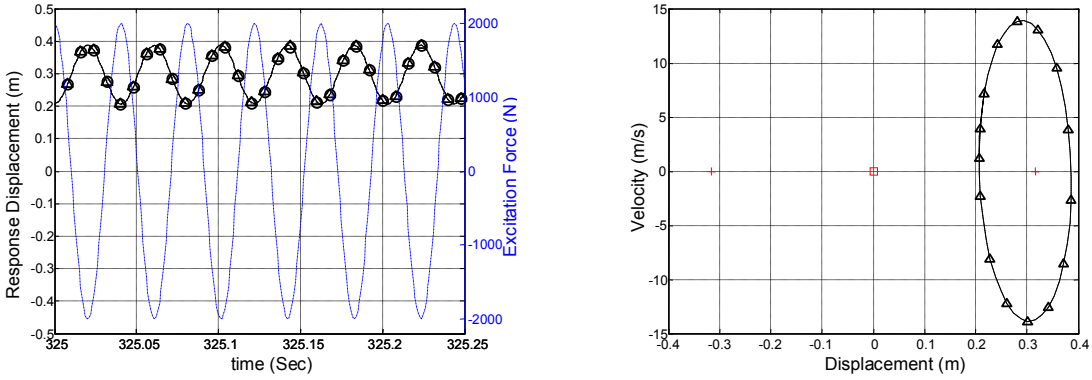

(a) **(b)**

Figure B - 2 (a) Time domain variation of displacement and excitation and (b) phase space trajectory of solution of the major harmonic response with a constant component *('-·-·-·-' external excitation, '___' time integration, '··○··○··○·· ' one harmonic (1) term included, '-Δ--Δ--Δ--' three harmonic (0, 1, 2) terms included.)*

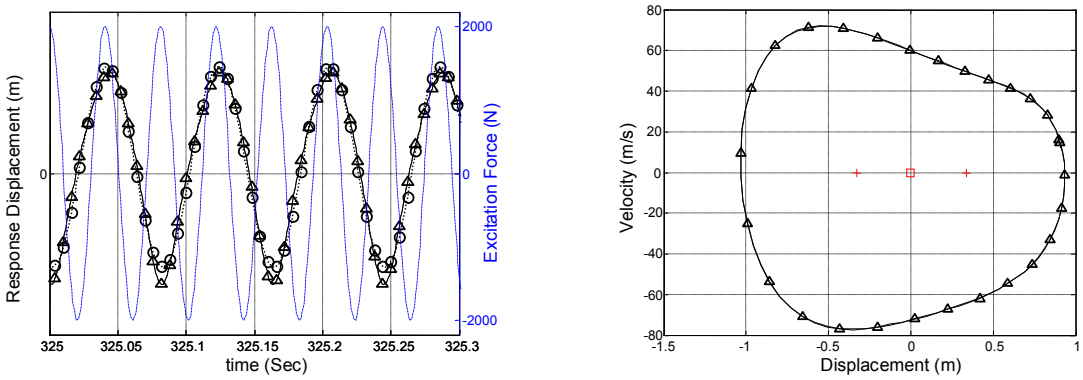

(a) **(b)**

Figure B - 3 (a) Time domain variation of displacement and excitation and (b) phase space trajectory of solution of 1/2 sub-harmonic response
('-·-·-·-' external excitation, '___' time integration, '··○··○··○·· ' two harmonic terms (0, 1/2) included, '-Δ--Δ--Δ--' four harmonic (0, 1/2, 2/2, 3/2) terms included.)

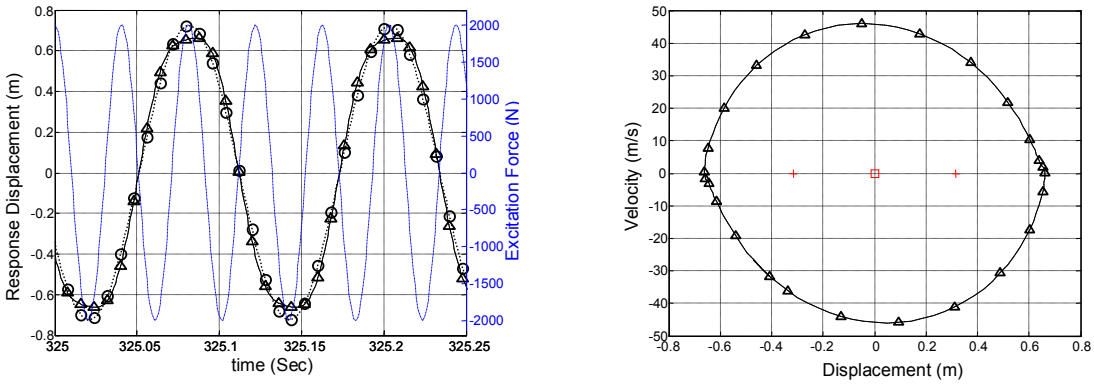

(a) **(b)**

Figure B - 4 (a) Time domain variation of displacement and excitation and (b) phase space trajectory of 1/3 sub-harmonic response
('-·-·-·-' external excitation, '___' time integration, '··○··○··○·· ' one harmonic term (1/3) included, '-Δ--Δ--Δ--' two harmonic terms (1/3, 3/3) included.)

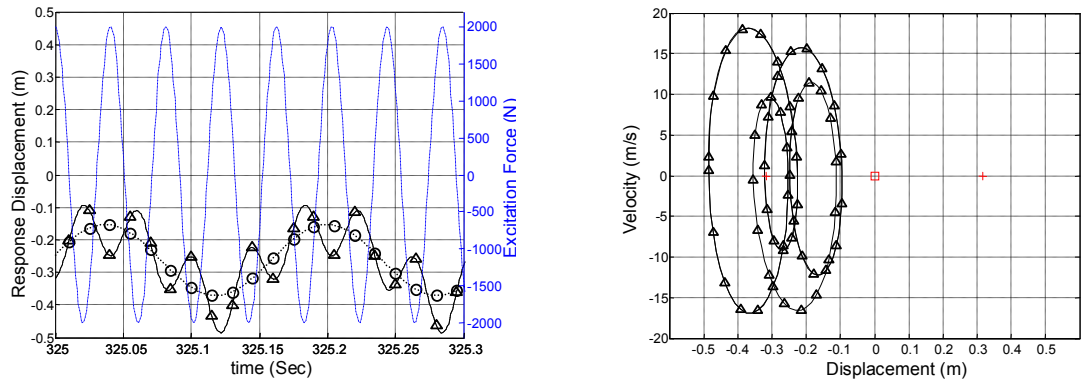

(a) **(b)**

Figure B - 5 (a) Time domain variation of displacement and excitation and (b) phase space trajectory of 1/4 sub-harmonic response
('-·-·-·-' external excitation, '___' time integration, '··○··○··○·· ' two harmonic terms (0, ¼) included, '-Δ--Δ--Δ--' five harmonic terms (0, ¼, 2/4, ¾, 4/4) included.)

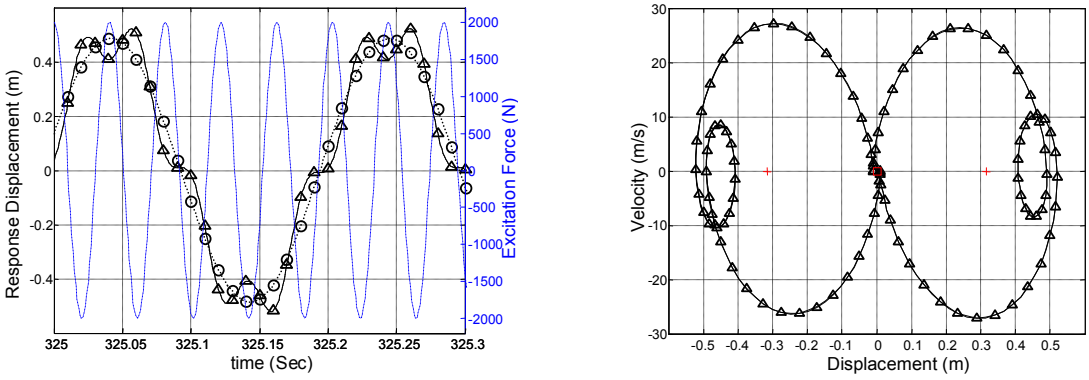

(a) **(b)**

Figure B - 6 (a) Time domain variation of displacement and excitation and (b) phase space trajectory of 1/5 sub-harmonic response

('-·-·-·-' external excitation, '___' time integration, '··○··○··○·· ' one harmonic term (1/5) included, '-Δ--Δ--Δ--' three harmonic terms (1/5, 3/5, 5/5) included.)

It is show from the above plots that the HBM calculation results are very close to the time-domain calculation results. In addition, HBM calculation is much more efficient, and more thorough in finding solutions that belong to the same harmonic regime. This is evident in Figure 4 - 3 and Figure 4 - 4 in Chapter 4.

B.2 Stability Check

The HBM calculation discovers a large group of steady-state solutions when the system is under fixed-amplitude periodic excitation, but it could not provide information whether the solutions are stable or not, i.e. whether or not the solutions exist in physical world. The stability of the steady-state response of this nonlinear system is not the emphasis in this study; however, some interesting findings were recorded, one of which, the system behaviour under varying excitation frequency, is reported here. This study is not only important to the understanding of the system's nonlinear behaviour, but also to some possible physical applications, e.g. the system behaviour in the run-up or run-down operation of the rotating machinery.

Figure B - 7 shows a cluster of subharmonic steady-state solutions, with the y-axis being the response amplitude. This is an extraction from Figure 4 - 4. Each black line represents the solution calculated by HBM over the whole frequency range. Blue dots are the calculation results from the Runge-Kutta method. In this exercise, time-domain calculation of the steady-state response first settles down on one of the sub-harmonic branch. The excitation frequency is gradually

reduced and the response is recorded. Figure B - 7 reveals that not all the HBM calculation results exist in the time-domain calculation.

All the subharmonic responses evolve in the same pattern as the excitation frequency decreases. Take the 1/3-subharmonic response branch for instance, at the higher frequency side, the response is symmetric to the global centre in the phase plane as shown in Figure B - 8. The symmetry is broken as the excitation frequency decreases and reaches a point that a DC term appears in the solution. The amplitude starts travelling on another branch. A typical time-domain variation and phase trajectory is shown in Figure B - 9. Further decrease of the excitation frequency leads to a point where the solution loses its stability. The loss of stability is preceded by a short span of frequency at which the steady-state response displays 'period-doubling' behaviour as shown in Figure B - 10. The red circles in the phase plane are called Poincaré Points. They are the record of the response every time the excitation is at the same phase angle. There are six Poincaré Points in the phase plot, which means that the response repeats itself after six cycles of excitation. The forced response then jumps to another branch after the 'period-doubling'. This jump can lead the solution to different steady-state response branches and the choice of branch appears to be so sensitive to the frequency variation speed that it can be considered as random. Figure B - 11 to Figure B - 13 shows the similar evolution on the branches of 1/5 subharmonic responses.

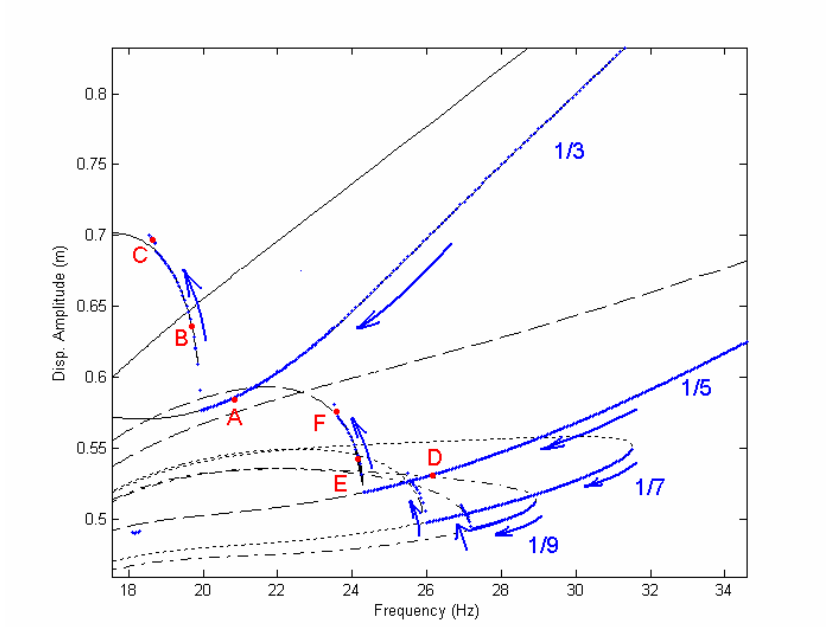

Figure B - 7 A cluster of sub-harmonic response branches

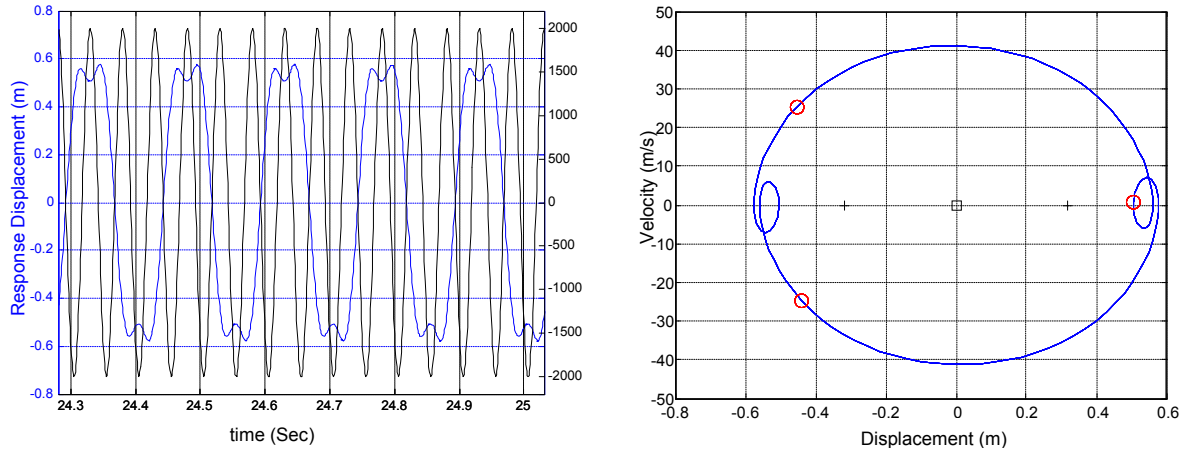

(a) **(b)**

Figure B - 8 (a) Time domain variation of displacement and excitation and (b) phase space trajectory of point A in Figure B - 7

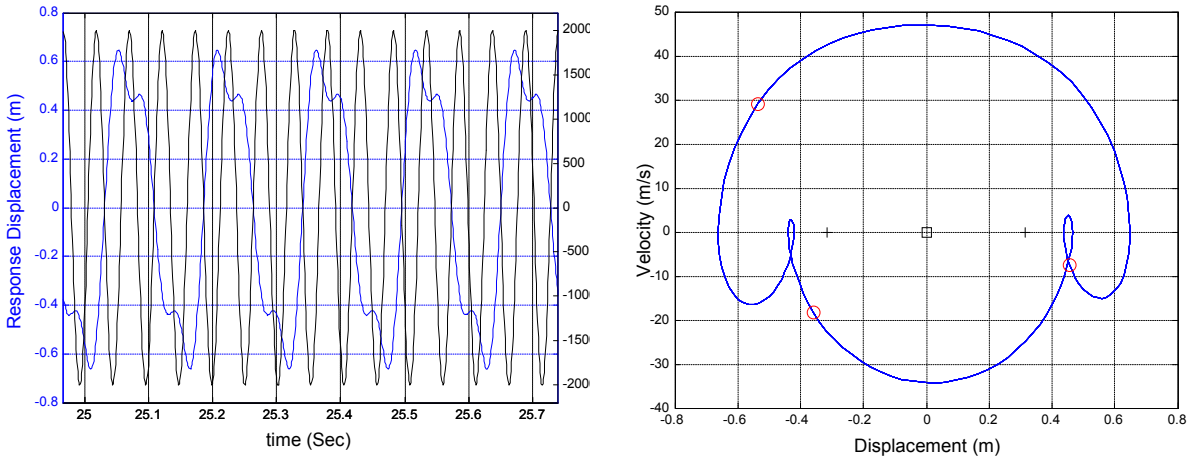

(a) **(b)**

Figure B - 9 (a) Time domain variation of displacement and excitation and (b) phase space trajectory of point B in Figure B - 7

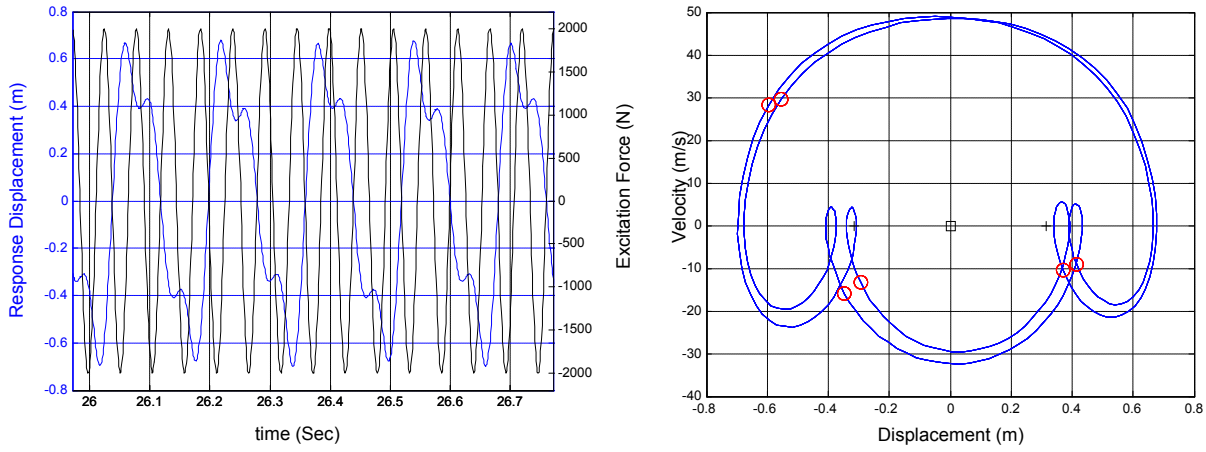

(a) **(b)**

Figure B - 10 (a) Time domain variation of displacement and excitation and (b) phase space trajectory of point C in Figure B - 7

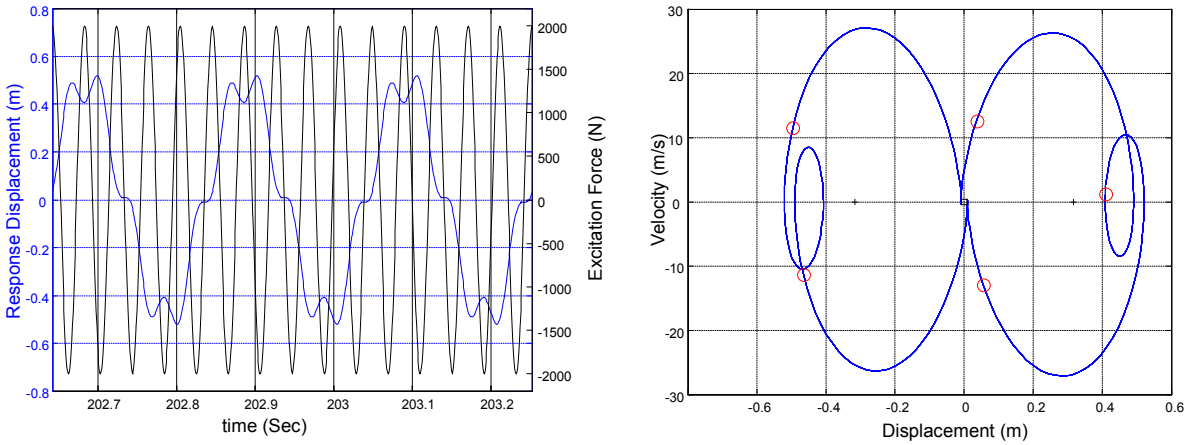

(a) **(b)**

Figure B - 11 (a) Time domain variation of displacement and excitation and (b) phase space trajectory of point D in Figure B - 7

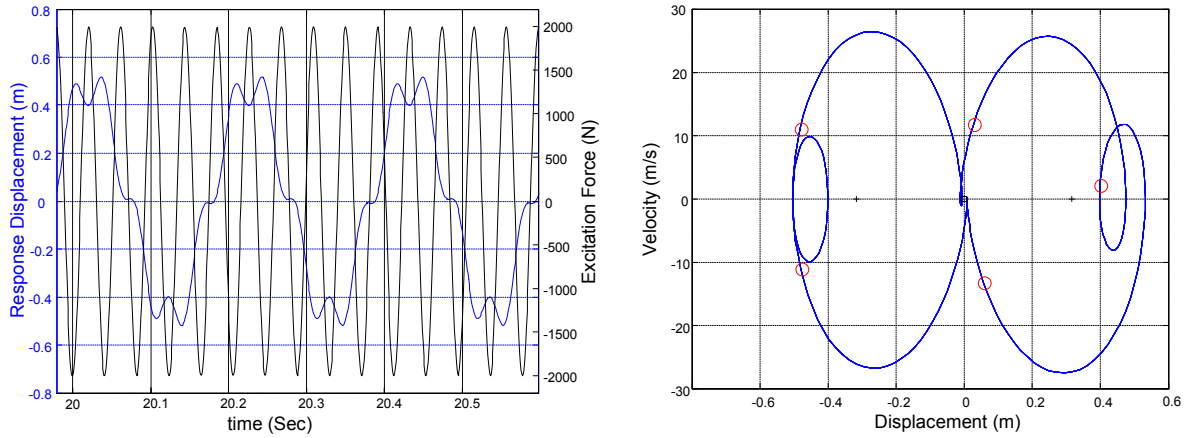

(a) **(b)**

Figure B - 12 (a) Time domain variation of displacement and excitation and (b) phase space trajectory of point E in Figure B - 7

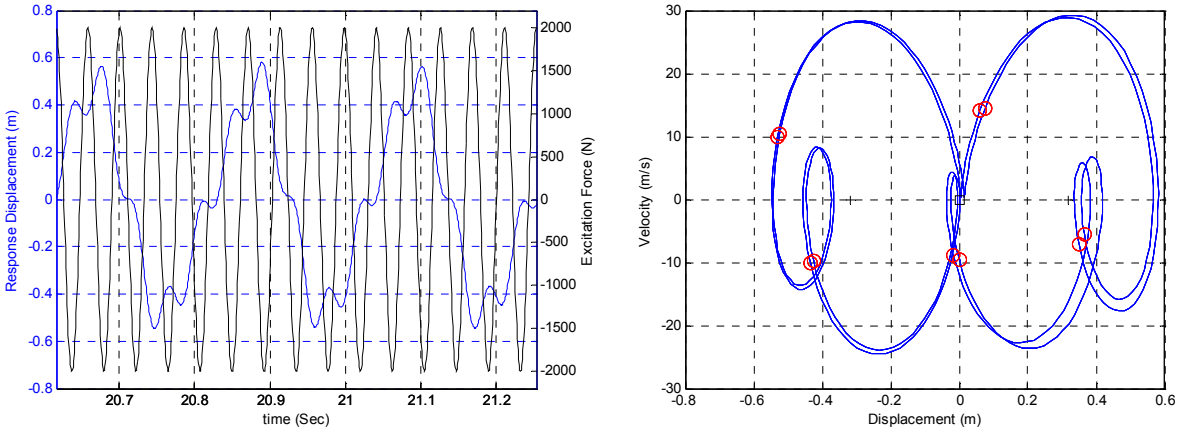

(a) **(b)**

Figure B - 13 (a) Time domain variation of displacement and excitation and (b) phase space trajectory of point F in Figure B - 7